Compressive Stress-strain of Unreinforced Masonry Boundary Element Prisms

Mohamed Yosry Mohamed Mohamed

A Thesis

in

The Department

of

Building, Civil and Environmental Engineering

Presented in Partial Fulfillment of the Requirements

for the Degree of Master of Applied Science (Civil Engineering) at

Concordia University

Montreal, Quebec, Canada

December 2018

CONCORDIA UNIVERSITY

School of Graduate Studies

This is to certify that the thesis prepared

By: **Mohamed Yosry Mohamed Mohamed**

Entitled: **Compressive Stress-strain Response of Unreinforced Masonry Boundary Element Prisms**

and submitted in partial fulfillment of the requirements for the degree of

Master of Applied Science (Civil Engineering)

complies with the regulations of the University and meets the accepted standards with respect to originality and quality.

Signed by the final Examining Committee:

_____ Chair
Dr. Ashutosh Bagchi

_____ External to Program
Dr. Rajamohan Ganesan

_____ Examiner
Dr. Lucia Tirca

_____ Examiner
Dr. Ashutosh Bagchi

_____ Supervisor
Dr. Khaled Galal

Approved by _____
Dr. Fariborz Haghighat, Ph.D., P. Eng, Graduate Program Director
Department of Building, Civil and Environmental Engineering

_____
Dr. Amir Asif, Ph.D., P. Eng, Dean
Gina Cody School of Engineering and Computer Science
Date 2018-12-04

Abstract

Compressive Stress-strain of Unreinforced Masonry Boundary Element Prisms

Mohamed Yosry Mohamed Mohamed

Reinforced masonry shear walls (RMSW) with masonry boundary elements (BE) are rectangular walls having integrated masonry BEs at the wall extremities. These BEs can be constructed using half pilaster block (i.e. C-shaped blocks) or regular stretchers. The compressive stress-strain response of the masonry BEs prisms built using stack-bonded C-shaped blocks (C-MSBEP) vary from that of regular stretchers prisms due to the continuity of the grout core (i.e. absence of block's webs) and the higher grout-to-shell area ratio. Understanding and enhancing the stress-strain response of the masonry BE is a key to enhance the overall response of the RMSW with BEs. One of the challenges limiting the use of RMSW in high-rise buildings is the low compressive strength of masonry compared to reinforced concrete. Many studies showed that for specific block strength increasing the grout strength will not result in a proportional increase in the masonry prism capacity. Although some factors that result in minimizing the grout contribution to the prism strength were previously investigated, a consensus on the main governing factors is yet to be established.

In this study, the compressive stress-strain relationships of half-scale fully-grouted C-MSBEP and its constituents (i.e. masonry shell and grout core) are studied. In total, eight fully-grouted masonry BE prisms, six un-grouted masonry BE shells, eighteen grout core prisms, nine running-bonded fully-grouted stretcher block prisms, and nine stack-bonded fully-grouted stretcher block prisms have been tested under concentric compression loading. Both the un-grouted masonry shells and the grout core prisms had the same height as the grouted C-MSBEPs. The test matrix is composed of two different prisms' aspect ratios, namely two and five. The grouted stretcher block prisms were grouted using normal strength grout while the grouted C-MSBEPs were grouted using two grout strengths, normal and high strength.

The study covers the effect of prism construction techniques in Canadian and US standards on the stress-strain response of C-MSBEPs, comparing the stress-strain of C-MSBEPs to regular stretcher block prisms, and the effect of the interaction between the masonry shell and the

grouted core on the masonry compressive strength. In addition, the effect of treatment, air and wet, on the stress-strain response was also examined on the grout core prisms. Moreover, the stress-strain relationship of the 200 mm x 100 mm grout cylinders is compared to that of the grout core prisms to study the shape and size effects. The results of the grouted C-MSBEPs were compared to four predictive equations from the literature and to the unit strength values provided by the Canadian and US standards to evaluate their ability to predict the peak strength of the grouted BEs.

The stress-strain response of C-MSBEPs was found to be different from that of regular stretcher block prisms and is affected differently by height-to-thickness ratio. Thus, two analytical models were proposed to predict the full stress-strain response of C-MSBEPs and stretcher block prisms. The shape and size effects on grout core prisms are evident especially for normal strength grout. The superposition of the load-displacement response of the grout core and the masonry shell was found to be not comparable to that of the grouted BE. The effect of treatment on the stress-strain relationship of the grout cores was found to be insignificant. The equations available in the literature that were used to predict the capacity of masonry prisms were found to misestimate the experimental results of the tested C-MSBEPs. The US Masonry Structures Joint Committee (MSJC 2013) design standard was found to introduce better estimation for C-MSBEP's compressive strength compared to the Canadian Standard Association CSA S304 (2014) "Design of Masonry Structures". Both the CSA A179 (2014) "Mortar and grout for unit masonry" grout cylinders and the ASTM C1019 (2014) "Standard Test Method for Sampling and Testing Grout" grout prisms were found not representing the actual grout stress-strain response within the C-MSBEP, mainly because they do not simulate the effect of grout shrinkage in actual masonry prisms. Therefore, an equation was proposed that considers the different factors affecting the contribution of the grout core to the strength of C-MSBEPs.

Dedication

To my supportive parents; Yosry and Aisha

To my beloved wife; Dina

To my son; Yusuf

To my Brothers; Ahmed and Mahmoud

Acknowledgements

All praise and gratitude be to Allah the Most Gracious, the Most Compassionate and the Most Merciful with the blessings of Whom the good deeds are fulfilled

I would like to thank my supervisor Dr. Khaled Galal for his support and guidance. Thanks to him, I learned many lessons about myself, the academia, and the world. My sincere thanks and gratitude are also due to postdoctoral fellow Dr. Ahmed Ashour for assisting and encouraging me throughout the past years. Their efforts cannot be denied in reviewing my journal papers and providing me with invaluable comments and suggestions.

The experimental work would have never been completed without the help of the structures laboratory staff at Concordia University: Riccardo Gioia, Andy Shin-pong, Roberto Avila-Perez, Nicolas Silva-Castellon and Jaime Yeargans. Due thanks also go to Dr. Ala' Obaidat for helping me with the experimental work of this study.

Special thanks are due to my older brother Mohammed Albutainy, my twin brother Nader Ali, and my younger brother Belal Abdelrahman for being more than friends to me. My thanks are also due to Dr. Khalid Al-Otaibi for providing me with technical tips and life lessons.

I would like to acknowledge the financial support from the Natural Sciences and Engineering Research Council of Canada (NSERC), l'Association des Entrepreneurs en Maçonnerie du Québec (AEMQ), the Canadian Concrete Masonry Producers Association (CCMPA) and Canada Masonry Design Centre (CMDC).

I am grateful for my parents, Yosry Zorainy and Aisha Nadi, for their love and emotional support. I am grateful also to my brothers, Ahmed and Mahmoud Yosry, for being there for me all the time.

No words can describe my gratitude to my wife Eng. Dina Said. I appreciate her continuous support, exceptional patience, and affectionate understanding. Finally, I am profoundly thankful to my son Yusuf. His smile provided me with the strength required to complete this work.

Table of Contents

1 Introduction 1

1.1 Background and Motivation 1

1.2 Objectives 3

1.3 Scope of Work 4

1.4 Thesis Layout 4

2 Literature Review 6

2.1 Canadian (CSA) and US (ASTM) Standards Requirements for Testing Masonry Prisms and their Individual Components 6

2.1.1 Sampling and testing of prism components 6

2.1.2 Construction and testing of prisms 8

2.1.3 Masonry Prisms of Boundary Elements fabricated with C-shaped Blocks 12

2.2 Canadian (CSA S304 2014) and US (MSJC 2013) standards Tabulated Compressive Strength values (Unit strength method) 12

2.3 Background on the effect of grout compressive strength on the prism strength 14

2.3.1 Incompatibility of longitudinal and transversal strains of masonry shell and grout-core 15

2.3.2 The representation of the grout core strength by the tested grout samples 15

3 Compressive Stress-Strain Response of Masonry Boundary Element Prisms 18

3.1 Experimental Work of Phase I 18

3.1.1 Test Matrix 18

3.1.2 Material Properties 20

3.1.3 Test Setup, Instrumentation, and Loading protocol 24

3.2 Results and Observations 25

3.2.1 Fully-grouted running-bonded stretcher block prisms 25

3.2.2 Fully-grouted stack-bonded stretcher block prisms 27

3.2.3 Fully-grouted Boundary Element Prisms 30

3.3 Effect of height-to-thickness ratio on the compressive strength of grouted masonry prisms 32

3.4 Stress-strain of boundary element prisms versus that of the stretcher block prisms 34

3.5 Stretcher block and boundary element prisms' experimental results versus the predicted values by CSA S304 (2014) and MSJC (2013) 37

3.6 Typical stress-strain responses and the proposed stress-strain models for standard stretcher block and boundary element prisms according to CSA and ASTM 39
4 The Interaction between the Masonry Shell and the Grout Core 45
4.1 Experimental Work of Phase II 45
4.1.1 Test Matrix 45
4.1.2 Material Properties 48
4.1.3 Test Setup, Instrumentation, and Loading protocol 50
4.2 Results and observations 51
4.2.1 Fully-grouted Boundary Element Prisms (high strength grout) 51
4.2.2 Un-grouted Boundary Element Shells 54
4.2.3 Grout Core Prisms 55
4.3 Comparing C-MSBEP strength with available prediction equations 59
4.3.1 Hamid et al. (1978) 60
4.3.2 Sturgeon et al. (1980) 61
4.3.3 Priestley and Chai Yuk Hon (1984) 62
4.3.4 Sarhat (2016) 63
4.4 Grout cylinders versus grout core prisms stress-strain responses 64
4.5 Superposition of masonry shell and grout core load-displacement curves versus that of the tested boundary elements 65
4.6 Factors influencing the reduction of the grout stress-strain response in the grouted prism 67
5 Summary, Conclusions and Future Work 72
5.1 Summary 72
5.2 Conclusions 73
5.3 Recommendations for Future Research 75
References 77
Appendix A Experimental Work 81
Appendix A.1 Material Characterization 81
Appendix A.2 Construction of Specimens 84
Appendix A.3 Specimens after Testing 88

List of Figures

Figure 1.1 Illustration of RMSW with BEs: (a) BE constructed using half pilaster block (C-shaped block), (b) Half-scale C-shaped concrete block compared to regular stretcher block, and (c) BE constructed using regular stretcher blocks 2
Figure 2.1 Grout prism specimens molding according to ASTM C1019 (2014) 8
Figure 2.2 Comparison of the correction factors for axial compressive strength of masonry prisms provided by ASTM C1314 (2014) and CSA S304 (2014) based on the prism height-to-thickness ratio 9
Figure 2.3 Comparison between the tabulated compressive strength values of MSJC (2013) and CSA S304 (2014) for concrete block grouted masonry prisms 13
Figure 3.1 Schematic drawing for the test specimens: (a) specimens with height to thickness ratio of two, (a) specimens with height to thickness ratio of five 18
Figure 3.2 Identification criteria for each tested sample 19
Figure 3.3 Dimensions of the half-scale stretcher blocks (left) and the half-scale C-shaped blocks (right) 21
Figure 3.4 Compression test for: (a) concrete block coupon, (b) mortar cube, (c) grout cylinder, (d) grout prism 21
Figure 3.5 Stress-strain response of: (a) grout cylinders, (b) grout prisms 23
Figure 3.6 Test setup and instrumentation for: (a) stretcher block prisms having height to thickness ratio= 2.0, (b) stretcher block prisms having height to thickness ratio= 5.0, (c) boundary element prisms having height to thickness ratio= 2.0, (b) boundary element prisms having height to thickness ratio = 5.0 24
Figure 3.7 Observed failure patterns for the fully-grouted running-bonded stretcher block prism of *h/t* = 2.0 (a) front, (b) right, (c) back, and (d) left 25
Figure 3.8 Observed failure patterns for the fully-grouted running-bonded stretcher block prism of *h/t* = 5.0 (a) front, (b) right, (c) back, and (d) left 26
Figure 3.9 Stress-strain curves for masonry stretcher block prisms of running bond pattern having *h/t* ratio of 5 and 2 27
Figure 3.10 Observed failure patterns for the fully-grouted stack-bonded stretcher block prism of *h/t* = 2.0 (a) front, (b) right, (c) back, and (d) left 28

Figure 3.11 Observed failure patterns for the fully-grouted stack-bonded stretcher block prism of *h/t* = 5.0 (a) front, (b) right, (c) back, and (d) left 28
Figure 3.12 Stress-strain curves for masonry stretcher block prisms of stack bond pattern having *h/t* ratio of 5 and 2 29
Figure 3.13 Observed failure patterns for the fully-grouted C-MSBEPs of *h/t* = 2.0 (a) front, (b) right, (c) back, and (d) left 30
Figure 3.14 Observed failure patterns for the fully-grouted C-MSBEPs of *h/t* = 5.0 (a) front, (b) right, (c) back, and (d) left 31
Figure 3.15 Stress-strain curves for boundary element masonry prisms (C-MSBEP) having *h/t* ratio of 5 and 2 32
Figure 3.16 Comparing the stress strain response of running bond pattern stretcher prisms, stacked bond pattern stretcher prisms, and B.E. prisms of *h/t* of 2.0 and 5.0 34
Figure 3.17 Comparison of stress-strain curves for the masonry prisms ST-S-2-FB (ASTM C1314 2014), ST-R-5-FS (CSA S304 2014), BE-2 and BE-5 36
Figure 3.18 Proposed stress-strain models by modifying Mander Model 41
Figure 3.19 Proposed stress-strain models by modifying Kent and Park Model 42
Figure 3.20 Proposed stress-strain models for ST-S-2-FB (ASTM) 43
Figure 3.21 Proposed stress-strain models for ST-R-5-FS (CSA) 43
Figure 3.22 Proposed stress-strain models for BE-2 44
Figure 3.23 Proposed stress-strain models for BE-5 44
Figure 4.1 Schematic drawing for the tested specimens: (a) Specimens with height to thickness ratio of two, (b) Specimens with height to thickness ratio of five 45
Figure 4.2 Identification method for each tested sample 46
Figure 4.3 Grout core specimens' molding: (a) Specimens representing BE prisms having *h/t* = 2.0, (b) Specimens representing boundary elements prisms having *h/t* = 5.0 47
Figure 4.4 Compression test for: (a) Concrete block coupon, (b) Mortar cube, (c) Grout cylinder 48
Figure 4.5 Stress-strain response of normal and high strength grout cylinders 50
Figure 4.6 Test setup and instrumentation for masonry prisms and shells having *h/t* ratio of: (a) two, (b) five, and grout core represents the grout in BE prism with *h/t* of: (c) two, and (d) five. 51

Figure 4.7 Observed failure patterns for the fully-grouted C-MSBEPs of *h/t* = 5.0 (a) front, (b) right, (c) back, and (d) left 52
Figure 4.8 Stress-strain curves for masonry boundary element masonry prisms C-MSBEP 53
Figure 4.9 Observed failure patterns for the un-grouted BE shells SH-0-2 and SH-0-5 54
Figure 4.10 Stress-strain curves for un-grouted masonry shells (stress computed based on net areas) 55
Figure 4.11 Stress-strain curves of normal strength grout cores representing the cores of BE prisms with *h/t* = 2.0 56
Figure 4.12 Stress-strain curves of normal strength grout cores representing the cores of BE prisms with *h/t* = 5.0 57
Figure 4.13 Stress-strain curves of high strength grout cores representing the cores of BE prisms with *h/t* = 2.0 57
Figure 4.14 Stress-strain curves of high strength grout cores representing the cores of BE prisms with *h/t* = 5.0 58
Figure 4.15 C-MSBEP ultimate strength (*h/t* = 5.0) against the prediction relationships using the grout strength of the tested cores and cylinders 60
Figure 4.16 Comparison of average stress-strain curves of grout core prisms and grout cylinders 64
Figure 4.17 Comparison of the load-displacement relationships of BE shells, grouted BE prisms, grout cores, and the superposition: (a) C-MSBEPs having *h/t* = 2.0 and grouted by normal strength grout, (b) C-MSBEPs having *h/t* = 5.0 and grouted by normal strength grout, (c) C-MSBEPs having *h/t* = 5.0 and grouted by high strength grout. 66
Figure 4.18 Cracked region in the grout cores of (a) Half-scale C-MSBEPs and (b) Full-scale stretcher block prisms 69
Figure 4.19 Illustration for the factors used in Equation 4.11 71
Figure A.1 Half-scale C-shaped block and Half-scale stretcher block compared to full-scale stretcher block 81
Figure A.2 Capping of stretcher blocks 81
Figure A.3 Failure of Stretcher blocks 81
Figure A.4 Capping of grout cylinders 82
Figure A.5 Failure of grout cylinders 82

Figure A.6 Failure of ASTM grout prisms 83
Figure A.7 Sampling and tamping of mortar cubes 83
Figure A.8 Building the specimens by the certified mason 84
Figure A.9 Stretcher block prisms and C-MSBEPs during construction 84
Figure A.10 Grouting the masonry prisms 85
Figure A.11 Keeping the prisms in sealed water tight bags 85
Figure A.12 Wet treatment of the grout cores 86
Figure A.13 Stretcher prisms of h/t = 2.0 before testing 86
Figure A.14 Stretcher prisms of h/t = 5.0 before testing 87
Figure A.15 C-MSBEPs before testing 87
Figure A.16 Stretcher block prisms after testing 88
Figure A.17 C-MSBEPs after testing 88

List of Tables

Table 2.1 Comparison between the requirements of CSA and ASTM for sampling and testing of masonry prisms and their constituents 7
Table 3.1 Experimental test matrix for stretcher block prisms 19
Table 3.2 Experimental test matrix for masonry boundary element prisms 20
Table 3.3 Materials properties 22
Table 3.4 Results of tested masonry stretcher block prisms 27
Table 3.5 Results of tested C-MSBEPs 32
Table 3.6 Comparison of the experimental results to the unit strength method values of CSA S304 (2014) 38
Table 3.7 Comparison of the experimental results to the unit strength method values of MSJC (2013) 38
Table 3.8 Values used for the proposed stress-strain models 41
Table 4.1 Experimental test matrix for C-MSBEPs 46
Table 4.2 Experimental test matrix for un-grouted masonry prisms (masonry shells) 46
Table 4.3 Experimental test matrix for grout core specimens 48
Table 4.4 Materials properties 49
Table 4.5 Results of tested masonry boundary element prisms C-MSBEP 53
Table 4.6 Results of un-grouted masonry prisms (shells) 55
Table 4.7 Results of tested grout core specimens 58
Table 4.8 Proposed values for grout strength reduction factors 71

Chapter 1

INTRODUCTION

1.1 Background and Motivation

Masonry has been used in construction for centuries. Currently, reinforced concrete block masonry is widely used in the construction of low-rise residential and commercial buildings. Reinforced masonry seismic force resisting systems (SFRS) have proven their efficiency in resisting seismic loadings on both the component and system levels (El-Dakhakhni and Ashour 2017). However, it is essential to enhance both the strength and ductility of the masonry seismic force resisting systems in order to introduce masonry as a competitive alternative in mid- and high-rise buildings. The highest specified compressive strength attainable using the unit strength method for a fully grouted prism is 13.5 MPa in the Canadian standards (CSA S304 2014), and 20.7 MPa in the US standards (MSJC 2013). These values are attained by using the highest block strength of approximately 30 MPa. Recent studies (Albutainy et al. 2017; Banting and El-Dakhakhni 2012; Ezzeldin et al. 2017; Shedid et al. 2010) have shown an enhancement in the wall ductility by introducing an integrated boundary element toward the wall ends (Figure 1.1) . Masonry boundary elements (BEs) allow the introduction of two layers of vertical steel rebars and, consequently, confining the wall most stressed zone by confining hoops.

Limited studies focused on the stress-strain relationship of reinforced masonry BEs. Abo El Ezz et al. (2015) investigated the effect of increasing the confinement ratio on the post-peak response and the strain ductility of masonry BEs constructed utilizing stretcher concrete blocks. It was found that more strain ductility is achieved by decreasing the hoops spacing. However, utilizing stretcher blocks to build the BEs imposed some limitations on the hoops spacing. Obaidat et al. (2017) tested full scale reinforced masonry BEs constructed by C-shaped blocks (Figure 1.1 b). These reinforced masonry BEs allow the installation of at least four longitudinal reinforcement bars confined by transverse hoops, at any desired spacing, which increases the ultimate strain of the BEs. Obaidat et al. (2018) further investigated the effect of changing the hoop spacing, the longitudinal reinforcement ratio, and the strength of grout on the axial stress-strain relationship of the half-scaled C-shaped reinforced masonry BEs. The study found that

increasing the longitudinal reinforcement ratio, increasing the grout strength, and decreasing the hoop spacing enhanced the peak and post-peak stress-strain performance. Nonetheless, the stress-strain response of the unreinforced BEs constructed using the C-shaped blocks is yet to be investigated.

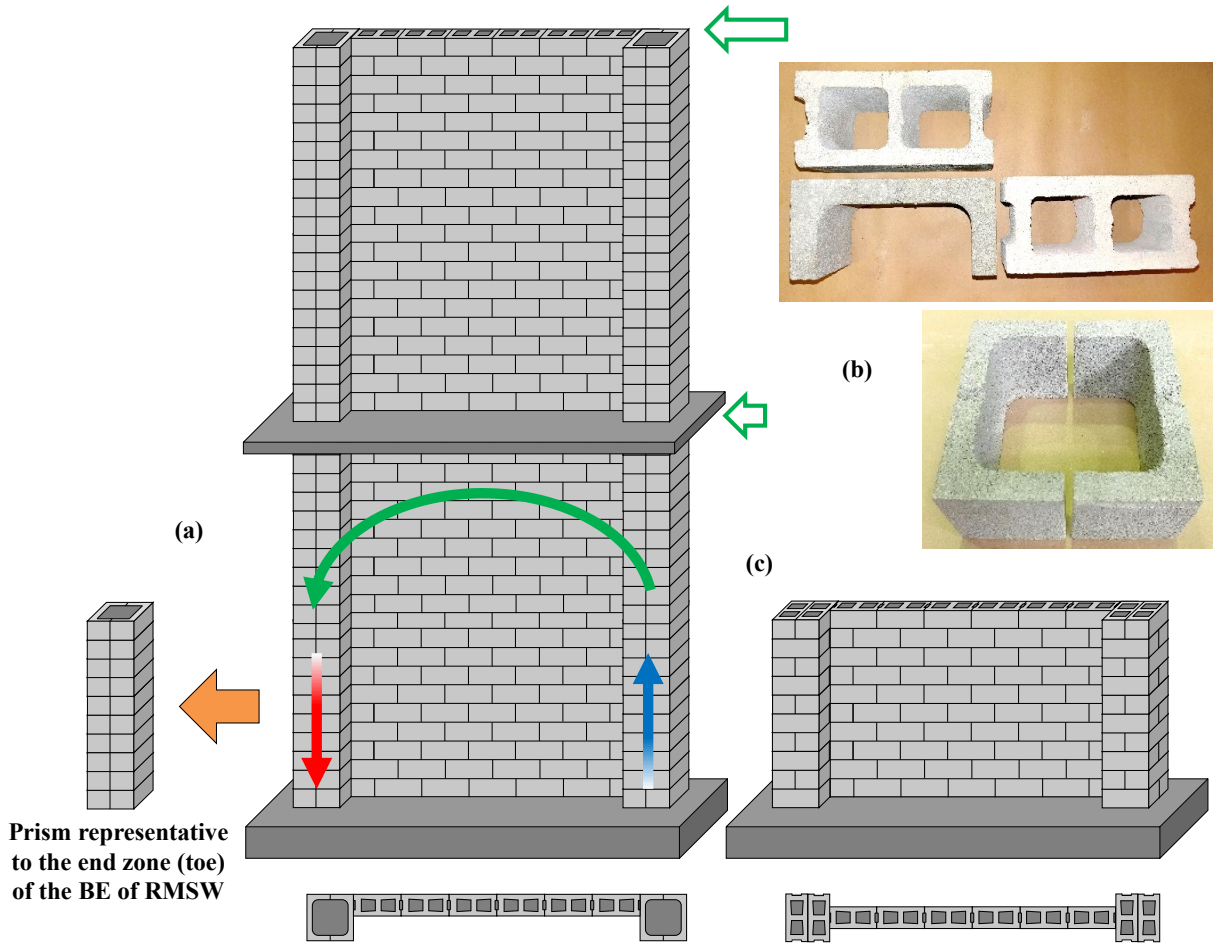

Figure 1-1 Illustration of RMSW with BEs: (a) BE constructed using half pilaster block (C-shaped block), (b) Half-scale C-shaped concrete block compared to regular stretcher block, and (c) BE constructed using regular stretcher blocks

Canadian and US standards specify dissimilar prism configurations as being representative to in-situ construction. This leads to two distinct specified compressive strength of masonry (f'_m) values for the same masonry element depending on which standard prism will be tested. Several researchers studied the requirements of each of the two standards with no consensus on which standard provide f'_m determination technique that is more representative to the actual

construction. While some studies showed that the prism construction requirements of CSA S304 (2014) is probably more representative of the actual wall construction (Hamid and Chukwunenye 1986; Hassanli et al. 2015), others supported the ability of the prism constructed according to ASTM C1314 (2014) "Standard Test Method for Compressive Strength of Masonry Prisms" to accurately represent the in-situ construction (Rizaee et al. 2016). This discrepancy also affects the tabulated f'_m values provided by the two standards for the unit strength method as these values follow each standard's procedure for the sake of consistency. Although the unit strength method allows getting f'_m while saving time, effort, and money invested in the testing of the prisms, the values provided in both standards are known to be conservative (Fortes et al. 2014; Korany and Glanville 2005), where the Canadian CSA S304 (2014) standard is more conservative than the American MSJC (2013).

Improving the stress-strain response of the unreinforced BE has a direct impact on the shear wall with BEs performance. Understanding and improving the interaction between the grouted core and the outer shell is the cornerstone of enhancing the unreinforced masonry performance. Several studies explored this interaction in masonry prisms fabricated by the different shapes and sizes of blocks (e.g. Hamid et al. 1978; Priestley and Chai Yuk Hon 1984; Sarhat 2016; Sturgeon et al. 1980). These studies are discussed in detail in the next chapter to highlight the main factors affecting the grout-shell interaction. Nonetheless, little is known about this interaction in the prisms built with C-shaped units. Moreover, the validity of the findings established in prisms with other types of blocks on the prisms constructed with C-shaped blocks is yet to be investigated.

1.2 Objectives

This thesis is part of an ongoing research project at Concordia University examining the response of reinforced masonry shear walls with boundary elements. Understanding the stress-strain relationship of the masonry boundary element prisms constructed with C-shaped blocks is vital for improving the response of the boundary elements and, in turn, the reinforced masonry shear walls.

The main objective of this study is to investigate the unreinforced masonry boundary element prisms constructed with stack-bonded C-shaped blocks (C-MSBEP). The goal is to identify the main factors affecting the stress-strain response of C-MSBEP and the interaction between its

shell and the grout core aiming to improve C-MSBEP's predictability. Moreover, the study considers assessing the suitability of the current requirements of the Canadian and the US standards for predicting the compressive strength of unreinforced masonry boundary element prisms constructed with stack-bonded C-shaped blocks (C-MSBEP).

1.3 Scope of Work

To achieve these objectives, five types of specimens were constructed and tested. The first type is grouted running-bonded stretcher blocks prisms. The second is grouted stack-bonded stretcher block prisms. These two types of specimens will be fully-grouted by normal strength grout. The third type is boundary element prisms constructed with C-shaped blocks. The C-MSBEPs will be fully-grouted by normal and high strength grouts. These three types will have two height-to-thickness ratios (*h/t*), namely, 2 and 5. The fourth type is C-MSBE shells. The shells are primarily un-grouted masonry prisms of the same (*h/t*) as the grouted C-MSBEPs. Finally, the fifth type is grout prisms that replicates the grouted cores of the C-MSBEPs. These grout prisms will be cast from the same normal and high strength grouts used for the C-MSBEPs and will have the same dimensions as the cores of these prisms. Figure 3.1 and 4.1 show schematic illustrations of the five tested groups.

1.4 Thesis Layout

Including the present chapter, this thesis consists of 5 chapters, a list of figures, a list of tables, appendix, and references. These chapters present all the details of the experimental and analytical investigation of C-MSBEPs as follows:

- *Chapter 1 – Introduction:* This chapter introduces the background and the motivation for this work followed by the objectives and the scope of work. The chapter ends with the layout of this thesis.
- *Chapter 2 – Literature Review:* This chapter reviews and compares the requirements of the Canadian and US standards for prism construction and testing. The comparison also covers the sampling and testing of the constituents of the prisms in both standards. The unit strength method values provided by both standards are also compared. Then, a review of the factors that affect the grout core contribution to the prism strength is presented.

- *Chapter 3 – Compressive Stress-Strain Response of Masonry Boundary Element Prisms:* This chapter presents the experimental work, observations, results, analysis, and discussion of phase I. The focus of this phase is the general compressive stress-strain response of the C-MSBEPs. The response is compared to that of the stretcher block prisms of different configurations. The effect of *h/t* on the peak stress of both types of prisms was investigated. The compressive strength values were compared to the unit strength method values of CSA S304 (2014) and MSJC (2013). Based on the results of the experimental work in this phase, 2 stress-strain models were proposed for C-MSBEPs and the stretcher block prims.
- *Chapter 4 – The Interaction between the Masonry Shell and the Grout Core:* This chapter presents the experimental work, observations, results, analysis, and discussion of phase II. The focus of this phase is to investigate the different factors that affect the grout contribution to the strength of C-MSBEPs. The effect of the grout shape and size, *h/t*, and treatment, air and wet, on the load capacity and the stress-strain response are examined. The results of the experimental work were compared to four predicative equations from the literature to examine the grout contribution factors suggested by other studies. A contribution factor is proposed for the grout that considers the shrinkage effect, the shape effect, the size effect, the aspect ratio, the water absorption, and the incompatibility of grout core and the masonry shell.
- *Chapter 5 – Summary, Conclusions and Future Work:* This chapter summarizes the work presented in the thesis and highlights the main conclusions. It also provides some recommendations for the future work to enhance the understanding of the stress-strain response of the C-MSBEPs.

Chapter 2

LITERATURE REVIEW

2.1 Canadian (CSA) and US (ASTM) Standards Requirements for Testing Masonry Prisms and their Individual Components

To properly address the similarities and discrepancies between the two masonry standards, the requirements of both standards are investigated. The investigation covers the methods of masonry prism testing as well as the sampling and testing of masonry block units, mortar, and grout. The comparison also covers the masonry prism construction techniques in both standards. A summary of the discussed comparison can be found in Table 2.1. The numbers between straight parentheses in the table mentions the provision(s) in the relevant standard that state each of these requirements.

2.1.1 Sampling and testing of prism components

Block Unit

Among the resemblances is the testing of the masonry block for compressive strength. CSA A165 (2014) indicates that the sampling and testing of concrete block masonry units for dimensions and physical properties shall be according to ASTM C140 (2015) "Standard Test Methods for Sampling and Testing Concrete Masonry Units and Related Units". CSA A165 (2014) "CSA Standards on concrete masonry units" specifies the minimum number of specimens to be tested as five specimens that should be increased to ten if the coefficient of variation (C.V.) is found to be more than 15%. However, ASTM C140 (2015) specifies the minimum number of specimens as six specimens. It should be noted that in the case of units that have unusual size or shape, such as open end and pilaster units, ASTM C140 (2015) indicates that coupons should be cut from the unit and tested. The coupon's height to thickness ratio should be two and the length to thickness ratio should be four.

Mortar

Another point of point of similarity between the two standards is the sampling and testing of the mortar. CSA A179 (2014) and ASTM C109 (2013) "Standard Test Method for Compressive

Strength of Hydraulic Cement Mortars (Using 2-in. or [50-mm] Cube Specimens)" both indicate sampling mortar as 50-mm cubes. The cubes after curing are tested for compressive strength. CSA A179 (2014) requires testing not fewer than six cubes while ASTM C109 (2013) allows testing 2 or 3 cubes for each period of test or test age.

Table 2.1 Comparison between the requirements of CSA and ASTM for sampling and testing of masonry prisms and their constituents

Comparison Aspect	CSA	ASTM
Block Unit Sampling and Testing		
Minimum Number of Specimens Required	5 (10 if C.O.V > 15%) *[10.2 (CSA A165-14)]*	6 *[5.2 (ASTM C140-15)]*
Mortar Sampling and Testing		
Specimen Shape and Dimensions	50 mm Cubes *[8.4.3.3 (CSA A179-14)]*	50 mm Cubes *[1.1 (ASTM C109-13)]*
Minimum Number of Specimens Required	6 *[8.4.1 (CSA A179-14)]*	2 *[8.1 (ASTM C109-13)]*
Grout Sampling and Testing		
Minimum Number of Specimens	3 *[8.4.1 (CSA A179-14)]*	3 *[5.2 (ASTM C1019-14)]*
Specimen Shape and Dimensions	200*100 Cylinders *[8.4.3.3 (CSA A179-14)]*	Prisms of square base of min. side length = 76 mm & $h/t = 2$ *[5.1 & 4.4 (ASTM C1019-14)]*
Prism Fabrication and Testing		
Minimum Number of Specimens Required	5 (10 if C.O.V > 15%) *[D.3.2.3 (CSA S304-14)]*	3 *[5.2 & 3.1.1 (ASTM C1314-14)]*
Minimum Number of Courses Required	3 *[D.3.2.2 (CSA S304-14)]*	2 *[5.7 (ASTM C1314-14)]*
Mortar Bedding Type Used	Face-Shell Bedding *[D.3.3.1{c} (CSA S304-14)]*	Full-Bedding *[5.6 (ASTM C1314-14)]*
Pattern Used	Replicates the wall pattern *[D.3.2.1 & D.6.3 (CSA S304-14)]*	Stack *[5.4 (ASTM C1314-14)]*
Standard Prism Height-to-Thickness Ratio	5 *[D.3.2.3 (CSA S304-14)]*	2 *[11.2 (ASTM C1314-14)]*

Grout

Although CSA A179 (2014) and ASTM C1019 (2014) both require testing a minimum of 3 specimens of grout to determine its compressive strength, they differ in the method of sampling

the grout. CSA A179 (2014) indicates that grout should be sampled as cylinders of 200 mm (8") diameter and 100 mm (4") length similar to these used for concrete. ASTM C1019 (2014), on the other hand, requires that the grout is sampled in molds constructed from the same blocks or bricks used for the actual construction of the masonry work. The mold should be proportioned to create a grout specimen of a square cross-section of a minimum side dimension of 76 mm (3") and a height-to-thickness ratio (h/t) equals to 2 (Figure 2.1).

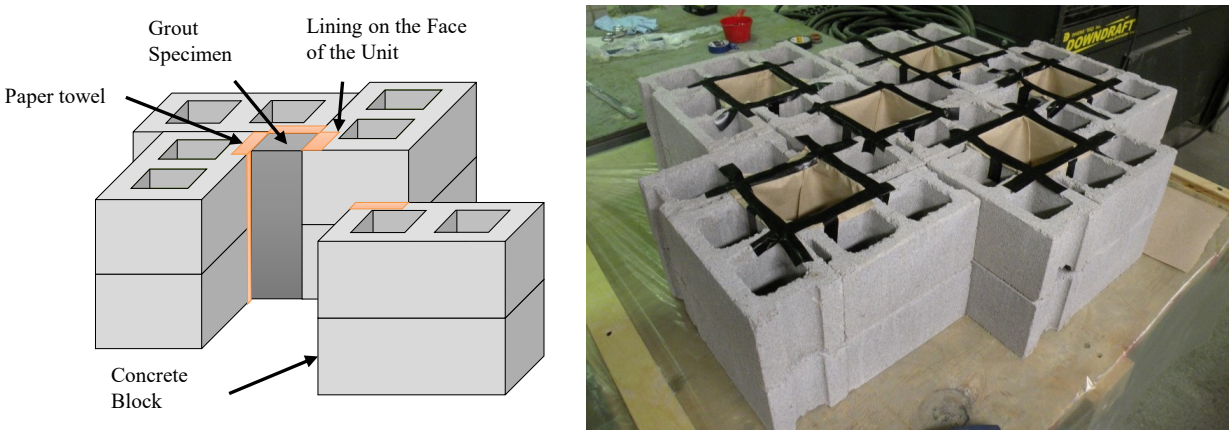

Figure 2-1 Grout prism specimens molding according to ASTM C1019 (2014)

2.1.2 Construction and testing of prisms

It can be observed that the testing of the individual constituents is similar in the two standards. However, the requirements of the two standards differ in the construction and testing of the masonry prism. CSA S304 (2014) specifies that the minimum number of prisms to be tested is five and should be increased to 10 if the coefficient of variation exceeds 15%. On the other hand, the ASTM C1314 (2014) allows testing only three prisms. Nonetheless, the main differences between the two standards that may affect the resulting specified compressive strength of masonry, f'_m, are the mortar bedding type, the pattern used, and the standard prism *h/t* along with the corresponding correction factors (Figure 2.2). The following discussion examines each of these factors in more details.

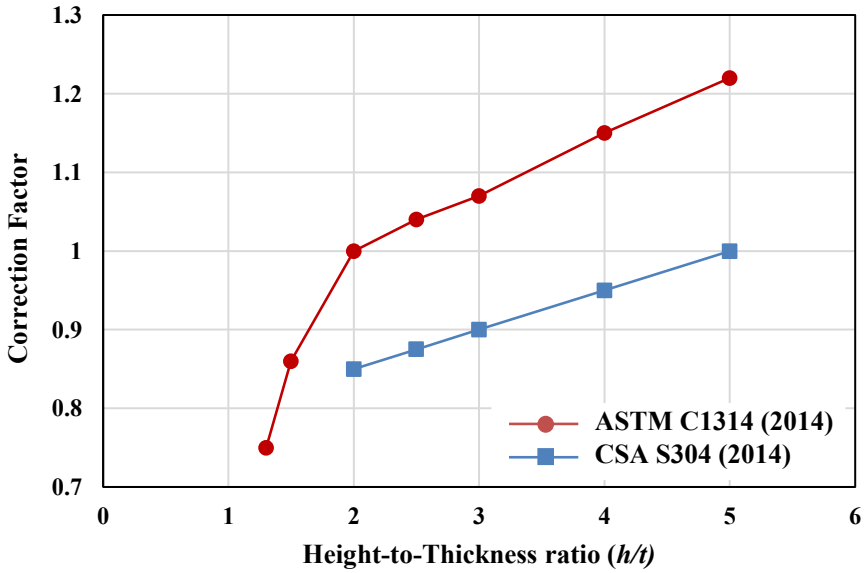

Figure 2-2 Comparison of the correction factors for axial compressive strength of masonry prisms provided by ASTM C1314 (2014) and CSA S304 (2014) based on the prism height-to-thickness ratio

Bond pattern

CSA S304 (2014) indicates that the pattern used for the prism should copy the exact pattern used in the actual masonry construction. ASTM C1314 (2014), on the other hand, requires that the pattern used for prisms is the stack pattern for any pattern used in the actual construction. It should be mentioned that CSA S304 (2014) allows using the stack pattern for running bonded wall if there is experimental evidence that shows there is no much difference between the two patterns or when there is an established relationship between the two patterns.

Bond pattern's effect on the compressive strength of masonry prisms was investigated by many researchers. Maurenbrecher (1980) mentioned that running bonded prisms result in slightly lower strength than stack bonded ones. Later, Scrivener and Baker (1988) found that the strength of running-bonded prisms of grouted concrete masonry can range from 75% to 99% of the strength of the equivalent stack-bonded prisms. Drysdale and Hamid (2005) mentioned that the strength of running bonded grouted concrete prisms are expected to be about 4 – 13% less than the strength of the stack bonded concrete prisms. Although, there is no consensus on the percentage of strength reduction for using running bond instead of stack bond, it is clear that in all cases the running bonded prisms are expected to result in lower strength compared to the stack bonded prisms.

It is worth mentioning that Ganesan and Ramamurthy (1992) showed that stack-bonded prisms do not represent the running-bonded construction as they tend to overestimate the capacity of the walls. As this finding contradicts the requirements of ASTM C1314 (2014) of using stack-bonded prism even for running-bonded construction, Ganesan and Ramamurthy (1992) recommended that these requirements should be reconsidered.

Mortar bedding

Type of mortar bedding is another point of discrepancy between the two standards. CSA S304 (2014) indicates the use of the face-shell bedding in the fabrication of the prisms built using hollow units. ASTM C1314 (2014) specify that the fabrication of the prisms should utilize full mortar beds (mortar on the face shells and all the webs).

Various studies investigated the effect of face-shell bedding and full-bedding on ungrouted stretcher block prisms. Hamid and Chukwunenye (1986) found that there is a significant difference in the mechanical behaviour between prisms fabricated by the each of the two bedding types. Hamid and Chukwunenye (1986) showed that the stress distribution across full-bedded three-course high prisms is uniform compared to face-shell three-course high bedded prisms of high non-uniform stress distribution. The results of this study were assured by Ganesan and Ramamurthy (1992) for five courses high prisms. Chahine and Drysdale (1989) showed that full-bedded prisms exhibit higher strength than face-shell prisms. These studies were focused on ungrouted full-scaled concrete units. The investigations of the effect of mortar bedding type on the compressive strength of grouted masonry prisms are few. This is believed to be a result of the established fact that the effect of other mortar properties such as the strength and the joint thickness on the grouted prism strength is not significant (Drysdale and Hamid 1979; Khalaf 1996).

Height-to-thickness ratio

The minimum number of courses in the prism construction allowed by CSA S304 (2014) is three courses for grouted masonry, but the *h/t* ratio should not be less than 2. The minimum number of courses allowed by ASTM C1314 (2014) is 2 with minimum *h/t* ratio of 1.3. The standard *h/t* in CSA S304 (2014) is 5.0 while it is 2.0 in ASTM C1314 (2014). The standard *h/t* here refers to the *h/t* that can be used in constructing the prisms and results in a compressive strength that do not need to be multiplied by any correction factors. In other words, if the prism

is built with the standard *h/t*, the compressive strength yielded is multiplied by 1. The correction factors applied to the resulting compressive strength in CSA S304 (2014) range from 0.85 for *h/t* of 2 to 1 for *h/t* of 5 or higher. However, the ASTM C1314 (2014) correction factors range from 0.75 for *h/t* of 1.3 to 1.22 for *h/t* of 5. All the correction factors mentioned in the two design standards and the corresponding *h/t* ratios are showed and compared in Figure 2.2.

Several studies have been carried out to investigate the effect of *h/t* on the compressive strength of masonry prisms. Drysdale and Hamid (1979) indicated that the 2-course high prism should not be used as a standard test specimen as it does not properly represent the strength as it shows a different failure mode. Boult (1979) found that the lower the *h/t* of the prisms, the higher the resulting compressive strength. This was also observed by Maurenbrecher (1980). Hamid and Chukwunenye (1986) stated that there is a certain mode of failure associated with the *h/t*. For *h/t* of 2, the mode of failure tends to be a shear failure while for *h/t* greater than two the typical tensile splitting is observed. Fahmy and Ghoneim (1995) performed a finite element study that showed that the strength decreases as the *h/t* of the prism increases but, it stops increasing at *h/t* of 5. The difference in resulting strength for different *h/t* is attributed to the effect of the loading machine end platens. They tend to constrain the prisms laterally at the upper and lower ends increasing its axial load capacity. As the *h/t* increases, this effect becomes less influential on the compressive strength. Hamid and Chukwunenye (1986) recommended that the practice of testing prisms of *h/t* of 2.0 should be discontinued and a prism of a number of mortar joints equal to or greater than 2.0 should be specified. Hamid and Chukwunenye (1986) recommended using a prism of *h/t* of 2.0 but with two-bed joints using a half block at top and bottom as a standard prism. Hassanli et al. (2015) investigated the effect of not only *h/t* on the compressive strength but also the length to thickness ratio (*l/t*). Hassanli et al. (2015) also suggested the alternation of the ASTM C1314 (2014) *h/t* of the standard prism to be 5.0 as the prism of *h/t* of 2.0 results in strength overestimation that ranges from 20-25%. In addition, Hassanli et al. (2015) provided a revision to the formulas of masonry modulus of elasticity, E_m, found in the ASTM standards and provided adjusted values for the correction factors of different *h/t* and provided new correction factors to account for *l/t*.

2.1.3 Masonry Prisms of Boundary Elements fabricated with C-shaped Blocks

Boundary elements (BE) attached to the edges of masonry shear walls have proven their enhancing influence on the behaviour of the shear walls. Boundary Elements fabricated with C-shaped units have the advantages of providing more space for steel reinforcements installation with hoops and easier installation of these reinforcements. As discussed earlier, the fabrication of the stretcher blocks prisms according to CSA S304 (2014) and ASTM C1314 (2014) leads to two different prism configurations. However, fabricating a C-shaped BE prism according to the two standards leads to the same prism. C-shaped BE prisms are built with mortar on all sides of the C-shaped units. So, there is no distinction between full-bedding or face-shell bedding in this type of prism. In addition, the C-shaped prisms are constructed in stack pattern. This facilitates the placement of the vertical reinforcement cage in the boundary elements. The C-shaped units are stacked on each other with one continuous vertical mortar joints separating the two C-shaped units in each course. The only difference between C-shaped BE prisms according to the two standards is the standard aspect ratio. So, the standard prism will be a 10-cousre prism if fabricated according to CSA S304 (2014) and 4-course prism if fabricated according to ASTM C1314 (2014). It is worth mentioning that testing 10-course high BE prisms for strength evaluation is practically challenging.

On the other hand, the previous discussion illustrates that a considerable number of researchers investigated the different factors that affect the prism strength and behaviour fabricated with different shapes of blocks. However, less is known about the effect of these factors on the strength and the behaviour of prisms fabricated with C-shaped units.

2.2 Canadian (CSA S304 2014) and US (MSJC 2013) standards Tabulated Compressive Strength values (Unit strength method)

The differences between the Canadian and the US standards are not only in the construction and testing of masonry prisms. They extend also to the tabulated values provided by the two standards for the unit strength method. The Canadian standard provide the specified unit strength values in Table 4 in CSA S304 (2014). For each combination of unit strength and mortar type, two values are given. One value is used for the ungrouted hollow units and the other for solid units or grouted hollow units. On the other hand, the US standard provide the unit strength values for concrete units in Table 2 in MSJC (2013). For each combination of unit strength and mortar

type, one value is given. This value can be used for ungrouted and grouted masonry prisms as long as the bed joints thickness is less than 15.9 mm. Moreover, for grouted prisms, if the masonry compressive strength, f'_m, is equal to or exceeds 13.79 MPa, the grout used should be equal to or exceeds the masonry compressive strength. The two standards provide different compressive strength values for the same combination of unit strength and mortar type (Figure 2.3). If concrete units of strength 30 MPa or more are used, CSA S304 (2014) specifies that the maximum grouted masonry f'_m to be considered is 13.5 MPa for type S mortar. However, the standard recommends the use of the prism testing method in this case as f'_m could exceed this value. On the other hand, MSJC (2013) does not specify f'_m values for units of strength higher than 33.10 MPa for type S mortar for which the predicted grouted masonry f'_m is 20.7 MPa. For the unit strength values that fall between the specified unit strength values, the two standards allow the use of interpolation to get the corresponding specified masonry compressive strength value.

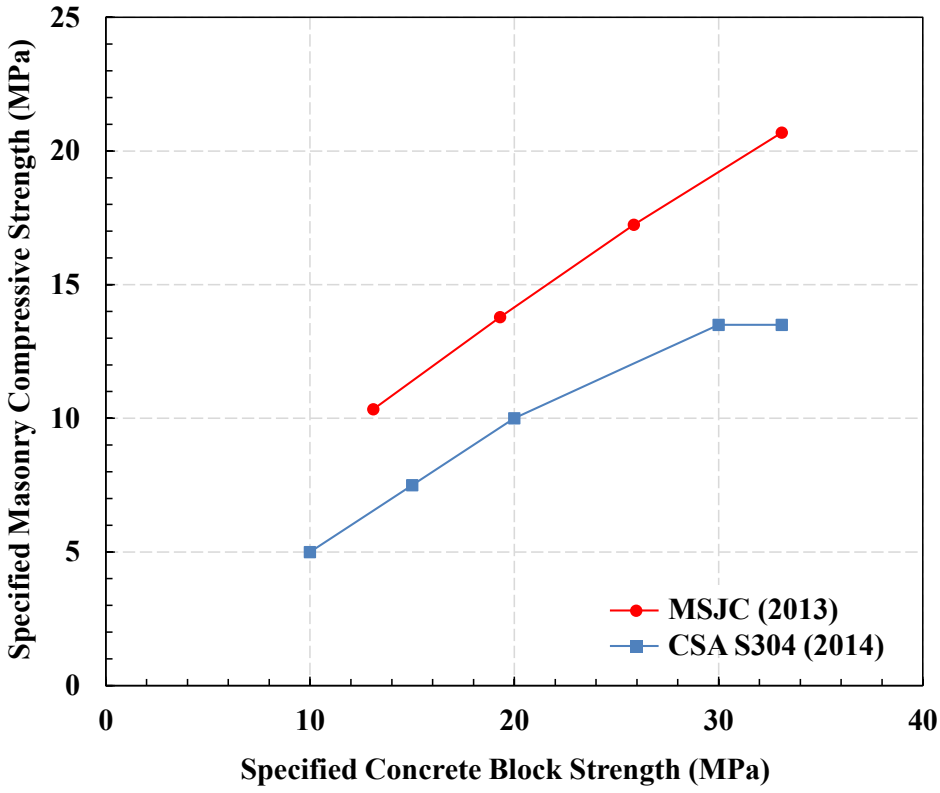

Figure 2-3 Comparison between the tabulated compressive strength values of MSJC (2013) and CSA S304 (2014) for concrete block grouted masonry prisms

2.3 Background on the effect of grout compressive strength on the prism strength

Several studies found that increasing the grout strength, increases the grouted prism strength (Hamid et al. 1978; Martins et al. 2018; Romagna and Roman 2002). Superposition of grout and masonry shell strengths has been tried as a simple method of predicating the strength of fully-grouted masonry prisms. One may assume that the prism ultimate strength can be easily obtained by multiplying the grout core stress by its area and adding to it the shell compressive stress multiplied by its area. Nonetheless, the invalidity of the strengths' superposition principle has long been argued. The simple superposition of strengths based on areas significantly overestimates the prism strength (Hamid et al. 1978; Priestley and Chai Yuk Hon 1984; Sturgeon et al. 1980). Therefore, a reduction factor is usually introduced to the grout and shell strength when predicting the masonry prism strength as shown in Eq. 2.1. However, the grout strength reduction factor varies dramatically between different researchers ($\alpha = 0.22 \sim 0.94$) (Hamid et al. 1978; Priestley and Chai Yuk Hon 1984; Sarhat 2016; Sturgeon et al. 1980). The variation in the reduction factor was a result of the different hypothesis used by researchers as will be discussed later in this study (see *comparing C-MSBEP strength with available prediction equations* section). Although many factors resulting in this grout-prism strength relationship were discussed in different studies, there is no consensus on the main factors. The various factors that result in minimizing the grout contribution to the prism strength are summarized below into two main categories.

$$f_m A_g = \alpha f_g A_c + \beta f_{sh} A_n \tag{2.1}$$

f_m : Grouted prism peak stress,
A_g : Grouted prism gross area,
f_g : Grout peak stress,
A_c : Prism core area,
f_{sh} : Shell peak stress,
A_n : Prism net area (A_g - A_c),
α, β : Reduction factors.

2.3.1 Incompatibility of longitudinal and transversal strains of masonry shell and grout-core

Incompatibility of strains in the longitudinal direction

The assumption that the peak stress resisted by both the masonry shell and the grout core occurs at the same strain is not valid (Hamid and Drysdale 1979). The peak stress of the masonry shell typically occurs at a longitudinal strain smaller than that of the grout core (Priestley and Chai Yuk Hon 1984). According to Priestley and Chai Yuk Hon (1984), the prism strength is associated with the shell strength, whereas the prism reaches its peak stress at the onset the shell reaches its peak stress. Therefore, a factor less than 1.0 must be multiplied by the grout peak stress to account for this incompatibility in the longitudinal strains.

Incompatibility in the Transversal direction

As pointed by Hamid et al. (1978), Hamid and Drysdale (1979), and Klinger (1986) the grout core's Poisson's ratio is usually larger than that of the masonry shell. Therefore, the grout core exerts lateral stresses on the surrounding shell which result in the shell's premature failure. According to this hypothesis, a reduction factor, β, is introduced to minimize the shell contribution to the prism compressive strength (Eq. 2.1).

It is worth mentioning that Khalaf et al. (1994) observed that a match between the concrete block and the grout Poisson's ratios can be achieved when the cube compressive strength of the grout is 45% - 50% more than that of the cube compressive strength of the concrete block material. Although this compatibility in transversal strains results in the highest prism compressive strength, the resulting strength values were still less than the values predicted by superposition.

2.3.2 The representation of the grout core strength by the tested grout samples

Superposition of strengths of the shell and the grout core is usually applied utilizing the strength of the tested grout cylinders or grout prisms. The 100 x 200 mm cylinders cast in non-absorbent molds are considered representative of the grout cores according to the CSA A179 (2014). On the other hand, ASTM C1019 (2014) requires the grout samples to be square cross-sectional prisms, of minimum side dimension 76 mm, cast between blocks from those used in the actual construction to consider the effect of water absorption on the grout compressive strength. Drysdale and Hamid (2005) mentioned that the grout prism molded according to ASTM is about 1.5 times the strength of the grout cylinder sampled according to CSA. The stress-strain response

of the grout samples could vary from that of the actual grout within the prism due to several factors as detailed below.

Water absorption and curing

Both the grout specimens, according to CSA A179 (2014) and ASTM C1019 (2014), are required to be cured in a moist cabinet. However, the blocks used for molding the ASTM specimen absorb a portion of the grout's mixing water. Drysdale and Hamid (2005) indicated that absorbing water from the grout before grout complete hydration lead to a lower water to cement ratio which produce a higher strength grout. On the contrary, Sturgeon et al. (1980) explained that the core strength is best represented by the moist grout cylinders as the water absorbed causes the shell to act as a barrier that prevents the evaporation and contains the mixing water especially in large grout cores. Hence, sufficient amount of water is sustained for the hydration process of cement. By comparing the ASTM molded specimens to grout specimens, of similar dimensions, cut from the center of grouted masonry prism core, Hedstrom and Hogan (1990) found out that the ASTM specimens are good representation of the grout in the core as the difference in the compressive strength was approximately 10%.

Aspect ratio, shape and size effects

Maurenbrecher (1980), Khalaf et al. (1994) and Hassanli et al. (2015) showed that the strength of the masonry prisms decreases with the increase of the *h/t* of the prisms tested. This behaviour was attributed to the confining effect of the end platens on the specimens affecting both the outer shell and the core of the prism tested. The *h/t* for CSA A179 (2014) and ASTM C1019 (2014) grout specimens is 2.0 while the *h/t* of the masonry prism grout core is usually larger. Therefore, the compressive strength of the prism core grout may be lower than that predicted by either the cylinder or the grout prism.

Hassanli et al. (2015) showed how the grout cylinder is characterized by a middle region, away from upper and lower platens, that is unaffected by lateral confining stresses. This implies that by testing grout cylinders, the *h/t* effect on the compressive strength can be avoided. If the same rational utilized by Hassanli et al. (2015) is applied, the grout prism specimen of square cross-section and $h/t = 2$ has the same free region from lateral confining platen stresses. Nonetheless, changing the sample shape from prism to cylinder may affect the stress strain response.

Moreover, Hassanli et al. (2015) found that the strength measured for concrete masonry prism decreases with the increase of the specimen size if the *h/t* is maintained. The results of testing 300 concrete cubes of different sizes of strengths ranging from 13 to 48 MPa showed that the 70 mm cube strength is higher than the 125 mm and the 150 mm cubes strengths (Neville 1956). In addition, the strength of the 150 x 300 mm concrete cylinders was observed to be lower than the strength of 100 x 200 mm cylinders for strengths ranging from 7 to 48 MPa (Malhotra 1976). Similarly, grout strength is also affected by the size of the specimen. The size of the grout in the core of the prism is usually multiple times larger than the cylinder or the grout prism size. Sturgeon et al. (1980) found that the grout core strength was around 0.74 of the cylinder strength.

Initial lateral tension due to restrained shrinkage of grout

A full bond between the shell and the grout core restrains the grout from shrinking. Therefore, lateral tension strains are induced to the grout core before applying the axial compression loading. This reduces the contribution of the grout core to the prism strength.

The effect of incomplete grout compaction

The incomplete and inadequate compaction of the grout contributes to the lower strength of the prism's grout core. To avoid this, a highly fluid grout should be used along with proper compaction. Therefore, a high grout slump of 250 mm was recommended by Drysdale and Hamid (2005) and a 275 mm slump was specified by CSA A179 (2014).

Other factors

Other factors may also affect the interaction between the grouted core and the outer shell in masonry prisms including the block shape and geometry (Drysdale and Hamid 2005; Sturgeon et al. 1980), and the effect of the flared or tapered shape of the face shells and webs of the stretcher concrete units (Drysdale and Hamid 1982). Flared or tapered shape of face shells and webs cause the webs and the face-shells to act as wedges to the grouted core. Consequently, this affects the interaction between the grout and the shell (Drysdale and Hamid 1982).

Chapter 3

COMPRESSIVE STRESS-STRAIN RESPONSE OF MASONRY BOUNDARY ELEMENT PRISMS

3.1 Experimental Work of Phase I

3.1.1 Test Matrix

As illustrated in Figure 3.1 the test matrix of the current study consisted of three groups: (1) fully-grouted running-bonded masonry stretcher block prisms, (2) fully-grouted stack-bonded masonry stretcher block prisms, and (3) fully-grouted masonry boundary elements prisms. The method used to identify each tested specimen is illustrated in Figure 3.2. The mortar used was Type S mortar. All the prisms were constructed by a certified mason, grouted by normal strength grout, and tested under concentric compression loading up to failure.

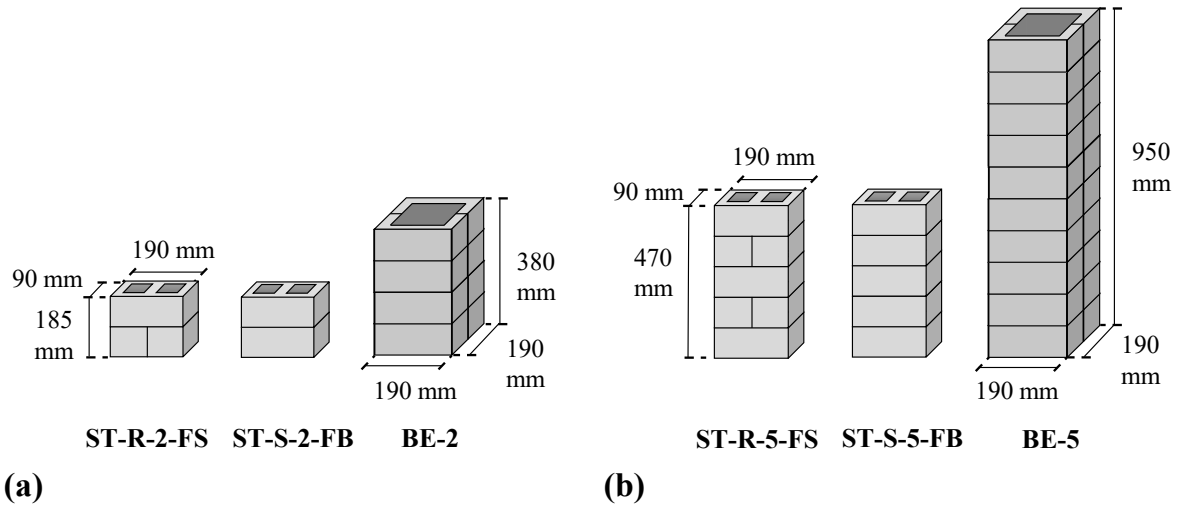

Figure 3-1 Schematic drawing for the test specimens: (a) specimens with height to thickness ratio of two, (a) specimens with height to thickness ratio of five

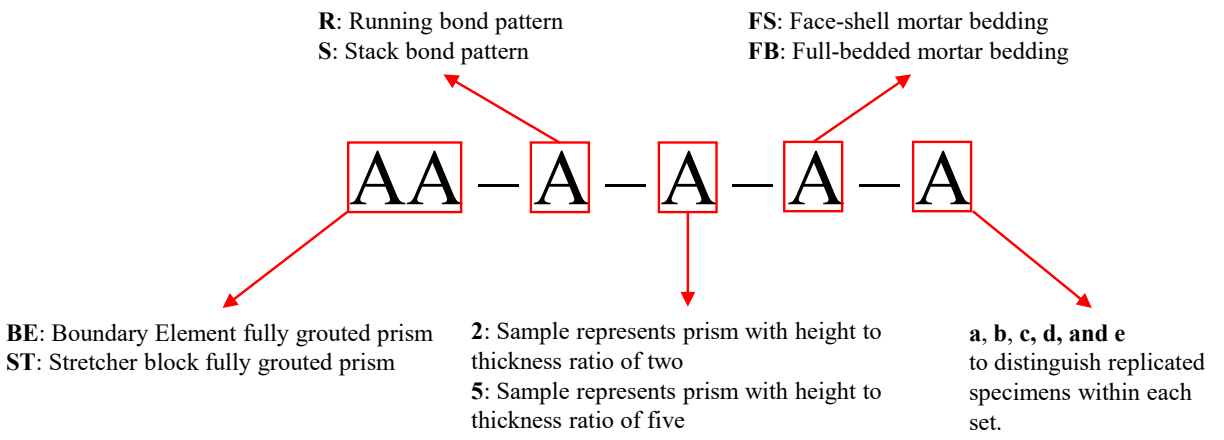

Figure 3-2 Identification criteria for each tested sample

Two sets of grouted masonry stretcher block prisms were constructed in running bond pattern with face-shell mortar bedding according to the requirements of CSA S304 (2014). The two sets ST-R-2-FS and ST-R-5-FS had *h/t* equals to two and five, respectively as shown in Table 3.1. Moreover, two sets of grouted masonry stretcher block prisms were constructed in stack bond pattern with full mortar bedding according to the requirements of ASTM C1314 (2014). The two sets ST-S-2-FB and ST-S-5-FB had *h/t* equals to two and five, respectively (Table 3.1).

Table 3.1 Experimental test matrix for stretcher block prisms

ID	Block Type	Pattern	Height-to-Thickness ratio	Mortar Bedding	Number of specimens	Standard Prism for
ST-R-2-FS	Stretcher	Running	2	Face-Shell	4	
ST-R-5-FS	Stretcher	Running	5	Face-Shell	5	CSA
ST-S-2-FB	Stretcher	Stack	2	Full-Bedded	4	ASTM
ST-S-5-FB	Stretcher	Stack	5	Full-Bedded	5	

In addition to the stretcher block prisms, two sets of masonry boundary elements prisms constructed using C-shaped concrete masonry blocks were constructed and tested. As listed in Table 3.2, the first set, BE-2, had a height to thickness ratio, *h/t*, equals to two (four-courses). The other set, BE-5, had a height to thickness ratio equals to five (ten-courses). It is worth mentioning that although there are no guidelines yet on testing boundary element prisms, *h/t* of five and two were chosen to follow the recommendations of CSA S304 (2014) and ASTM C1314 (2014), respectively, in testing masonry prisms for compressive strength.

Table 3.2 Experimental test matrix for masonry boundary element prisms

ID	Block Type	Height-to-Thickness ratio	Number of specimens
BE-2	C-shaped	2	2
BE-5	C-shaped	5	3

3.1.2 Material Properties

Blocks

The blocks used in this experimental work are half-scaled units due to the limited capacity of the available testing frame (Figure 3.3). The C-shaped and the stretcher blocks were tested for the compressive strength according to requirements of CSA A165 (2014) and ASTM C140 (2015). According to ASTM C140 (2015), the C-shaped units fall in the category of unusual shape units while the stretcher blocks fall in the category of ordinary shaped units. Consequently, they were tested under dissimilar procedures. The stretcher blocks were tested in full shape while coupons were cut from the C-shaped blocks and tested for compressive strength in the same direction of the actual loading as shown in Figure 3.4 (a). Each coupon has a height to thickness ratio of two to one and a length to thickness ratio of four to one following the requirements of ASTM C140 (2015). In total, five stretcher blocks were tested, and five coupon specimens were cut of dimensions 100 mm (length) x 50 mm (height) x 25 mm (thickness) and tested. All the specimens were hard-capped by high-strength gypsum before testing.

As shown in Table 3.3, the average compressive strength of the C-shaped block coupons was 22 MPa with computed coefficient of variation of 13.8%. The average compressive strength of the stretcher blocks was 14.5 MPa with coefficient of variation of 5.64%. The difference between the two types of blocks in compressive load capacity is partially attributed to the dissimilarity of testing procedures.

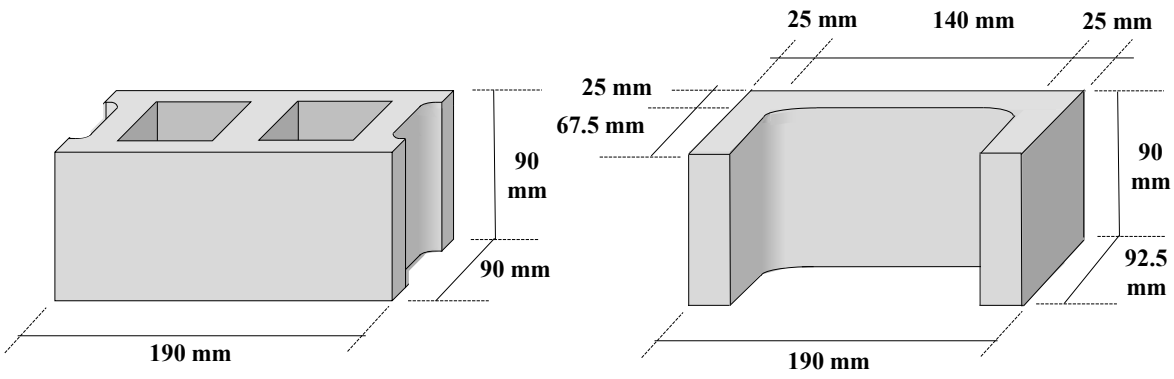

Figure 3-3 Dimensions of the half-scale stretcher blocks (left) and the half-scale C-shaped blocks (right)

(a) **(b)**

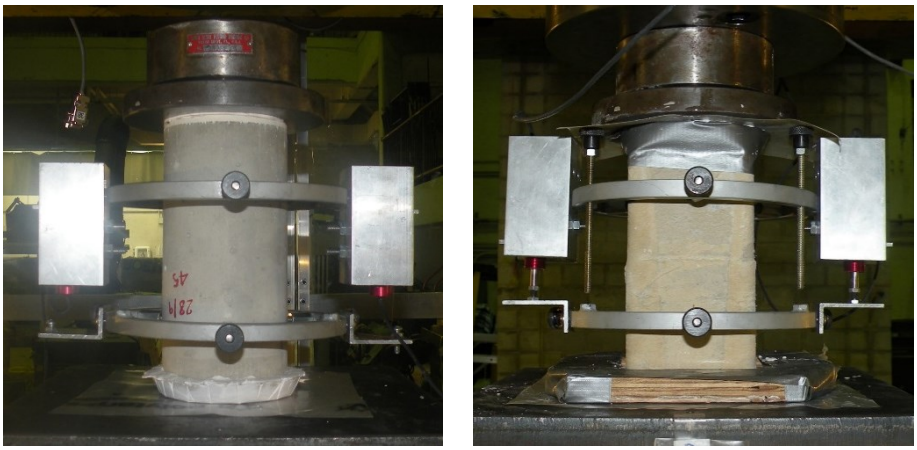

(c) **(d)**

Figure 3-4 Compression test for: (a) concrete block coupon, (b) mortar cube, (c) grout cylinder, (d) grout prism

Table 3.3 Materials properties

Item	Batch #	Ultimate Load (kN)	Strength (MPa)	C.V.	Number of Specimens
Stretcher Block	-	123.1	14.5	5.64%	5
C-shaped Block	-	55.0	22.0	13.80%	5
Mortar (Cubes)	-	32.3	12.9	7.94%	6
Grout (Cylinders)	*Batch 1	157.0	20.0	6.96%	3
	**Batch 2	117.0	14.9	8.70%	3
Grout (Prisms)	-	256.0	31.6	1.39%	3

*Batch 1 used for fully-grouted stretcher block prisms.
**Batch 2 used for fully-grouted boundary element prisms.

Mortar

Prebagged type S mortar was used for joining the stretcher blocks in the stretcher block prisms and the C-shaped block units in the grouted C-MSBEPs. The mortar joints thickness was approximately 5 mm each. The compressive strength of the mortar was evaluated according to CSA A179 (2014). Six 50 mm mortar cubes were tested for each mortar batch as shown in Figure 3.4 (b). No capping was needed for the mortar cubes according to the requirements of CSA A179 (2014) and ASTM C109 (2013). The average compressive strength was 12.9 MPa with coefficient of variation equals to 7.94% (Table 3.3).

Grout

Three cylinders were sampled from each grout batch. The cylinders had 100 mm diameter (4") and 200 mm height (8"). The grout cylinders were tested for compressive strength according to CSA A179 (2014) as illustrated in Figure 3.4 (c). All the cylinders were cured in water before testing. They were capped by high-strength gypsum as specified by ASTM C617 (2014) "Standard Practice for Capping Cylindrical Concrete Specimens". Due to the large number of samples two grout batches have been used. Their average compressive strengths were 20.0, and 14.9 MPa with 6.96, and 8.70% coefficients of variation for the first and second batches, respectively (Table 3.3). Three grout prims were molded between the half-scaled stretcher blocks from each grout batch (Figure 2.1). The grout prisms had 90 mm square cross section and 180 mm height. The molded grout specimens were tested according to ASTM C1019 (2014) as illustrated in Figure 3.4 (d). The average compressive strength of the normal strength grout molded was 31.6 MPa with 1.39% coefficient of variation. High slump grout was used to avoid

gaps or voids in the grouted core. The prisms were filled by grout in three layers with thorough compaction for each layer.

The stress-strain responses for the normal strength grout cylinders and prisms are shown in Figure 3.5. The change in displacement was measured by linear variable differential transformers (LVDTs). Two LVDTs were positioned diametrically opposite to one another for the cylinders and on two opposite sides for the grout prisms. The gauge length was half the height for both the cylinder (100 mm) and the prism (90 mm). The gauge lines were parallel to the axis of grout specimens and centered about its mid-height following the requirements of ASTM C469 (2014) "Standard Test Method for Static Modulus of Elasticity and Poisson's Ratio of Concrete in Compression". High-strength gypsum was used to cap the grout cylinders and the grout prisms before testing. The peak stresses for the grout cylinders and grout prisms occurred at a strain of 0.0017. The initial stiffness for the average compressive strength of the grout cylinders and the prims were 13.16 GPa and 23.03 GPa respectively.

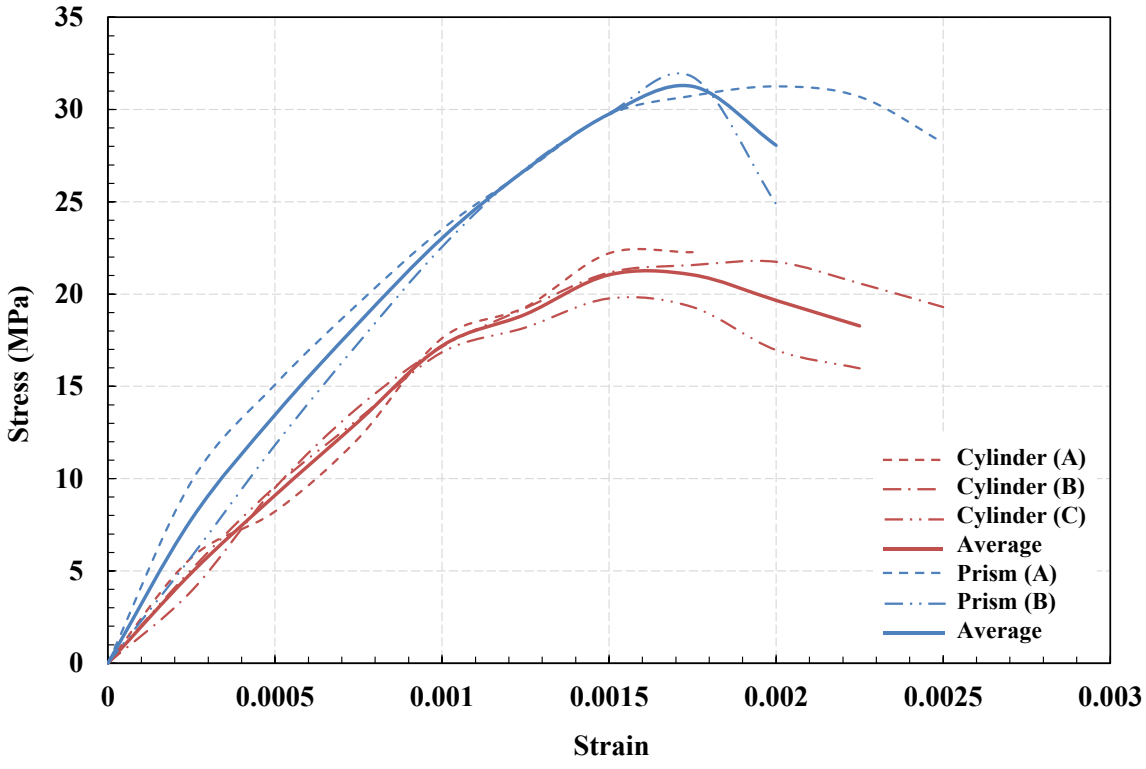

Figure 3-5 Stress-strain response of: (a) grout cylinders, (b) grout prisms

3.1.3 Test Setup, Instrumentation, and Loading protocol

All specimens were tested in servo-controlled 2000 kN reaction frame under quasi-static concentric compression loading up to failure. High-strength gypsum was used between the upper and lower steel plates and the sample to ensure sample leveling and to prevent any voids between the specimen and the loading plates. The plates' dimensions and material followed the requirements of CSA S304 (2014). The verticality of the specimens was checked by two laser aligning devices positioned in two perpendicular directions. A spherical-head was situated between the top of the specimen and the loading cylinder. The spherical-head was checked before each test that it is free to tilt in any direction and that it is centered with the upper plate and the sample. Four LVDTs were used to measure the displacement across the full height of all the specimens. The LVDTs were positioned so that there is one LVDT centered on each side of the tested prism. The full test setup can be seen in Figure 3.6.

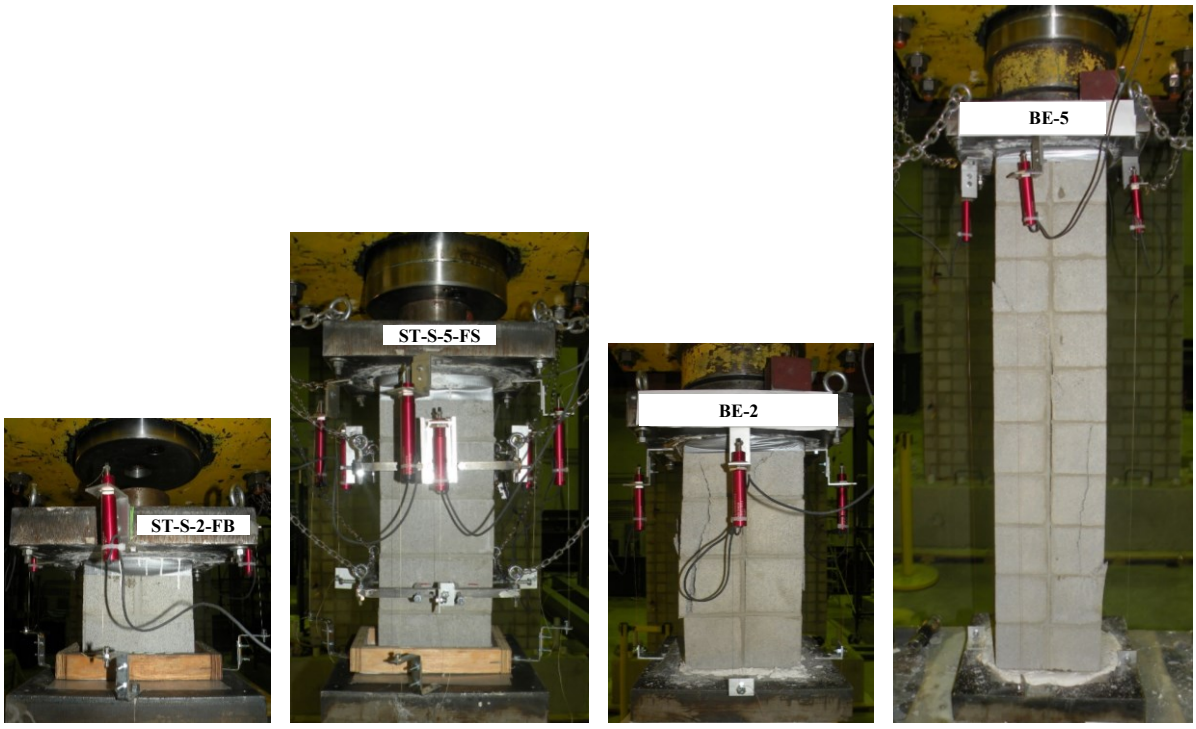

Figure 3-6 Test setup and instrumentation for: (a) stretcher block prisms having height to thickness ratio= 2.0, (b) stretcher block prisms having height to thickness ratio= 5.0, (c) boundary element prisms having height to thickness ratio= 2.0, (b) boundary element prisms having height to thickness ratio = 5.0

According to CSA S304 (2014), any rate of loading can be used to load the prism up to one-half of the capacity. Then, the rate should be adjusted so that the remaining load is applied in a uniform manner till the failure of the prism. However, the application of the remaining load should take a minimum of 1 minutes and a maximum of 2 minutes. A rate of 0.005 mm/sec was utilized in the current study up to a 0.002 axial strain. After that, a slower rate of 0.001 mm/sec was applied to capture the post-peak response. It is worth noting that following the above loading rate fulfilled the CSA S304 (2014) limits for most of the specimens. Nonetheless, it was decided to use the same loading protocol for all specimens to rule out the effect of changing the loading rate on the resulting stress-strain relationship.

3.2 Results and Observations

3.2.1 Fully-grouted running-bonded stretcher block prisms

The observed failure patterns at the end of the tests for the face-shell running-bonded masonry prisms of h/t = 2.0 and 5.0 can be found in Figures 3.7 and 3.8, respectively. For the prisms of h/t = 2.0 (ST-R-2-FS) a shear mode conical shaped failure pattern was dominant. It was more obvious in the sides of the prisms. On the other hand, a splitting failure was dominant for the prisms of h/t = 5.0 (ST-R-5-FS).

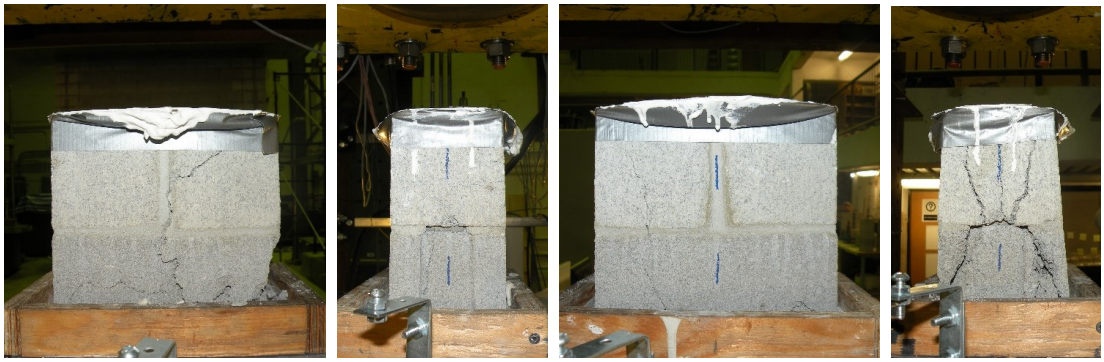

(a) **(b)** **(c)** **(d)**

Figure 3-7 Observed failure patterns for the fully-grouted running-bonded stretcher block prism of h/t = 2.0 (a) front, (b) right, (c) back, and (d) left

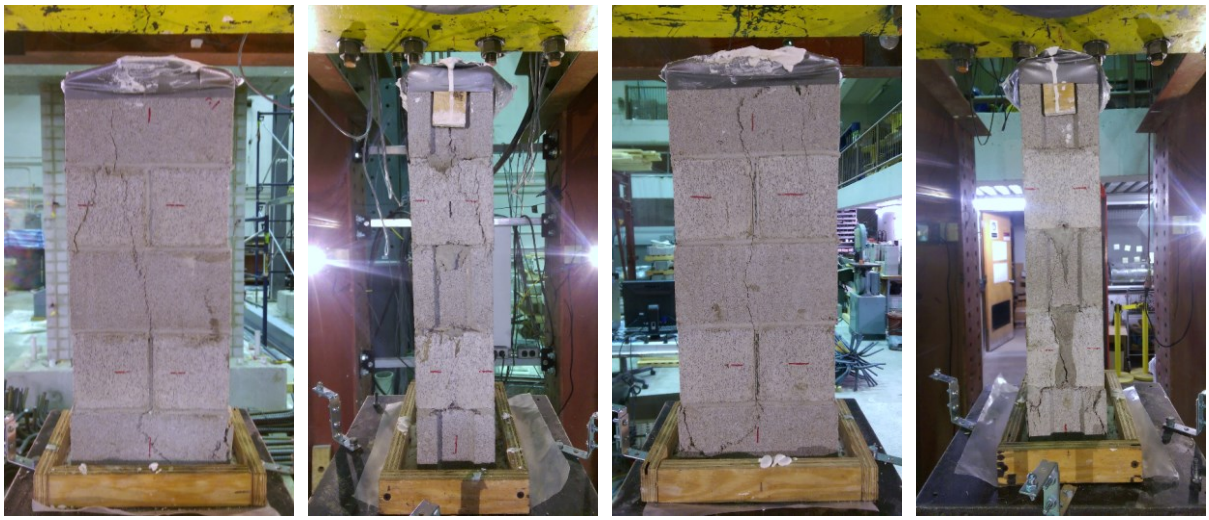

(a) **(b)** **(c)** **(d)**

Figure 3-8 Observed failure patterns for the fully-grouted running-bonded stretcher block prism of *h/t* = 5.0 (a) front, (b) right, (c) back, and (d) left

The stress-strain responses are illustrated in Figure 3.9. The average response was calculated by averaging the stresses at each strain level for all the specimens in each category. It is worth mentioning that these stresses are the average stresses observed against the strains measured by the four LVDTs on the four sides of each specimen at each strain level. The stresses were calculated based on the gross area of the specimen (i.e. 190 mm x 90 mm = 17100 mm^2). The results of testing the running-bonded masonry prisms are summarized in Table 3.4.

The average peak stress of the prisms of *h/t* of two (ST-R-2-FS) was 15.74 MPa having C.V. = 3.28%. This stress was achieved at a peak strain of 0.0034 (C.V. = 12.18%). The average initial stiffness of ST-R-2-FS was 7.68 GPa (C.V. = 16.96%). The average peak stress of the prisms of *h/t* of five (ST-R-5-FS) was 11.15 MPa (C.V. = 6.24%). This result is 29.2% less than the results of the prisms ST-R-2-FS. This stress was achieved at a peak strain of 0.0017 (C.V. = 8.59%) which is half the peak strain of the prisms ST-R-2-FS. The initial stiffness for ST-R-5-FS was 8.19 GPa (C.V. = 8.71%) which is only 6.64% more than the results observed for ST-R-2-FS.

Considering the aforementioned failure patterns, the prisms of different heights show different peak stresses due to the confining effect of the loading machine end platens. The constraining effect of the platens on the top and bottom of the prisms alters the compressive stress-strain

response of the prisms leading to two distinctive failure modes, peak stress values, and elastic moduli for the prisms of h/t = 2.0 and 5.0.

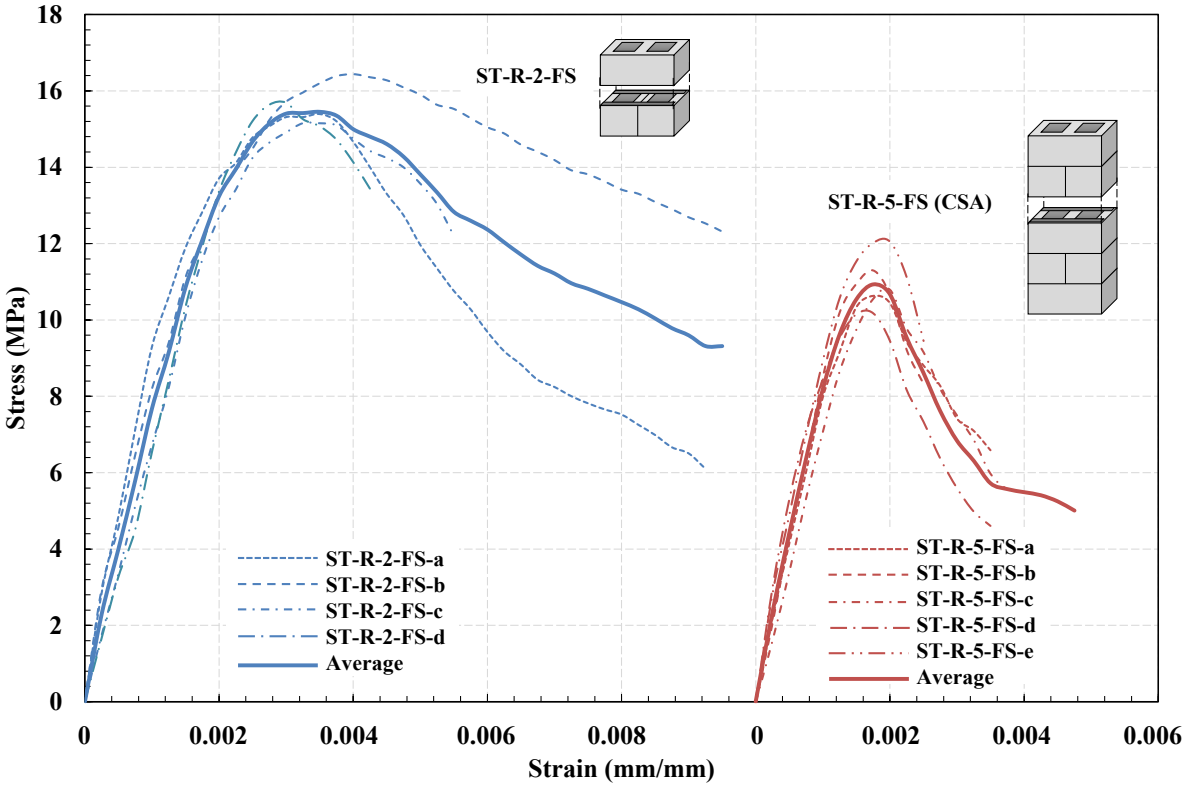

Figure 3-9 Stress-strain curves for masonry stretcher block prisms of running bond pattern having h/t ratio of 5 and 2

Table 3.4 Results of tested masonry stretcher block prisms

Code	Ultimate Load (kN)	Strength (MPa)	C.V.	Strain at Peak	C.V.	Elastic Modulus (GPa)	C.V.
ST-R-2-FS	269.2	15.74	3.28 %	0.0034	12.18 %	7.68	16.96%
ST-R-5-FS	190.7	10.93	6.24 %	0.0017	8.59 %	8.19	8.71%
ST-S-2-FB	299.6	17.30	6.66 %	0.0030	6.29 %	8.57	4.83%
ST-S-5-FB	227.1	13.28	11.39 %	0.0018	18.13 %	9.43	5.95%

3.2.2 Fully-grouted stack-bonded stretcher block prisms

The observed failure patterns at the end of the tests for the full-bedded stack-bonded masonry prisms of h/t = 2.0 and 5.0 can be found in Figures 3.10 and 3.11, respectively. Similar to the running-bonded prisms, the prisms of h/t = 2.0 (ST-S-2-FB) had a dominant shear mode conical

shaped failure pattern and a splitting failure was dominant for the prisms of h/t = 5.0 (ST-S-5-FB).

(a) **(b)** **(c)** **(d)**

Figure 3-10 Observed failure patterns for the fully-grouted stack-bonded stretcher block prism of h/t = 2.0 (a) front, (b) right, (c) back, and (d) left

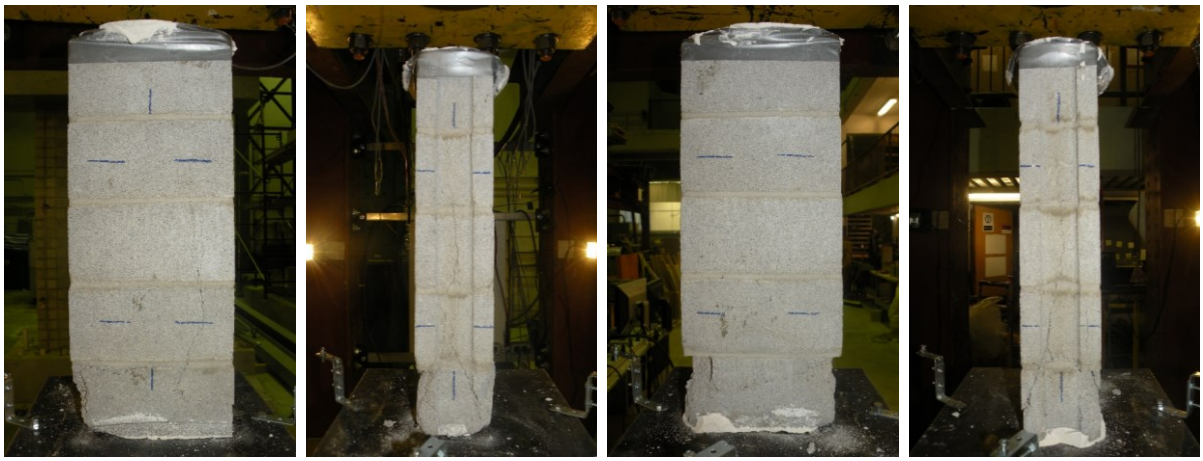

(a) **(b)** **(c)** **(d)**

Figure 3-11 Observed failure patterns for the fully-grouted stack-bonded stretcher block prism of h/t = 5.0 (a) front, (b) right, (c) back, and (d) left

The stress-strain responses are presented in Figures 3.12. The figure shows the stress, computed as the measured load divided by the area (i.e. 17100 mm^2) against the average longitudinal strains (i.e. average of the four LVDTs readings). The results of testing the stack-bonded masonry prisms are summarized in Table 3.4.

The average peak stress of the prisms of *h/t* of two (ST-S-2-FB) was 17.52 MPa having C.V. = 6.66%. This stress was achieved at a peak strain of 0.0030 (C.V. = 6.29%). The average initial stiffness of ST-S-2-FB was 8.57 GPa (C.V. = 4.83%). The average peak stress of the prisms of *h/t* of five (ST-S-5-FB) was 13.28 MPa (C.V. = 11.39%). This result is 31.9% less than the results of the prisms ST-S-2-FB. This stress was achieved at a peak strain of 0.0018 (C.V. = 18.13%) which is 60% the peak strain of the prisms ST-S-2-FB. The initial stiffness for ST-S-5-FB was 9.43 GPa (C.V. = 5.95%) which is 10% more than the results observed for ST-S-2-FB.

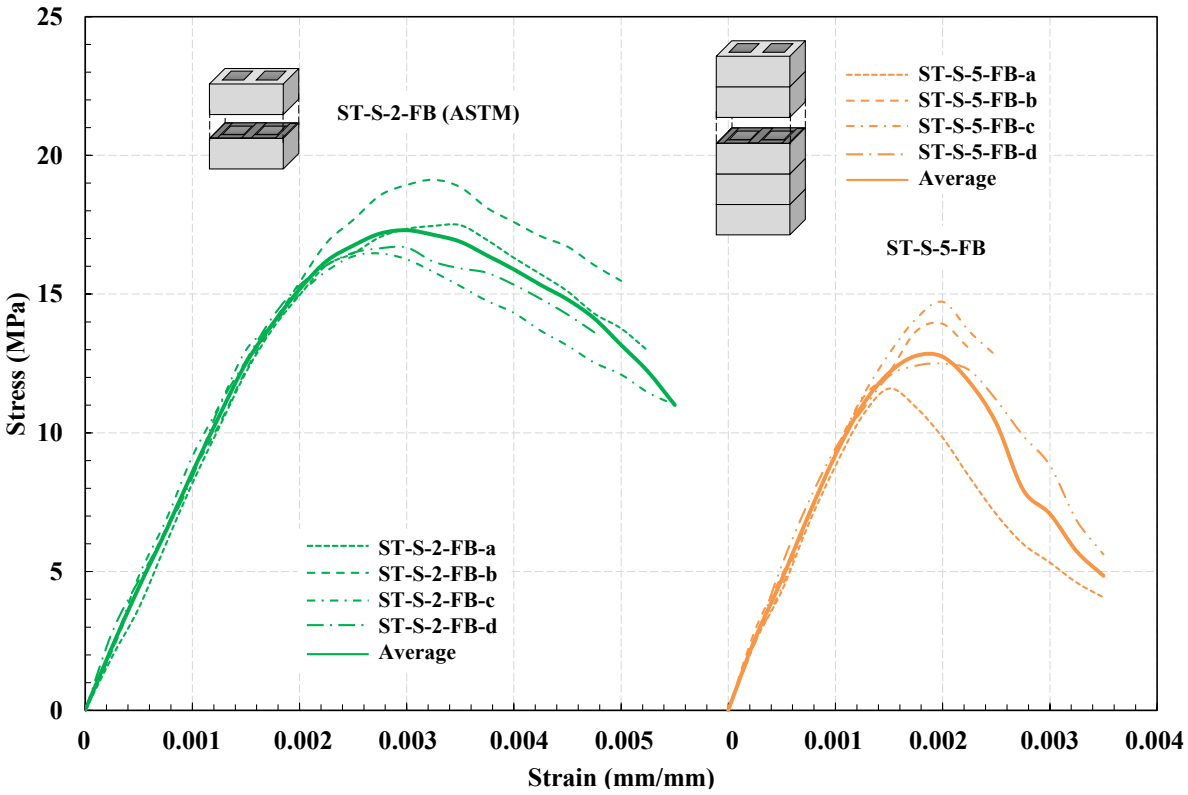

Figure 3-12 Stress-strain curves for masonry stretcher block prisms of stack bond pattern having *h/t* ratio of 5 and 2

The average compressive strength of ST-S-2-FB is 11.3% more compared to the compressive strength of ST-R-2-FS. These stresses were achieved at similar peak strains in the two prisms. The initial stiffness of ST-S-2-FB is also 11.6% more than that of ST-R-2-FS. The average compressive strength of ST-S-5-FB is 19.1% more compared to the compressive strength of ST-R-5-FS. These stresses were achieved at similar peak strains in the two prisms. The initial stiffness of ST-S-5-FB is 15.1% more than that of ST-R-5-FS.

3.2.3 Fully-grouted Boundary Element Prisms

The observed failure patterns at the end of the tests of the third group of specimens, fully-grouted masonry boundary element prims of *h/t* = 2.0 and 5.0 can be found in Figures 3.13 and 3.14, respectively. For C-MSBEPs of *h/t* = 2.0 (BE-N-2), a shear mode conical shaped failure pattern was observed with no spalling of the blocks. On the other hand, a splitting failure was observed for the C-MSBEPs with *h/t* = 5.0 (BE-N-5 and BE-H-5). This suggest that the failure mode is mainly affected by the *h/t* of the prism not the block geometry. However, the splitting failure in C-MSBEPs started with vertical cracks in the vertical joints after reaching the maximum load followed by partial spalling of the C-shaped units initiated by the expansion of the grout core. The lateral expansion of the grout core continued under the axial compression loading till its crushing at the end of the test. For all specimens, no buckling was observed during testing till the failure.

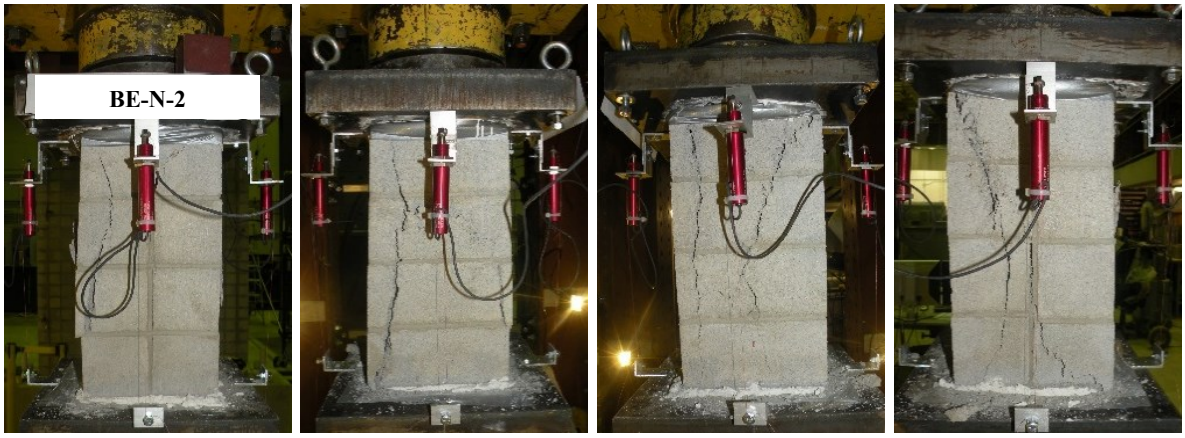

(a) **(b)** **(c)** **(d)**

Figure 3-13 Observed failure patterns for the fully-grouted C-MSBEPs of *h/t* = 2.0 (a) front, (b) right, (c) back, and (d) left

The stress-strain relationships can be seen in Figure 3.15. The figure shows the stress-strain response of the individual specimens tested along with the average response for each category of prisms. The stress-strain responses of the individual specimens in each category as well as the average response were calculated similar to what mentioned before in the stretcher block

masonry prims. However, the area used for stress calculations for these prisms is the gross area of the grouted BE constructed with C-shaped blocks (i.e. 190 mm x 190 mm = 36100 mm^2).

The results of testing the C-MSBEPs are summarized in Table 3.5. The average peak stress of the prisms having *h/t* = 2.0 and grouted with normal strength grout (BE-2) was 12.66 MPa (C.V. = 0.28%). This stress was achieved at a peak strain of 0.002 (C.V. = 2.83%). The initial stiffness of this category of specimens was 8.88 GPa (C.V. = 14.14%). The average peak stress of the prisms grouted with the same grout but having *h/t* of five (BE-5) is 10.48 MPa (C.V. = 3.24%), thus 17.2% less than the results of the prisms BE-2. This stress was achieved at a peak strain of 0.0019 (C.V. = 8.61%) which is similar to the prisms BE-2. The initial stiffness for BE-5 was 6.15 GPa (C.V. = 9.22%) which is 31% less than the results observed for BE-2.

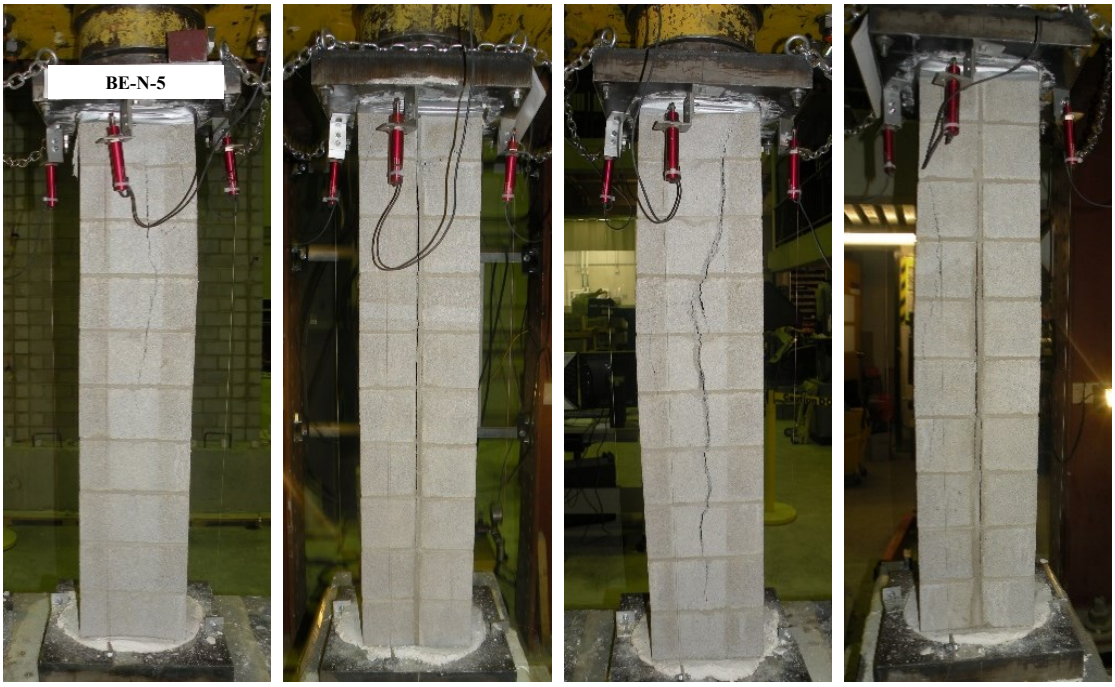

Figure 3-14 Observed failure patterns for the fully-grouted C-MSBEPs of *h/t* = 5.0 (a) front, (b) right, (c) back, and (d) left

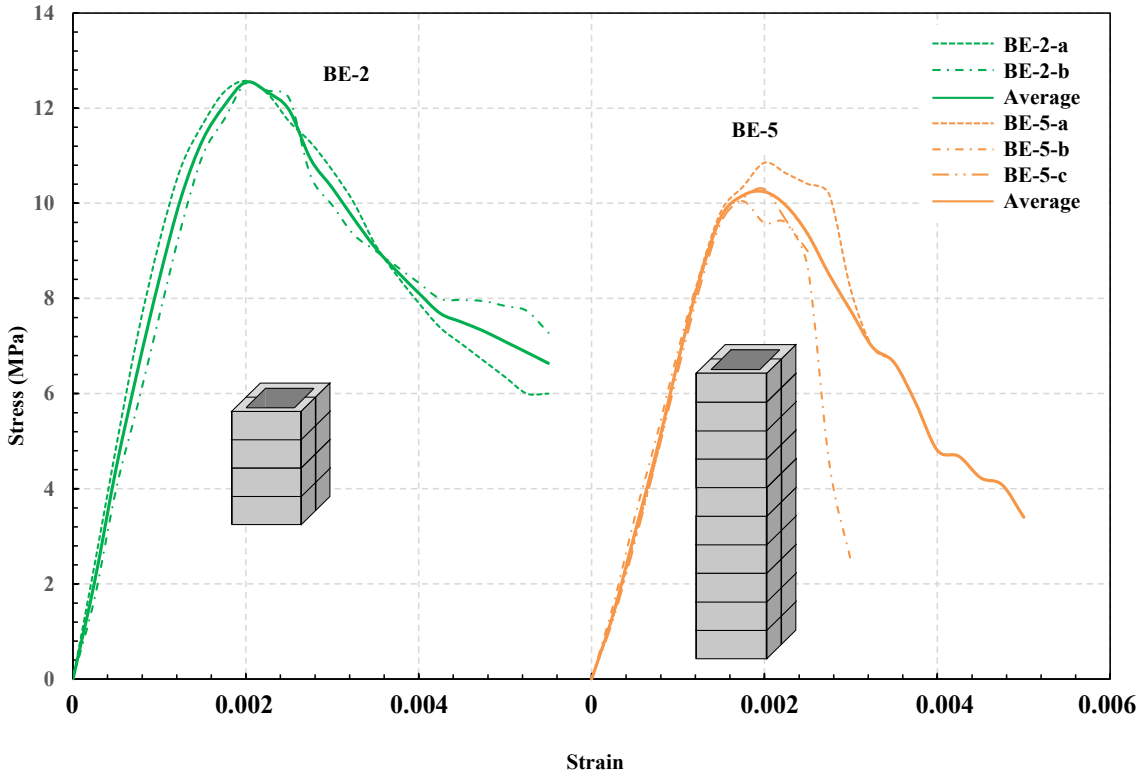

Figure 3-15 Stress-strain curves for boundary element masonry prisms (C-MSBEP) having *h/t* ratio of 5 and 2

Table 3.5 Results of tested C-MSBEPs

ID	Ultimate Load (kN)	Strength (MPa)	C.V.	Strain at Peak	C.V.	Elastic Modulus (GPa)	C.V.
BE-2	457.0	12.55	0.28%	0.0020	2.83%	8.88	14.14%
BE-5	380.5	10.24	2.83%	0.0019	9.03%	6.15	9.22%

3.3 Effect of height-to-thickness ratio on the compressive strength of grouted masonry prisms

The stress-strain response of ST-S-2-FB and ST-S-5-FB are compared in Figure 3.16. Changing the *h/t* from two to five significantly affected the peak stress and the peak strain. Stack-bonded prisms of full mortar bedding and *h/t* = 2.0 showed a 32% decrease in peak stress compared to the same prisms but of *h/t* = 2.0. This increase percentage is almost 1.5 times the 22% predicted by the ASTM C1314 (2014). Moreover, the peak strain of the prisms of *h/t* equals

to two is more than 1.5 times the peak strain of prisms of *h/t* equals to five. However, the initial stiffness for both prisms is almost the same.

The stress-strain relationships of ST-R-2-FS and ST-R-5-FS are compared in Figure 3.16. Similar to the stack-bonded prisms of full mortar bedding, changing the *h/t* from two to five significantly affected the peak stress and the peak strain. Running-bonded prisms of face-shell mortar bedding and *h/t* = 2.0 showed a 41% increase in peak stress compared to the same prisms but of *h/t* = 5.0. This increase percentage is more than double the percentage indicated by the correction factor of CSA S304 (2014). The peak strain value of the prisms of *h/t* = 2.0 is double the peak strain value of prisms of *h/t* = 5.0. Similar to the stack-bonded full mortar bedded prisms, the initial stiffness of the running-bonded prisms for both aspect ratios is almost the same.

To consider the effect of changing the *h/t* in BEs, the stress-strain relationships of BE-2 and BE-5 are compared in Figure 3.16. The grouted boundary element prisms of *h/t* = 2.0 showed a 20% increase in the peak stress compared to the same prisms of *h/t* = 5.0. This increase percentage falls between the percentage predicted by the correction factors of CSA S304 (2014) and the percentage predicted by the correction factor of ASTM C1314 (2014). Considering that CSA S304 (2014) requires prisms of *h/t* = 2.0 to be converted to prisms of *h/t* = 5.0 and ASTM C1314 (2014) requires the opposite, the two standards result in a slight overestimation of the effect of *h/t* on BE prism strength. This overestimation value is negligible and can be safely ignored. Moreover, the peak strain values of the BE prisms of *h/t* = 2.0 and of *h/t* = 5.0 are nearly equal. Nonetheless, the prisms of lower aspect ratio tend to be stiffer than the prisms of the higher aspect ratio.

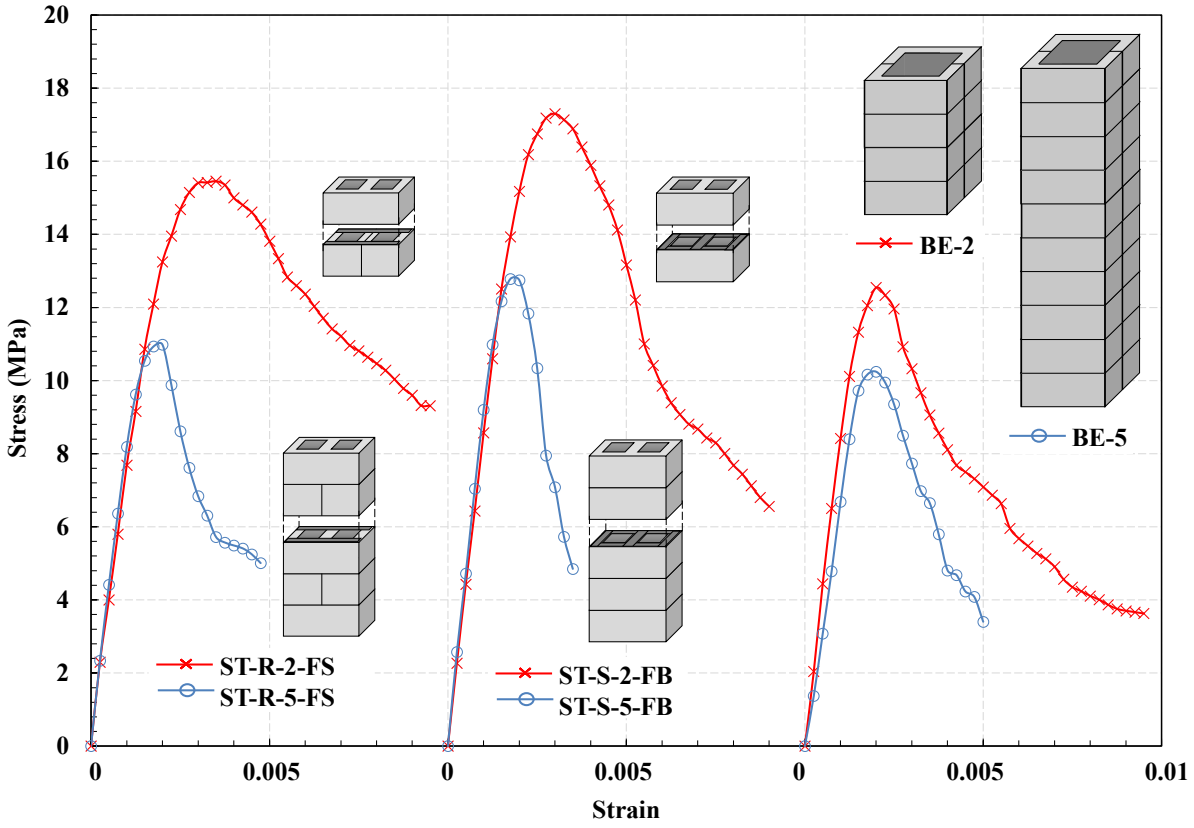

Figure 3-16 Comparing the stress strain response of running bond pattern stretcher prisms, stacked bond pattern stretcher prisms, and B.E. prisms of *h/t* of 2.0 and 5.0

It can be observed that the change in *h/t* (loading machine platen influence) has less effect on C-MSBEPs than the stretcher block prisms. This is attributed to the combined effect of *h/t* with *l/t* as shown by Hassanli et al. (2015) and discussed before. According to Hassanli et al. (2015), specimens of *l/t* = 2.0 and *h/t* = 2.0 show more increase in strength when compared to specimens of the same *l/t* but with *h/t* = 5.0 than the specimens of *l/t* = 1.0 and *h/t* = 2.0 when compared to specimens of the same *l/t* but with *h/t* = 5.0. Thus, C-MSBEPs of *l/t* = 1.0 are less influenced by the platen effect than the stretcher block prisms of *l/t* = 2.0 when comparing the prisms of *h/t* = 2.0 to the prisms of *h/t* = 5.0.

3.4 Stress-strain of boundary element prisms versus that of the stretcher block prisms

Comparing the stress-strain responses of BE-5 to that of the stretcher block prism ST-S-5-FB of the same *h/t* (5.0), bond pattern (stack bond), and mortar bedding (full bedding), It can be observed that the boundary element prisms have less peak stress and initial stiffness. The peak

stress of BE-5 is 21% less than that of ST-S-5-FB. Also, it is 27% less stiff than ST-S-5-FB. It can be concluded that boundary element prisms constructed with C-shaped blocks cannot be represented by stretcher block prisms of the same aspect ratio, mortar bedding and block pattern. It is believed that the reason for this distinction in stress-strain responses is the continuous vertical mortar joint in the BE prisms constructed with C-shaped blocks. In stretcher block prisms, the lateral expansion of the grout core due to the axial compression is resisted by the tensile strength of the stretcher block. This grout-block interaction works as a sort of a confinement to the grout core increasing the overall prism peak stress. The same mechanism occurs in the C-MSBEPs. However, the presence of the vertical mortar joint in the C-MSBEPs in each course leads to the formation of a weak line that decreases the confinement effect of the blocks to the grout core leading to a less peak stress compared to the stretcher block prisms. The vertical joint is also responsible for the difference in the initial stiffness between the two types of prisms.

As mentioned before, the requirements of prism construction in CSA S304 (2014) and in ASTM C1314 (2014) result in two distinct prisms. The two prisms are affected by a combination of the factors discussed earlier. Testing these two prisms lead to incomparable stress-strain responses as shown in Figure 3.17. The ASTM stack-bonded prism of full-bedded mortar joints and h/t = 2.0 showed a significant increase in peak stress and peak strain compared to the CSA running-bonded prism of face-shell mortar bedding and h/t = 5.0. The peak stress of the ASTM prism is more than 1.5 times the peak stress of the CSA prism. In addition, the peak strain of the ASTM prism is 1.76 times the peak strain of the CSA prism. Nonetheless, both prisms have almost the same initial stiffness. It can be concluded that the CSA S304 (2014) and ASTM C1314 (2014) stretcher block prisms show significantly distinct stress-strain responses. Recalling that stretcher block prisms of h/t = 2.0 leads to peak stress which is 20 ~ 25% more than these of h/t = 5.0 (Hassanli et al. 2015) and that stack-bonded prisms results in a peak stress that can be up to 25% more than these of running-bonded prisms, this distinction is mainly attributed to the combined effect of the different h/t ratios and different bond-patterns between the CSA and ASTM standard prisms.

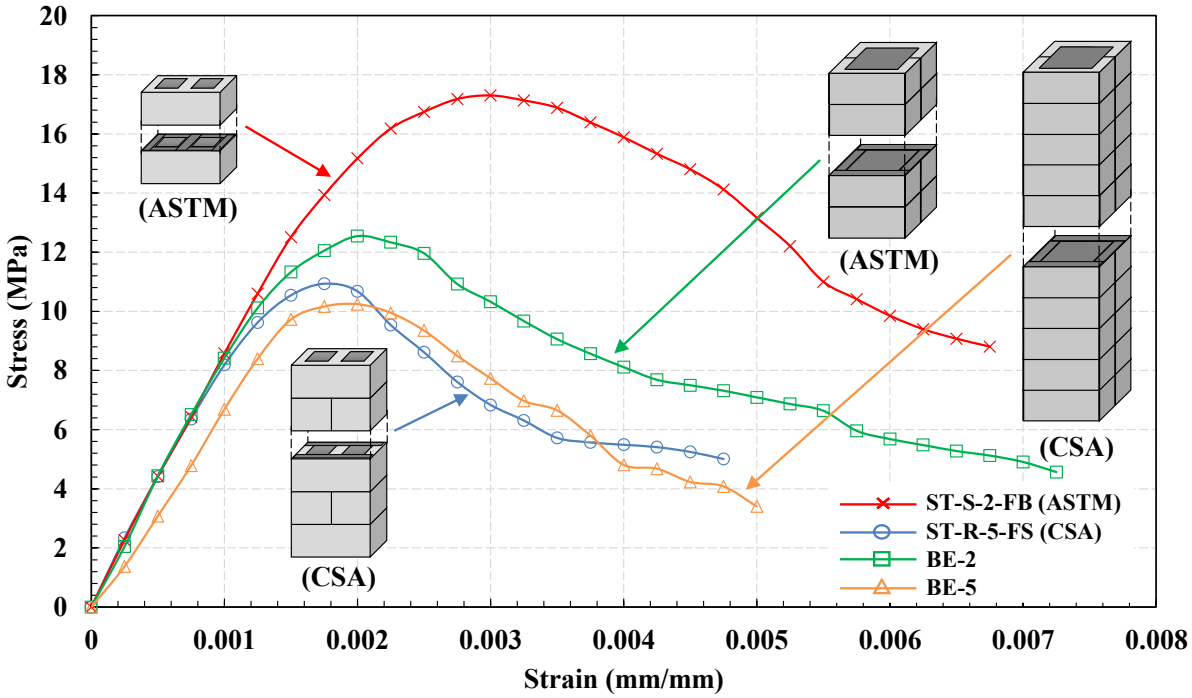

Figure 3-17 Comparison of stress-strain curves for the masonry prisms ST-S-2-FB (ASTM C1314 2014), ST-R-5-FS (CSA S304 2014), BE-2 and BE-5

The stress-strain relationships of stack-bonded stretcher block prism of full bedding and h/t = 2.0 (ST-S-2-FB) and the BE prism constructed with C-shaped blocks of h/t = 2.0 (BE-2) have similar initial stiffness. However, the peak stress and peak strain of the stretcher block prism are 38% and 50% more than these of the BE prism, respectively. In addition, the stress-strain relationship of BE-5 is compared to that of ST-R-5-FS in Figure 3.17. The peak stress of the stretcher block prism is only 6% more than that of the BE and its peak strain is 11% less compared to that of the BE. However, the initial stiffness of ST-R-5-FS is 22% higher than that of BE-5. These percentages are less significant compared to the percentages in the case of comparing ST-S-2-FB to BE-2 or in the case of comparing ST-S-5-FB to BE-5.

BE-5 was expected to have less peak stress than ST-R-5-FS. The BE prisms were expected to have less peak stress than stretcher block prisms as explained before in the comparison of BE-5 with ST-S-5-FB. However, the difference in peak stresses is small because the stretcher block prism in this comparison (ST-R-5-FS) is running-bonded which results in less peak stress than the stack-bonded prism (ST-S-5-FS). On the other hand, the large difference between BE-2 and ST-S-2-FB could be attributed to the combined effect of the vertical mortar joint in the C-

MSBEPs and the effect of the different *l/t* between the C-MSBEPs and the stretcher block prisms.

The masonry compressive strength, f'_m, for a wall constructed with stretcher blocks (web of a shear wall with boundary elements) is evaluated by testing the prisms ST-S-2-FB (according to ASTM C1314 2014) and ST-R-5-FS (according to CSA S304 2014). However, the compressive strength of a BE constructed with C-shaped blocks shall be evaluated by testing the prism BE-2 and BE-5 following the requirements of the same two standards, respectively. The dissimilarity of the stress-strain relationships of ST-S-2-FB and BE-2 highlights the importance of testing BE prisms along with stretcher block prisms for a full compressive strength evaluation for a shear wall with boundary elements if ASTM standards are to be followed. On the other hand, the similarity of the stress-strain relationships of ST-R-5-FS and BE-5 shows that testing the stretcher block prism only is enough for an acceptable compressive strength evaluation for a shear wall with boundary elements if CSA standards to be followed.

3.5 Stretcher block and boundary element prisms' experimental results versus the predicted values by CSA S304 (2014) and MSJC (2013)

Tables 3.6 and 3.7 compare the results of the prisms in this experimental work to the predicted values by Table 4 in CSA S304 (2014) and Table 2 in MSJC (2013), respectively. The specified compressive strength for masonry unit in Table 3.6 was calculated according CSA S304 (2014) using Eq. 3.1. It should be noted that these specified values were used to determine the corresponding tabulated masonry compressive strength values from Table 4.

$$f'_{unit} = f_{av}(1 - 1.64v) \quad (3.1)$$

f'_{unit} : Masonry unit specified compressive strength,

f_{av} : Masonry unit average compressive strength,

v : Coefficient of variation,

Moreover, the corrected specified compressive strength in the same table was calculated following CSA S304 (2014) using Eq. 3.2 and then multiplying the results by the *h/t* correction factor.

$$f'_m = f_{av}(1 - 1.64v) \quad (3.2)$$

f'_m : Masonry specified compressive strength,

f_{av} : Prism average compressive strength,

v : Coefficient of variation,

On the other hand, in Table 3.7, the masonry unit average strength was used to determine the corresponding masonry compressive strength value from Table 2 in MSJC (2013). The obtained values were compared to average prism compressive strengths (corrected for *h/t*) (NCMA 2014).

Table 3.6 Comparison of the experimental results to the unit strength method values of CSA S304 (2014)

ID	Unit Specified Strength (MPa)	Grout Strength (MPa)	Prism		CSA S304 (2014)			
			Average Strength (MPa)	C.V. %	*h/t* Correction Factor	Corrected Specified Strength (MPa)	Table 4 Value	Error
ST-R-2-FS	12.1	20	15.74	3.28	0.85	11.18	7.25	-35%
ST-R-5-FS			10.93	6.24	1	9.14		-21%
ST-R-2-FB			17.3	6.66	N/A	N/A	N/A	N/A
ST-R-5-FB			13.28	11.39				
BE-2	17	14.9	12.55	0.28	0.85	8.92	10.7	20%
BE-5			10.24	2.83	1	8.56		25%

Table 3.7 Comparison of the experimental results to the unit strength method values of MSJC (2013)

ID	Unit Average Strength (MPa)	Grout Strength (MPa)	Prism		MSJC (2013)			
			Average Strength (MPa)	C.V. %	*h/t* Correction Factor	Corrected Average Strength (MPa)	Table 2 Value	Error
ST-R-2-FS	14.5	20	15.74	3.28	N/A	N/A	N/A	N/A
ST-R-5-FS			10.93	6.24				
ST-R-2-FB			17.3	6.66	1	17.30	11.12	-36%
ST-R-5-FB			13.28	11.39	1.22	16.20		-31%
BE-2	22	14.9	12.55	0.28	1	12.55	15.2	21%
BE-5			10.24	2.83	1.22	12.49		22%

A significant underestimation of the capacity of the stretcher block prisms by both standards can be observed. This finding agrees with the findings of previous studies that showed that the unit strength method values are conservative. On the other hand, both standards overestimate the

capacity of the BE prisms. Moreover, the percentages of overestimation by the two standards for the capacity of the BE prisms are similar (range from 20-25%). This suggests that the unit strength method values provided by the two standards are not suitable for predicting the C-MSBEP compressive strength. However, according to MSJC (2013), the unit strength method values provided shall be multiplied by 0.85 if the unit used is less than 102 mm in height. If this reduction is applied to Table 2 values in Table 3.7, the overestimation percentage for BE prisms falls to only 3% while the underestimation for stretcher block prisms rises to more than 40%.

These results show that while a revision for the values presented by both standards regarding the stretcher block prisms is worth reconsidering, it is believed that MSJC (2013) tabulated values can be used for predicting the capacity of the BE prisms.

3.6 Typical stress-strain responses and the proposed stress-strain models for standard stretcher block and boundary element prisms according to CSA and ASTM

The typical stress-strain response of the masonry prisms, stretcher block prisms and C-MSBEPs, starts with a short linear elastic relationship of a slope equals to the elastic modulus of elasticity. This relationship ends with the occurrence of the first crack. After this point, the stress-strain curve starts to have a steeper slope. The first crack in stretcher block prisms is a vertical crack that appears in the sides of the stretcher block. However, in the C-MSBEPs, the first crack appears in the vertical mortar joint. The cracking starts in the C-MSBEPs earlier than the cracking in stretcher block prisms because the vertical mortar joint is weaker, in compression and in tension, than the stretcher block. The cracking in both types of prisms is initiated by the grout core lateral expansion under the compressive axial loading. The slope of the stress-strain curve becomes steeper as the cracks appear and develop in the four sides of the stretcher block prism and as the vertical joint cracks become longer and wider in the C-MSBEPs. Meanwhile, the compressive strength of the blocks in the two types of prisms decrease due to cracking and transfer bigger part of their load share to the grout cores as loading proceeds. The increasing loading combined with the load transferred from the blocks and the decreased grout core axial compression capacity due to shrinkage (see *factors influencing the reduction of the grout stress-strain response in the grouted prism* section) lead to the grout core reaching its peak stress rapidly and prematurely. Therefore, as the blocks reach their peak stress, the grout core reaches its peak stress shortly after. At this point, the slope of the stress-strain curve becomes a plateau. The post-peak response is characterized by the rapid reduction in the blocks load carrying

capacity and the excessive lateral expansion of the grout cores. The grout cores excessive expansion leads to the spalling of parts of the blocks in the stretcher block prisms and the appearance of vertical cracks in the sides with no vertical mortar joints in C-MSBEPs followed by partial spalling of the blocks. This causes the slope of the stress-strain curve to decrease acquiring a negative sign. The slope of the curve continues to decrease till the crushing of the grout cores which marks the total failure and the inability of the stretcher block prisms and C-MSBEPs to carry any loads.

Testing of boundary element prisms is more challenging than testing stretcher block prisms especially if a boundary element prism of *h/t* = 5.0 (10-course prism) is required to be tested according to CSA S304 (2014). Thus, two simplified stress-strain models are proposed to facilitate the prediction of the stress-strain relationship of the boundary element prisms from the standard stretcher block prisms of CSA S304 (2014) and ASTM C1314 (2014). The models also allow the conversion between the two standards' prisms.

The first model were developed by modifying the peak stress, the strain at peak, and the tangent modulus of elasticity in Mander model for unconfined concrete (Mander et al. 1988a; b). The model is illustrated in Figure 3.18. The axial compressive stress f is given by Eq. 3.1 to Eq. 3.4.

$$f = \frac{f_m \, x \, r}{r - 1 + x^r} \tag{3.1}$$

$$x = \frac{\varepsilon}{\varepsilon_m} \tag{3.2}$$

$$r = \frac{E_m}{E_m - E_{sec}} \tag{3.3}$$

$$E_{sec} = \frac{f_m}{\varepsilon_m} \tag{3.4}$$

f_m : Masonry peak stress (MPa),

ε : Axial compressive strain,

ε_m : Strain corresponding to peak stress,

E_m : Masonry tangent modulus of elasticity (MPa).

E_{sec} : Masonry secant modulus of elasticity (MPa).

The values of the peak stress and the strain corresponding to peak stress, ε_m, and the tangent modulus of elasticity, E_m, are listed in Table 3.8.

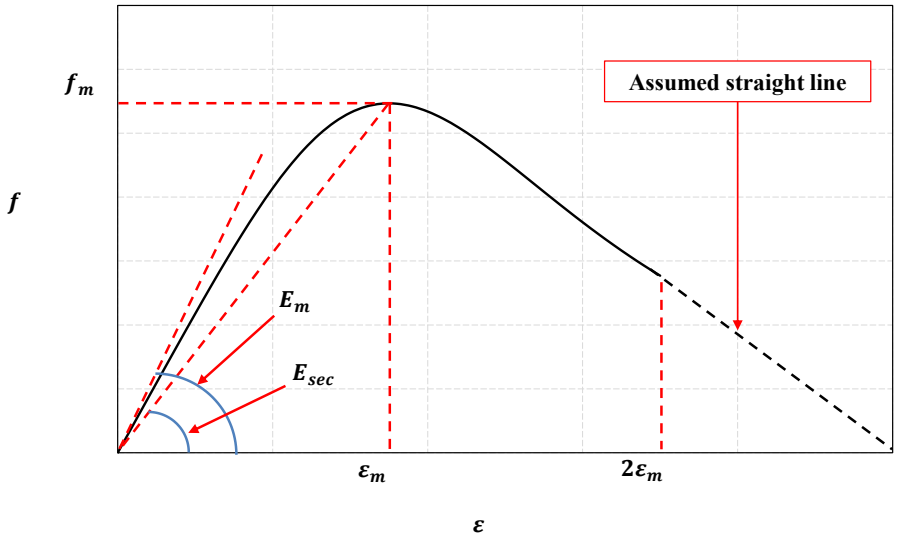

Figure 3-18 Proposed stress-strain models by modifying Mander Model

Table 3.8 Values used for the proposed stress-strain models

Model		Value of	ASTM Standard Stretcher block Prism	ASTM Standard BE Prism ($h/t = 2$)	CSA Standard Stretcher block Prism	CSA Standard BE Prism ($h/t = 5$)
Kent and Park	Mander	f_m(MPa)	17.30	12.55	10.93	10.24
		ε_{mu}	0.0030	0.0020	0.0018	0.0020
		E_m (MPa)	$500f_m$	$750f_m$	$800f_m$	$700f_m$

The second model was developed by modifying the peak stress and the strain at peak in Kent and Park model for unconfined concrete (Kent and Park 1971). The model is illustrated in Figure 3.19. The ascending branch of the curve ($\varepsilon \leq \varepsilon_m$) for the axial compressive stress f is given by Eq. 3.5 while the descending branch ($\varepsilon > \varepsilon_m$) is given by Eq. 3.6 to Eq. 3.8.

$$f = f_m\left[\frac{2\varepsilon}{\varepsilon_m} - \left(\frac{\varepsilon}{\varepsilon_m}\right)^{1.8}\right] \tag{3.5}$$

$$f = f_m[1 - Z(\varepsilon - \varepsilon_m)] \tag{3.6}$$

$$Z = \frac{0.5}{\varepsilon_{50} - \varepsilon_m} \tag{3.7}$$

$$\varepsilon_{50} = 0.00037 * f_m \tag{3.8}$$

ε_{50} : Strain corresponding to 50% reduction in the peak stress,

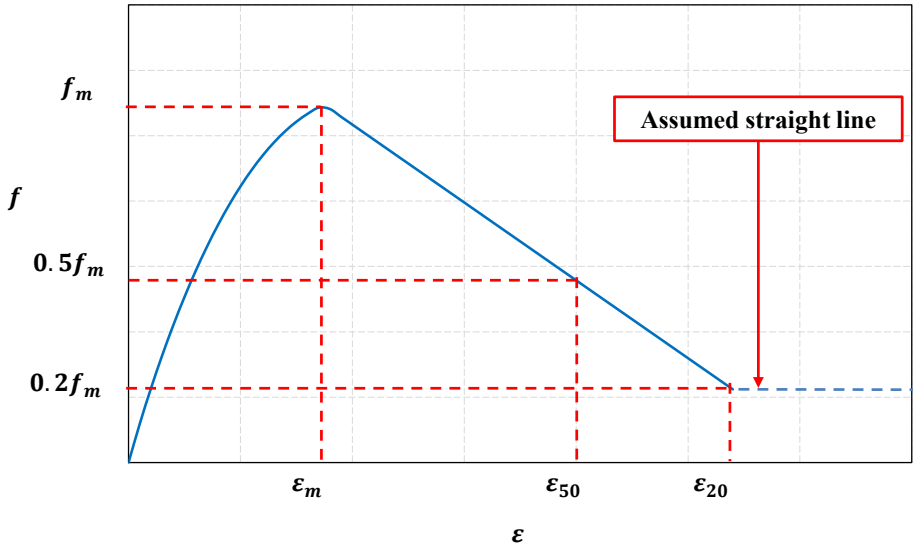

Figure 3-19 Proposed stress-strain models by modifying Kent and Park Model

The values of the peak stress and the strain corresponding to peak stress, ε_m, are listed in Table 3.8. The stress-strain relationships resulted from the two proposed models are compared to the stress-strain relationships resulted from the experimental work in Figures 3.20 to 3.23.

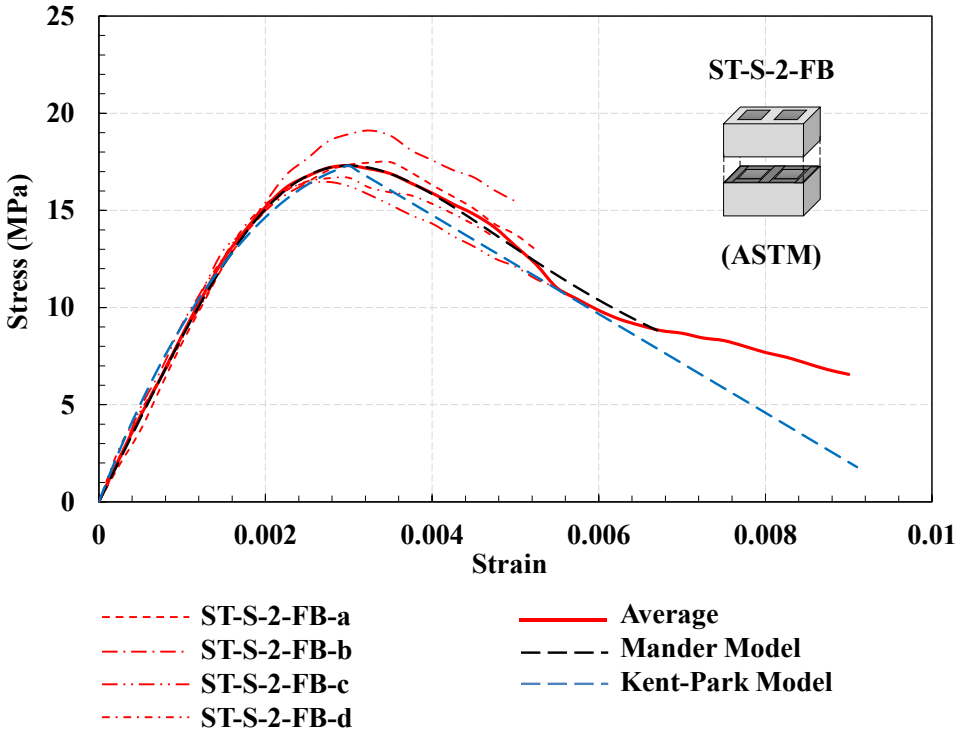

Figure 3-20 Proposed stress-strain models for ST-S-2-FB (ASTM)

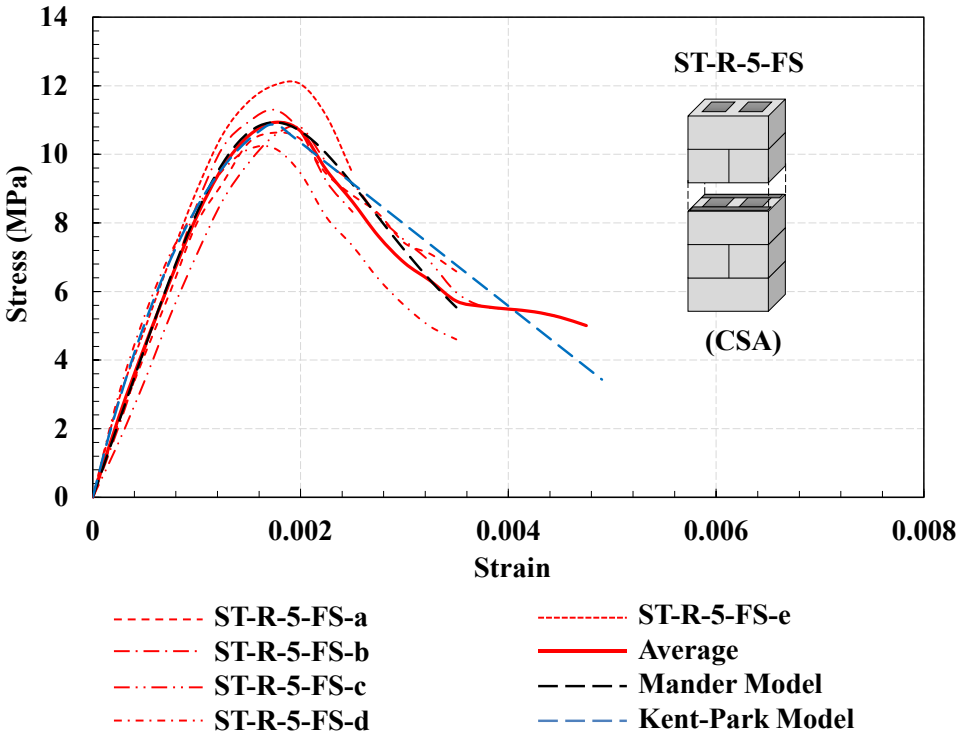

Figure 3-21 Proposed stress-strain models for ST-R-5-FS (CSA)

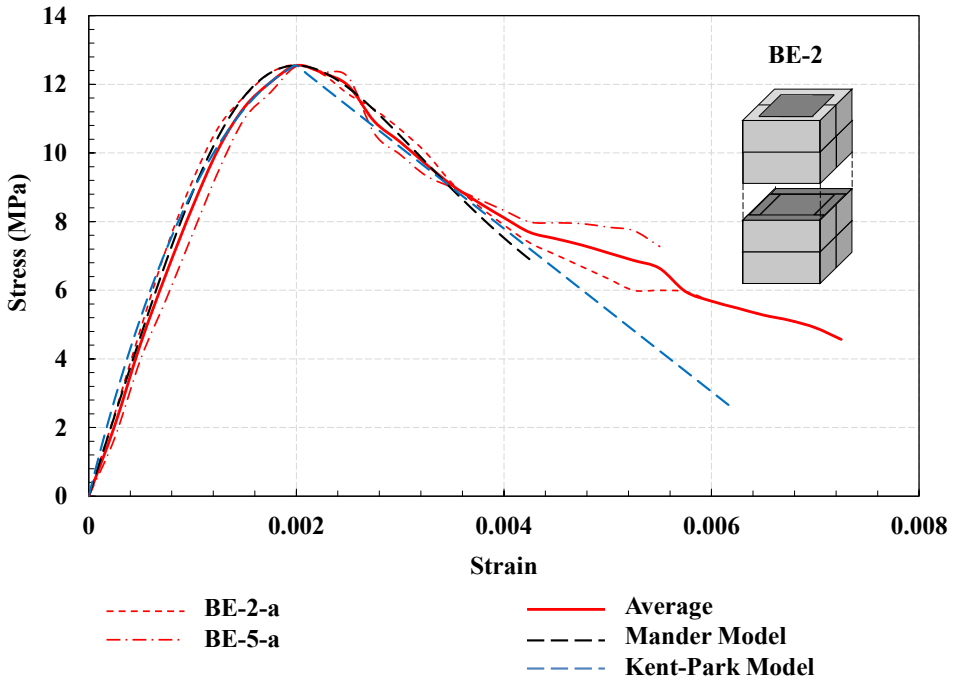

Figure 3-22 Proposed stress-strain models for BE-2

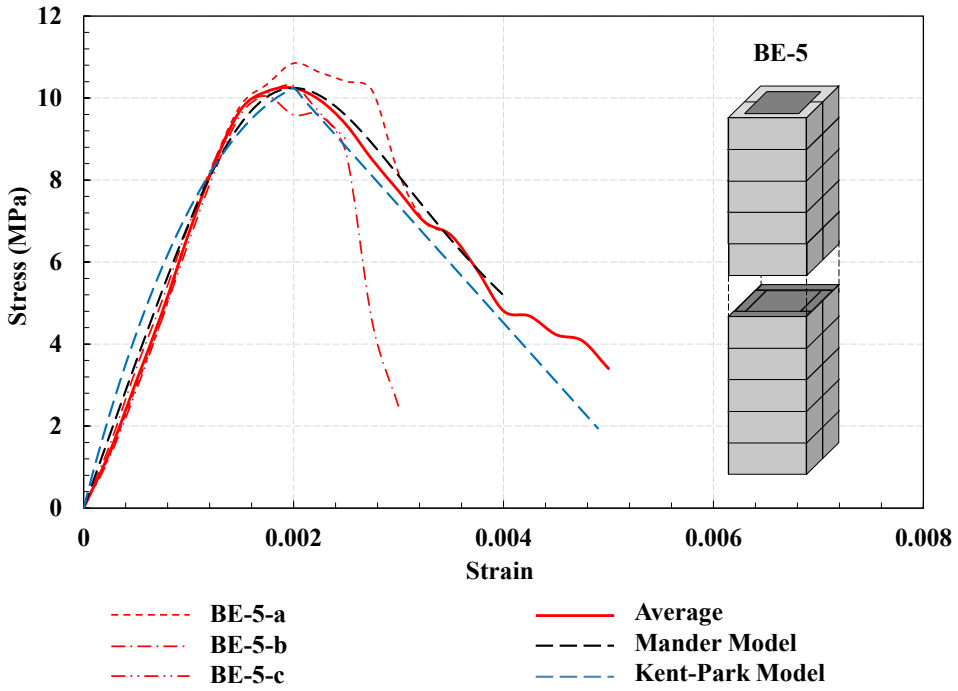

Figure 3-23 Proposed stress-strain models for BE-5

Chapter 4

THE INTERACTION BETWEEN THE MASONRY SHELL AND THE GROUT CORE

4.1 Experimental Work of Phase II

4.1.1 Test Matrix

As illustrated in Figure 4.1 the test matrix of this phase consists of three groups: (1) fully-grouted masonry BE prisms constructed using C-shaped blocks, (2) un-grouted masonry BE shells, and (3) C-MBE grout core prisms. The method used to identify each tested specimen is illustrated in Figure 4.2. In addition to the two sets of the fully-grouted C-MSBEPs tested in the first phase, a third set was tested in this phase. The third set had h/t = 5.0 and was grouted by high strength grout. The masonry BE prisms constructed using C-shaped concrete masonry blocks were tested under concentric compression loading up to failure. Table 4.1 lists all the C-MSBEPs tested. It should be noted that the other two sets, grouted with normal strength grout, were renamed in this table, and throughout the chapter, according to the method used to identify the specimens in this chapter to facilitate the comparisons.

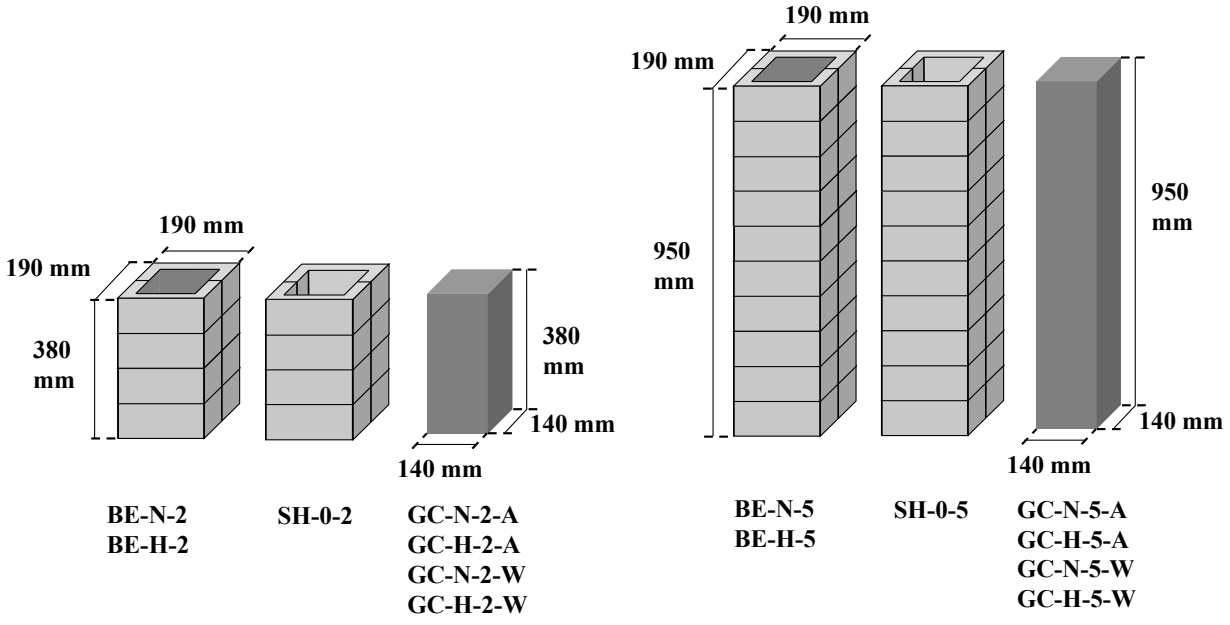

Figure 4-1 Schematic drawing for the tested specimens: (a) Specimens with height to thickness ratio of two, (b) Specimens with height to thickness ratio of five

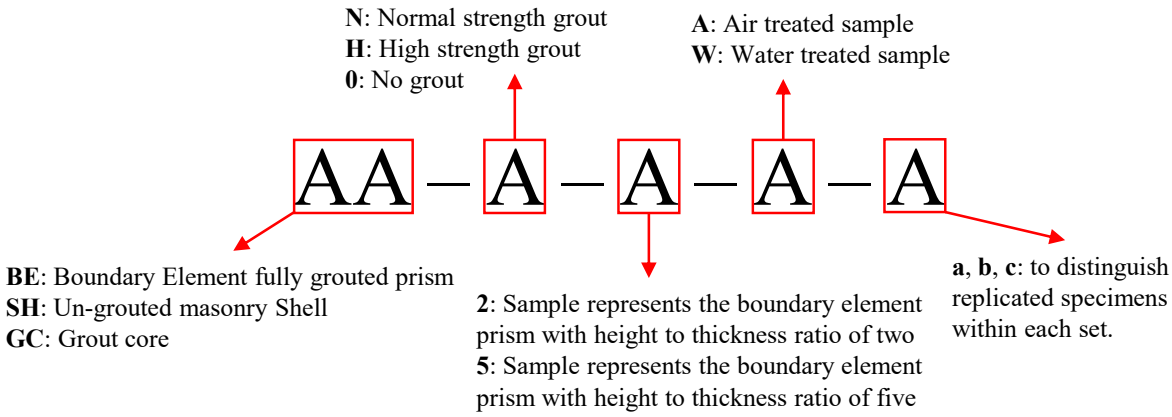

Figure 4-2 Identification method for each tested sample

Table 4.1 Experimental test matrix for C-MSBEPs

ID	Grout Strength	Height-to-Thickness ratio	Number of specimens
BE-N-2	Normal	2	2
BE-N-5	Normal	5	3
BE-H-5	High	5	3

In addition to the fully grouted BE prisms, two sets of un-grouted masonry BE shells were constructed and tested under similar loading procedure. The two sets, SH-0-2, and SH-0-5, had *h/t* equals to 2 and 5, respectively (Table 4.2).

Table 4.2 Experimental test matrix for un-grouted masonry prisms (masonry shells)

ID	Height-to-Thickness ratio	Number of specimens
SH-0-2	2	3
SH-0-5	5	3

Moreover, eight sets of grout prisms mimicking the grout cores inside the BE prisms were cast and tested under concentric compression loading. Each grout core had square cross-section of side length equals to 140 mm and a height of 380 mm or 950 mm (Figure 2.1). These dimensions replicate the dimensions of the grout core corresponding to each tested C-MSBEPs. All the grout cores were constructed by casting the grout following ASTM C1019 (2014)

guidelines. As illustrated in Figure 4.3, the blocks were laid in a way to act as molds for the grout cores. The inner face of each space specified for casting a grout specimen was lined with paper towels as recommended by ASTM C1019 (2014). The paper towels act as a permeable surface that allow the absorption of water from the grout core by the surrounding blocks while preventing the bond between them.

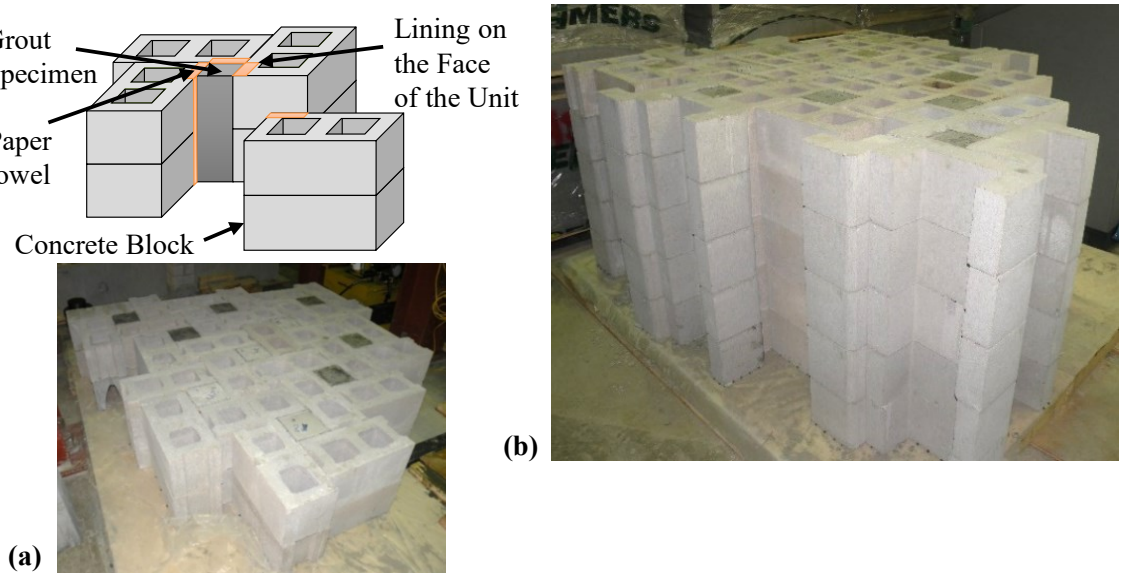

Figure 4-3 Grout core specimens' molding: (a) Specimens representing BE prisms having *h/t* = 2.0, (b) Specimens representing boundary elements prisms having *h/t* = 5.0

Four pairs of grout cores were constructed with *h/t* equals to 2.7 and 6.8 representing the grout core in BE prism having *h/t* equal to 2 and 5, respectively (Table 4.3). For each *h/t*, two sets were cast using normal and high strength grout. To investigate the effect of curing, following the construction, one set of grout cores was cured in water (i.e. 24 hours after pouring the grout) and the other was air cured between the blocks' molds. Both sets were removed from the molds 24 hours before testing.

Table 4.3 Experimental test matrix for grout core specimens

ID	Grout Strength	Nominal Height-to-Thickness ratio	Actual Height-to-Thickness ratio	Curing	Number of specimens
GC-N-2-A	Normal	2	2.7	Air	3
GC-N-5-A	Normal	5	6.8	Air	1
GC-H-2-A	High	2	2.7	Air	3
GC-H-5-A	High	5	6.8	Air	1
GC-N-2-W	Normal	2	2.7	Water	3
GC-N-5-W	Normal	5	6.8	Water	1
GC-H-2-W	High	2	2.7	Water	3
GC-H-5-W	High	5	6.8	Water	3

4.1.2 Material Properties

Blocks

Half-scaled blocks were used due to the limited capacity of the available testing frame. The C-shaped blocks were tested for compressive strength according to requirements of CSA A165 (2014) and ASTM C140 (2015). ASTM C140 indicates that coupons should be cut from the unit and tested in the case of units that have unusual size or shape, such as open end and pilaster units. Each coupon shall have a height to thickness ratio of two to one and a length to thickness ratio of four to one. Therefore, 5 coupon specimens were cut of dimensions 100 mm (length) x 50 mm (height) x 25 mm (thickness). The coupons were tested for compressive strength in the same direction of the actual loading as shown in Figure 4.4 (a). As shown in Table 4.4, the average compressive strength was 22 MPa with computed coefficient of variation of 13.8%.

(a) **(b)** **(c)**

Figure 4-4 Compression test for: (a) Concrete block coupon, (b) Mortar cube, (c) Grout cylinder

Table 4.4 Materials properties

Item	Batch #	Ultimate Load (kN)	Compressive Strength (MPa)	C.V.	Number of Specimens
C-shaped Block	-	55.0	22.0	13.80%	10
Mortar	-	30.8	12.3	7.15%	12
Grout (NS)	Batch 1[a]	117.0	14.9	8.70%	3
	Batch 2[b]	122.5	15.6	4.34%	6
Grout (HS)	Batch 1[a]	353.0	45.0	4.75%	3
	Batch 2[b]	361.1	46.0	6.41%	6

[a]Batch 1 used for fully-grouted boundary element prisms.
[b]Batch 2 used for grout-core specimens.

Mortar

Prebagged type S mortar was used for joining the C-shaped block units in the shells and the grouted C-MSBEPs. The mortar joints thickness was approximately 5 mm each. The compressive strength of the mortar was evaluated according to CSA A179 (2014). Six 50 mm mortar cubes were tested for compressive strength for each mortar batch as shown in Figure 4.4 (b). The average compressive strength was 12.3 MPa with coefficient of variation equals to 7.15% (Table 4.4).

Grout cylinders

Three cylinders were sampled from each grout batch. The cylinders had 100 mm diameter and 200 mm height. The grout was tested for compressive strength according to CSA A179 (2014) as illustrated in Figure 4.4 (c). All the cylinders were cured in water before testing. The grout cylinders were capped by high-strength gypsum as specified by ASTM C617 (2014). Due to the large number of samples two grout batches have been used. The average compressive strength of the high strength grout was 45.2, and 46.0 MPa with 4.75, and 6.41% coefficient of variation for the first and second batches, respectively. As shown in Table 4.4, the first batch was used in the construction of the fully grouted masonry prisms. However, the second batch was used in the construction of the grout prisms. High slump grout was used to avoid gaps or voids in the grouted core. The prisms were filled by grout in three layers with thorough compaction for each layer.

The stress-strain responses for the normal and the high strength grouts' cylinders are shown in Figure 4.5. The testing was carried out under displacement-controlled loading. A rate of 0.005 mm/sec was utilized in the current study up to a 0.002 axial strain. After that, a slower rate of

0.001 mm/sec was applied to capture the post-peak response. The change in displacement was measured by linear variable differential transformers (LVDTs). Two LVDTs were positioned diametrically opposite to one another. The gauge length was half the height of the cylinder (100 mm). The gauge lines were parallel to the axis of the cylinder and centered about its mid-height following the requirements of ASTM C469 (2014). The peak stress for the normal strength grout occurred at a strain of 0.002 while the peak stress for the high strength grout occurred at a strain of 0.0028. The initial stiffness for the high strength grout was 18.71 GPa which is more than double that of the normal strength grout (7.52 GPa).

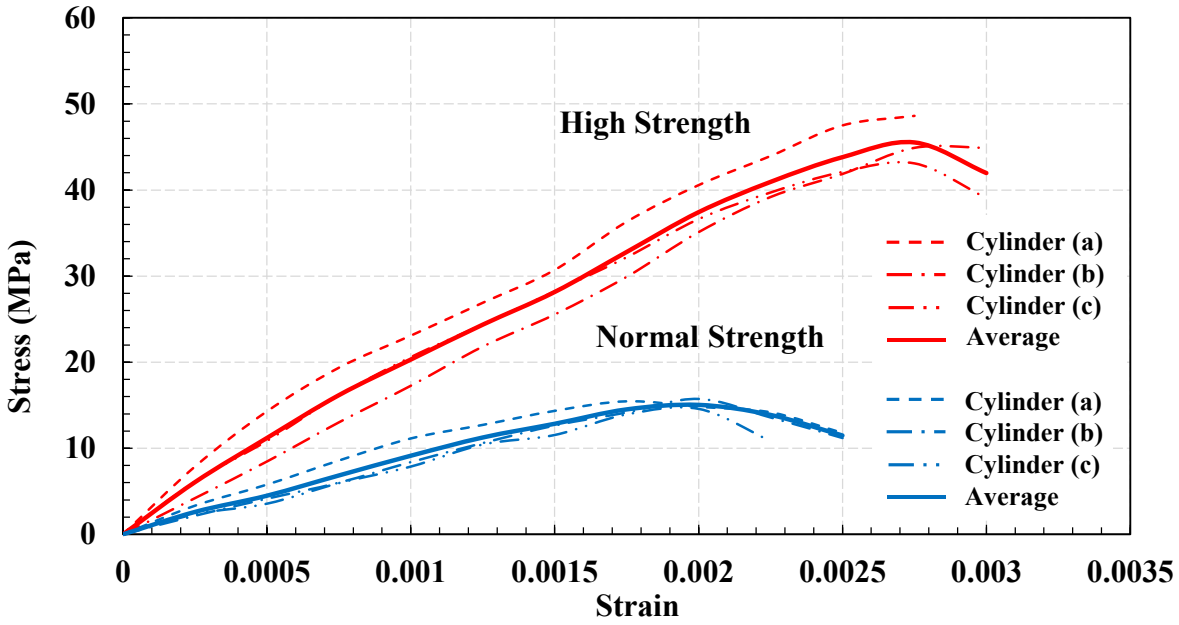

Figure 4-5 Stress-strain response of normal and high strength grout cylinders

4.1.3 Test Setup, Instrumentation, and Loading protocol

All specimens were tested in servo-controlled 2000 kN reaction frame under quasi-static concentric compression loading up to failure. High-strength gypsum was used between the upper and lower steel plates and the sample to ensure sample leveling and to prevent any voids between the specimen and the loading plates. The plates' dimensions and material followed the requirements of CSA S304 (2014). The verticality of the specimens was checked by two laser aligning devices positioned in two perpendicular directions. A spherical-head was situated between the top of the specimen and the loading cylinder. The spherical-head was checked before each test that it is free to tilt in any direction and that it is centered with the upper plate

and the sample. At least four LVDTs were used to measure the displacement across the full height of all the specimens. The LVDTs were positioned so that there is one LVDT centered on each side of the tested prism. The full test setup can be seen in Figure 4.6.

(a) **(b)** **(c)** **(d)**

Figure 4-6 Test setup and instrumentation for masonry prisms and shells having *h/t* ratio of: (a) two, (b) five, and grout core represents the grout in BE prism with *h/t* of: (c) two, and (d) five

Similar to the cylinders testing, a rate of 0.005 mm/sec was utilized during testing up to a 0.002 axial strain. A slower rate of 0.001 mm/sec was applied after that to capture the post-peak response. It is worth noting that following the above loading rate fulfilled the CSA S304 (2014) limits for most of the specimens. Nonetheless, it was decided to use the same loading protocol for all specimens to rule out the effect of changing the loading rate on the resulting stress-strain response.

4.2 Results and observations

4.2.1 Fully-grouted Boundary Element Prisms (high strength grout)

The observed failure patterns at the end of the tests of the first set of specimens, fully-grouted masonry boundary element prims, can be found in Figure 4.7. A splitting failure was observed

for the C-MSBEPs with h/t = 5.0 and high strength grout (BE-H-5). The splitting failure started with vertical cracks in the vertical joints after reaching the maximum load followed by partial spalling of the C-shaped units initiated by the expansion of the grout core. For all specimens, no buckling was observed during testing till the failure. The final failure mode was vertical splitting cracks along the four sides, with the sides containing the vertical mortar joints having bigger and longer cracks, accompanied by partial spalling of the blocks and the crushing of the grout core.

Figure 4-7 Observed failure patterns for the fully-grouted C-MSBEPs of h/t = 5.0 (a) front, (b) right, (c) back, and (d) left

Figure 4.8 shows the stress-strain relationship of the individual specimens tested along with the average relationship for each category of BE prisms. The average relationship was calculated by averaging the stresses at each strain level for all the specimens in each category. It is worth mentioning that these stresses are the average stresses observed against the strains measured by the four LVDTs on the four sides of each specimen at each strain level. The stresses were calculated based on the gross area of the specimen (i.e. 36100 mm^2). The results of testing the C-MSBEPs are summarized in Table 4.5.

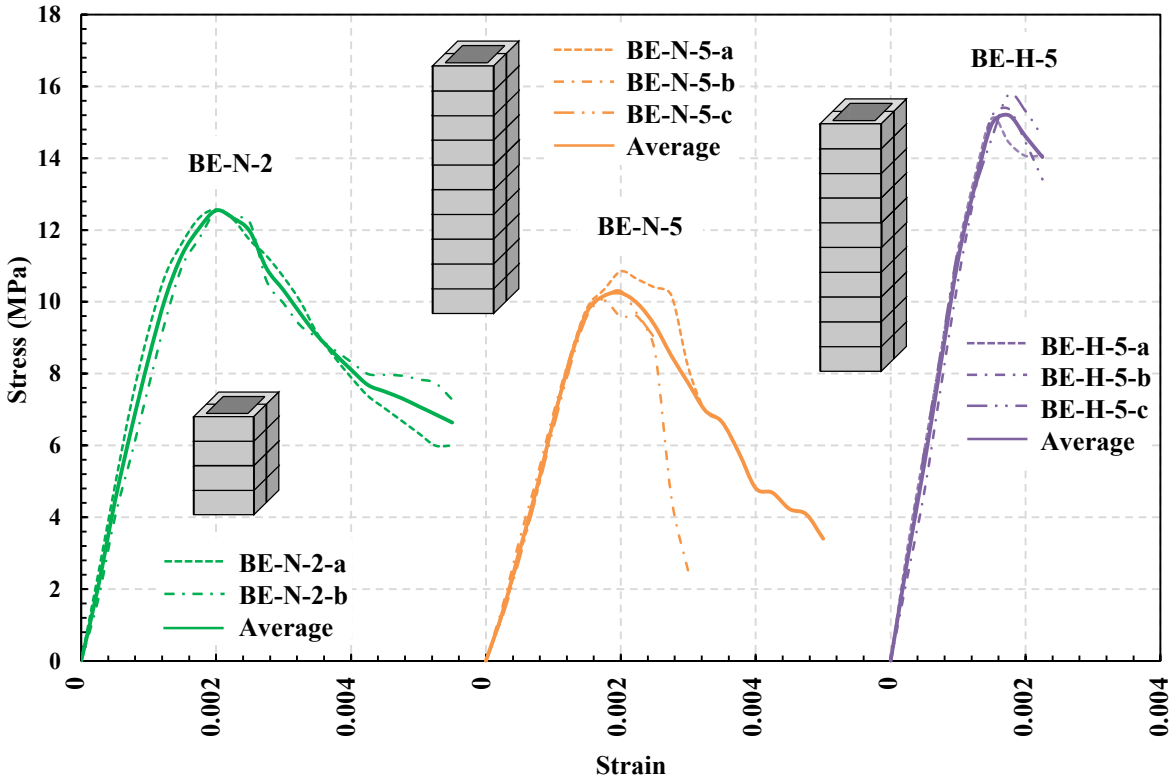

Figure 4-8 Stress-strain curves for masonry boundary element masonry prisms C-MSBEP

Table 4.5 Results of tested masonry boundary element prisms C-MSBEP

ID	Ultimate Load (kN)	Strength (MPa)	C.V.	Strain at Peak	C.V.	Elastic Modulus (GPa)	C.V.
BE-N-2	457.0	12.66	0.28%	0.0020	2.83%	8.88	14.14%
BE-N-5	380.5	10.54	2.83%	0.0019	9.03%	6.15	9.22%
BE-H-5	563.2	15.60	2.43%	0.0016	6.31%	10.98	12.03%

The effect of increasing the grout strength can be observed by comparing BE-H-5 to BE-N-5. Trebling the grout core compressive strength from 14.9 MPa to 45 MPa, increased the peak stress by 50%. Considering that the grout core area is approximately half the gross area of the prism, this increase value indicates the invalidity of applying the superposition principle without the need for reduction factors. Increasing the grout strength also led to a stiffer prism by increasing the elastic modulus by almost 1.8 times (from 6.15 GPa to 10.98 GPa). However, this increase in stiffness had a slight effect on peak strain.

4.2.2 Un-grouted Boundary Element Shells

The observed failure patterns at the end of the tests of the un-grouted masonry boundary element prims are shown in Figure 4.9. The patterns for the shells of h/t = 2.0 (SH-0-2) was a shear mode conical shaped failure pattern. On the other hand, a splitting failure was observed for the shells of h/t = 5.0 (SH-0-5). The splitting failure started with vertical cracks in the vertical joints after reaching the maximum load followed by the fracture of the C-shaped units. For all specimens, no buckling was observed during testing till the failure.

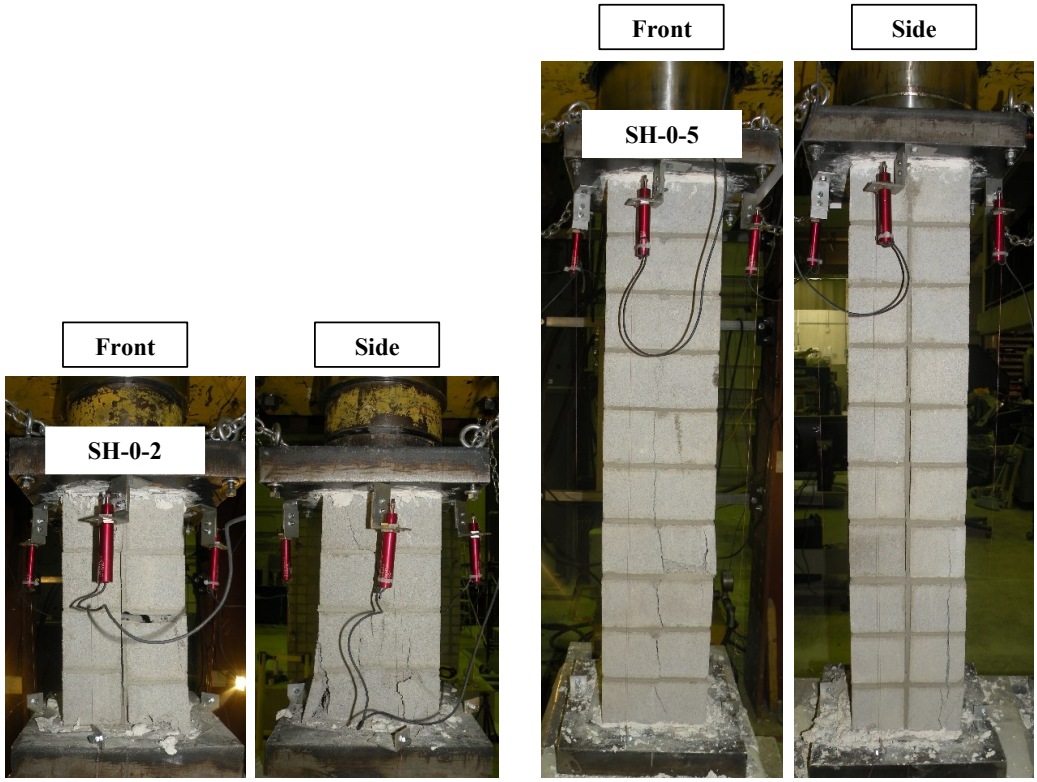

Figure 4-9 Observed failure patterns for the un-grouted BE shells SH-0-2 and SH-0-5

The stress-strain relationships for the second group of specimens, un-grouted C-MBE shells, are illustrated in Figure 4.10. The stress-strain relationships of the individual specimens in each category as well as the average relationships were calculated similar to the procedure adopted for the fully-grouted masonry BE prims. However, the area used for stress calculations for these shells is the net area of the prisms (i.e. 190 mm x 190 mm – 140 mm x 140 mm = 16500 mm^2).

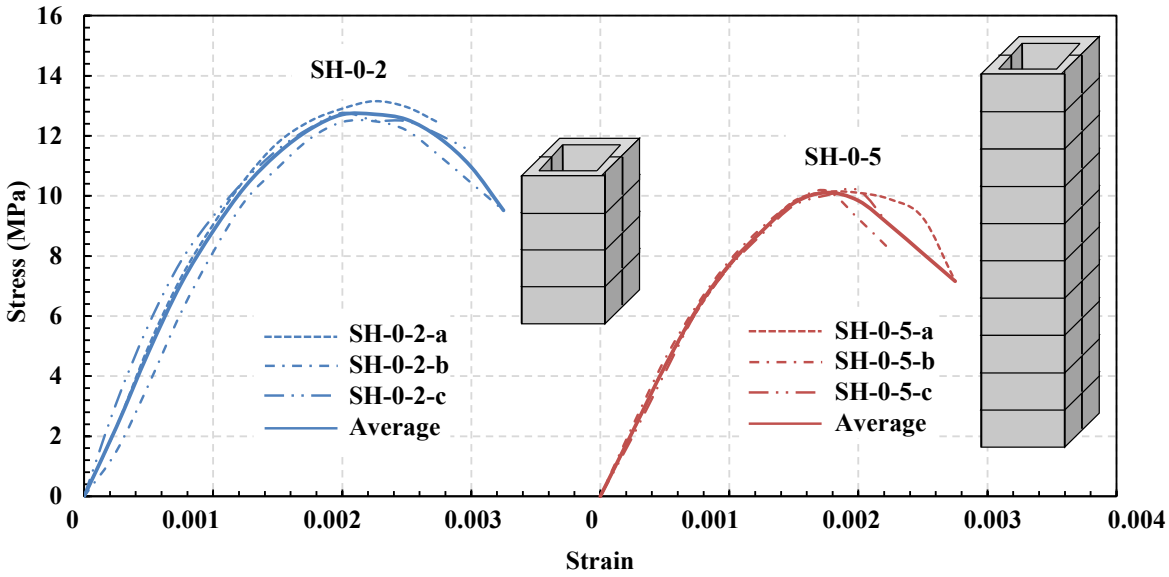

Figure 4-10 Stress-strain curves for un-grouted masonry shells (stress computed based on net areas)

The results of testing the un-grouted masonry BE shells are summarized in Table 4.6. Similar to the results of the grouted prisms, the platen effect is evident in the response and results of the ungrouted prisms. The average peak stress for the prisms of h/t = 2.0 (13 MPa) is 1.25 times that of the prisms of h/t = 5.0 (10.37 MPa). The average peak strains for both sets of prisms are around 0.002. The ratio of 1.25 is also comparable to the 1.2 corresponding to the grouted prisms. It can be concluded that shells and grouted prisms of h/t = 2.0 and 5.0 are affected by the platen confinement in the same manner.

Table 4.6 Results of un-grouted masonry prisms (shells)

ID	Ultimate Load (kN)	Strength (MPa)	C.V.	Strain at Peak	C.V.	Elastic Modulus (GPa)	C.V.
SH-0-2	214.5	13.0	1.90%	0.0021	8.31%	9.42	12.43%
SH-0-5	171.1	10.37	1.09%	0.0018	7.95%	8.32	1.92%

4.2.3 Grout Core Prisms

The stress-strain relationships of the grout-core prisms are presented in Figures 4.11 to 4.14. The figure shows the stress, computed as the measured load divided by the core area (i.e. 140 mm x 140 mm = 19600 mm^2), against the average longitudinal strains (i.e. average of the four LVDTs readings). All the grout cores did not show any visible cracking before failure. The

specimens resisted the loads applied while being intact till the brittle failure which was more intense in the high strength grout specimens. The results of testing the grout cores are summarized in Table 4.7. It should be noted that calculating the coefficients of variation was not applicable for the specimen sets GC-N-5-A, GC-N-5-W and GC-H-5-A. This was dictated by the fact that 2 specimens in each set were damaged before testing which highlights the fragility of these unreinforced and slender specimens.

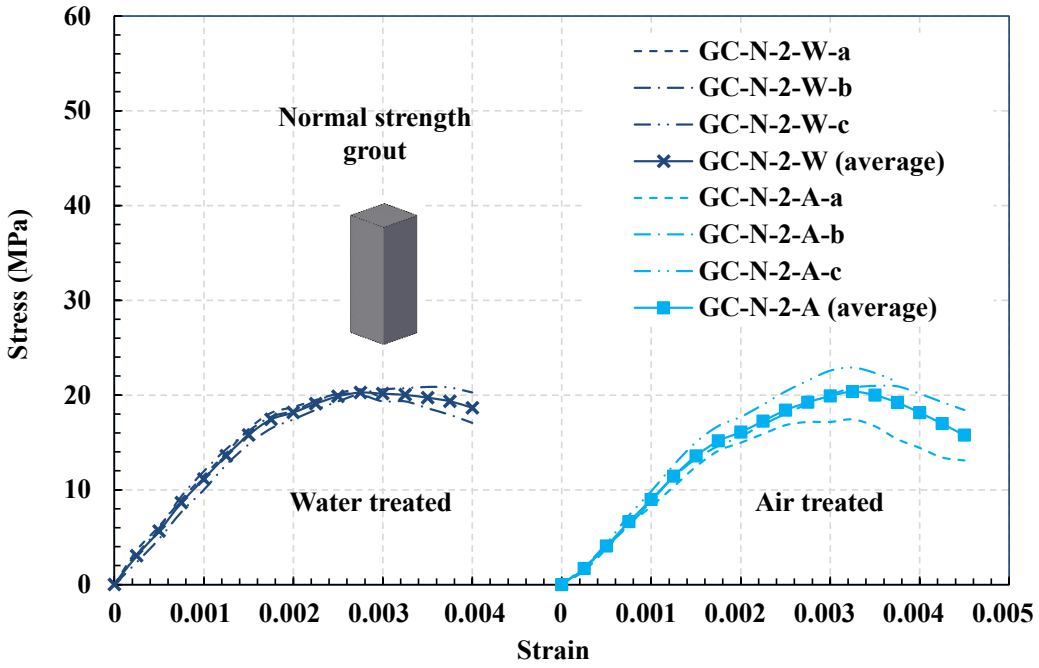

Figure 4-11 Stress-strain curves of normal strength grout cores representing the cores of BE prisms with $h/t = 2.0$

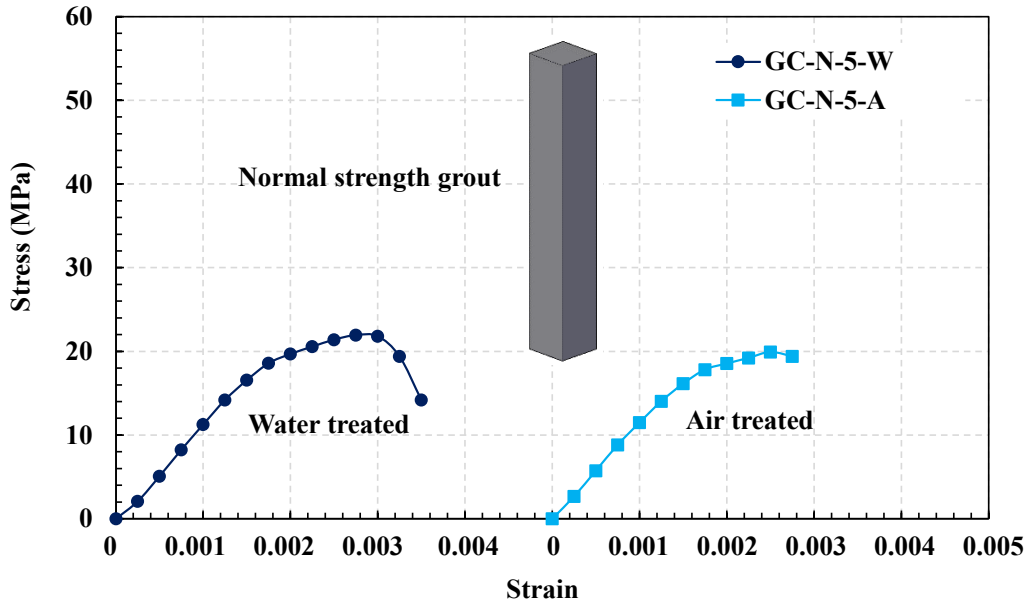

Figure 4-12 Stress-strain curves of normal strength grout cores representing the cores of BE prisms with $h/t = 5.0$

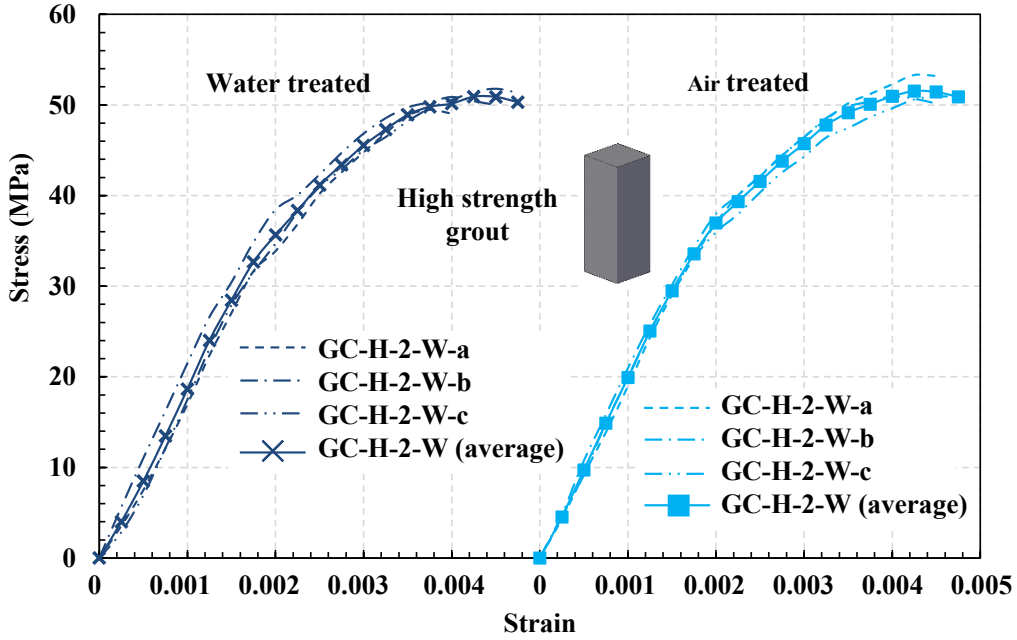

Figure 4-13 Stress-strain curves of high strength grout cores representing the cores of BE prisms with $h/t = 2.0$

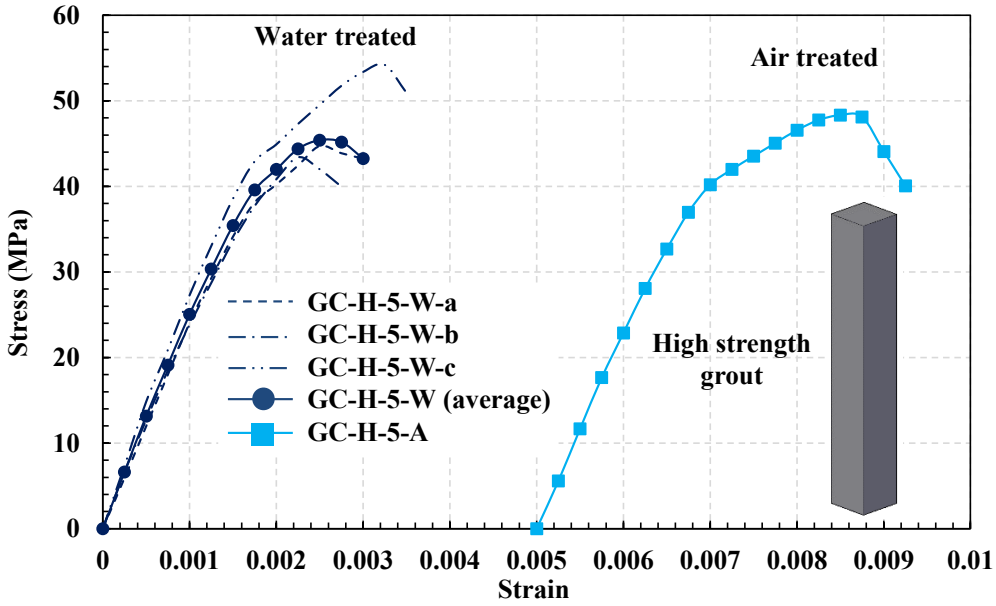

Figure 4-14 Stress-strain curves of high strength grout cores representing the cores of BE prisms with $h/t = 5.0$

Table 4.7 Results of tested grout core specimens

ID	Ultimate Load (kN)	Strength (MPa)	C.V.	Strain at Peak	C.V.	Elastic Modulus (GPa)	C.V.
GC-N-2-A	402.8	20.55	13.61%	0.0034	5.81%	8.97	9.04%
GC-N-5-A	392.0	20.00	N/A	0.0025	N/A	10.65	N/A
GC-H-2-A	1018.8	51.98	2.76%	0.0043	3.97%	19.42	9.15%
GC-H-5-A	948.1	48.37	N/A	0.0034	N/A	22.28	N/A
GC-N-2-W	405.0	20.66	1.63%	0.0030	17.69%	11.27	11.79%
GC-N-5-W	437.1	22.30	N/A	0.0028	N/A	8.37	N/A
GC-H-2-W	996.7	50.85	2.17%	0.0041	8.16%	17.96	17.59%
GC-H-5-W	935.1	47.71	12.28%	0.0026	15.31%	26.44	10.54%

The average peak stress of the water cured grout cores of $h/t = 2$ (GC-N-2-W) is only 0.5% higher than the average peak stress of the air cured cores (GC-N-2-A) and is 7.4% lower than the average peak stress of the core specimen of $h/t = 5$ (GC-N-5-W). The average peak stress of the water cured grout cores of $h/t = 5$ (GC-N-5-W) is 11.5% more than the average peak stress of the air cured cores (GC-N-5-A). The average peak stress of the water cured grout cores of $h/t = 2$

(GC-H-2-W) is 2.2% less compared to the average peak stress of the air cured cores (GC-H-2-A) and is 6.6% more compared to the water cured grout cores of h/t = 5 (GC-H-5-W). Finally, the average peak stress of the water cured grout cores of h/t = 5 (GC-H-5-W) is 1.4% less than the average peak stress of the air cured cores (GC-H-5-A).

No significant difference observed between specimens cured in water and these left to cure between the blocks. This can be explained in the light of the assumption presented in the study of Sturgeon et al. (1980) that the surrounding blocks retain the mixing water for the grout cores. This is supported by the fact that after the failure of the cores in this study, the core specimens were found to be moist from the inside. The platen effect on the peak stress is less obvious in the grout cores than the shells and grouted prisms. This is attributed to the actual h/t of the shorter grout-core prisms being close to 3.0. This h/t combined with length-to-thickness ratio of 1.0, results in peak stresses that are approximately equal to these of the longer prisms (Hassanli et al. 2015).

4.3 Comparing C-MSBEP strength with available prediction equations

The ultimate strength of the grouted and un-grouted C-MSBEPs are plotted against the grout strength based on the grout core and cylinder strength in Figure 4.15. It should be noted that the un-grouted C-MSBEPs strength is calculated based on the gross area of the prism for consistency with grouted C-MSBEPs results. It can be observed from the figure that the strength of the BE prisms increases with the increase of the grout strength. However, the contribution of the grout strength to the C-MSBEPs strength tends to decrease at high strength levels. Hamid et al. (1978), Sturgeon et al. (1980), Priestley and Chai Yuk Hon (1984), and Sarhat (2016) represented this relationship through linear regression best fit model, nonetheless, each recommended different slope based on the hypothesis and the available database.

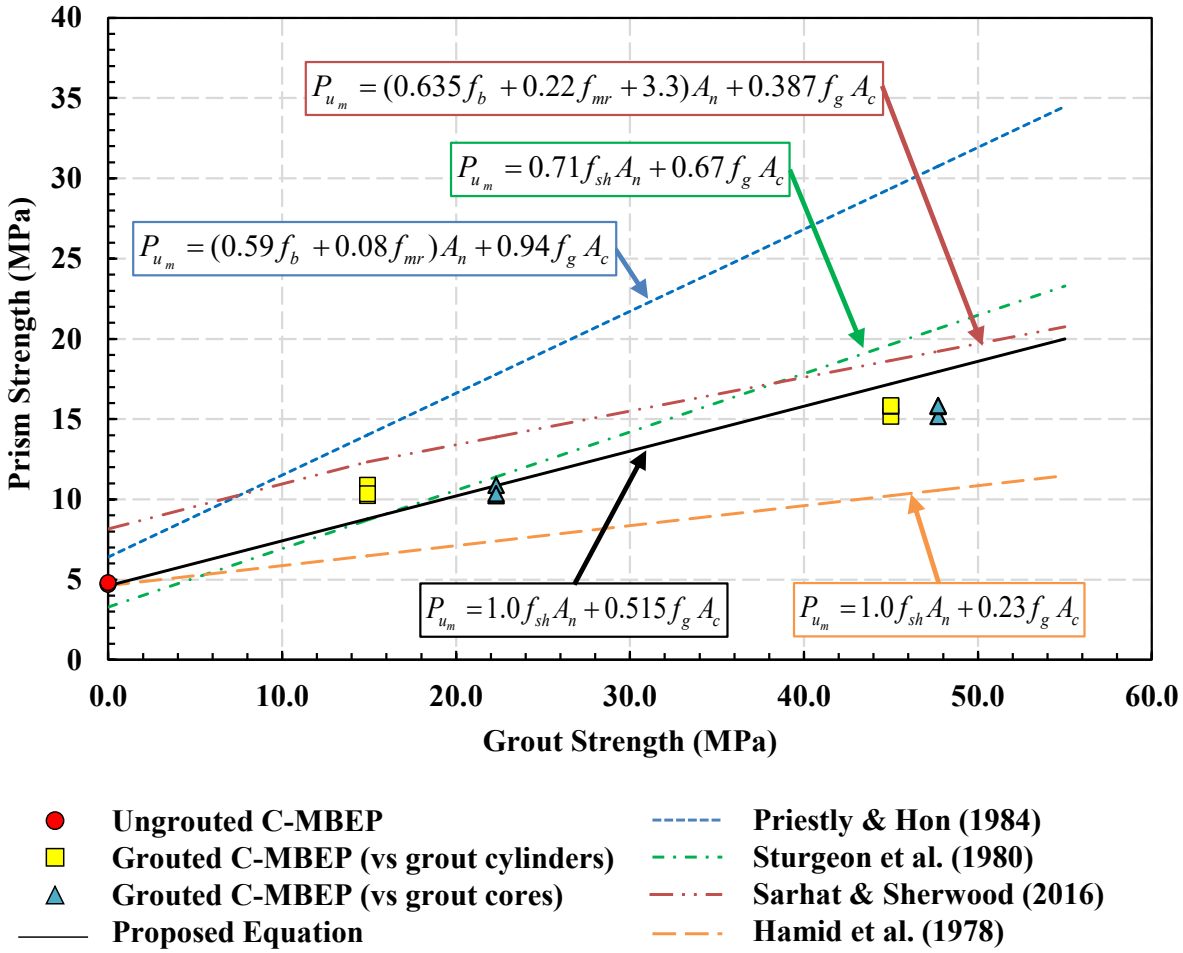

Figure 4-15 C-MSBEP ultimate strength (h/t = 5.0) against the prediction relationships using the grout strength of the tested cores and cylinders

4.3.1 Hamid et al. (1978)

The linear equation of Hamid et al. (1978) was based on an experimental work done on full-scale single core stretcher block prisms having h/t = 3. Hamid et al. (1978) presented a linear regression equation based on the peak stresses resulted (Eq. 4.1). Hamid et al. (1978) suggested that the shell strength was not permitted to develop fully due to the lateral expansion of the grout leading to a reduced contribution from the shell to the prism strength. However, this was not reflected in the relationship of Hamid et al. (1978), as it can be observed that the shell strength developed fully, and the grout was the constituent that failed prematurely (Eq. 4.2).

$$f_m = (\eta + 0.143 f_g / \mu f_b) f_{sh} \quad \text{(MPa, Grout cylinder)} \tag{4.1}$$

$$P_{u_m} = 1.0 f_{sh} A_n + \left(\frac{0.143}{(1-\eta)\mu f_b} f_{sh} \right) f_g A_c \quad (4.2)$$

η : Masonry block solid ratio (A_n / A_g) which equals 0.457,

μ : Cylinder to molded prism conversion factor (Hamid et al. 1978) which equals 0.553,

f_b : Masonry block peak stress which equals 22 MPa,

P_{u_m} : Masonry prism peak load (kN).

Substituting for η, μ, f_b and f_{sh} with the values from this experimental work Eq. 4.3 is reached.

$$P_{u_m} = 1.0 f_{sh} A_n + 0.23 f_g A_c \quad (4.3)$$

The equation predicts that the grout contributes by only 23% of its strength. As shown in Figure 4.15 the equation of Hamid et al. (1978) is the most conservative relationship which underestimates the peak stresses of the grouted C-MSBEPs. It is worth noting that the values computed by Eq. 4.3 and presented in Figure 4.15 were multiplied by a reduction factor of 0.9 to account for the different *h/t* ratio as recommended by CSA S304 (2014).

4.3.2 Sturgeon et al. (1980)

The equation of Sturgeon et al. (1980) was based on an experimental work done on full-scale pilaster block prisms of *h/t* = 2. From the results of the tested prisms, Sturgeon et al. (1980) deduced linear regression equations relating prism strength to grout strength. The stresses and loads equations are reproduced here in Eq. 4.4 and 4.5. As shown in Eq. 4.5, almost 70% of the grout strength is contributing to the masonry prism strength. It is worth noting that the values computed by Eq. 4.5 were multiplied by a factor of 0.85 to obtain the compressive strength of a prism having *h/t* = 5.0 as recommended by CSA S304 (2014).

$$f_m = 0.41 f_g + 2.94 \quad \text{(MPa, Gross Area)} \quad (4.4)$$

$$P_{u_m} = 0.71 f_{sh} A_n + 0.67 f_g A_c \quad (4.5)$$

This finding contradicts the regression equation established before by Hamid et al. (1978). Sturgeon et al. (1980) argued that it is the grout not the shell that was not permitted to fully develop its strength in the prisms tested by Hamid et al. (1978). This suggests that lateral expansion and excessive cracking caused the grout to fail before the full development of the shell capacity. On the other hand, according to Sturgeon et al. (1980) equation, the grout can develop up to 67% of its capacity and the shell is able to develop up to 71% of its capacity (Eq. 4.5). Sturgeon et al. (1980) suggested that this discrepancy can be explained by comparing the (net area/gross area) for both prisms. For the pilaster units used in Sturgeon et al. (1980) experimental work, this ratio was 0.393 while for the single core masonry units used by Hamid et al. (1978), the ratio is 0.623. Thus, it was suggested that due to the higher net area to gross area, the lateral strains of the grout in his specimens were able to induce significant tensile stress on the shell causing their premature failure. This hypothesis may explain the different values for the contribution of the shell in the two experimental programs. It is worth mentioning that the ratio of net area to gross area for the half-scaled C-shaped masonry units tested in this study is 0.457. This value falls in between the two values mentioned earlier and the results for the grouted prisms falls in between the two equations.

4.3.3 Priestley and Chai Yuk Hon (1984)

The relationship presented in Eq. 4.6 is based on an analytical study by Priestley and Chai Yuk Hon (1984). The ability of the equation to predict the compressive strength of the masonry prisms was assessed against five experimental studies including Hamid et al. (1978). This relation suggests a larger contributions of grout strength to the prism strength compared to the relationships of Hamid et al. (1978) and Sturgeon et al. (1980). Also, the equation considers the contribution of the mortar peak stress, f_{mr}, separately. It is worth mentioning that this equation is adopted by the New Zealand standards to predict the prism strength (NZS 2004).

$$f_m = 5.871\eta(0.1f_b + 0.0136f_{mr}) + 0.9375f_g(1-\eta) \tag{4.6}$$

$$P_{u_m} = (0.5871f_b + 0.08f_{mr})A_n + 0.9375f_g A_c \tag{4.7}$$

f_{mr} : Mortar peak stress which equals to 12.9 MPa in this study,

As shown in Figure 4.15, the equation of Priestley and Chai Yuk Hon (1984) highly overestimated the grouted C-MSBEP especially at high level of grout strength. One of the main assumptions on which the equation was built is that the shell peak stress occurs at 0.0015 strain while the grout core peak stress occurs at a strain of about 0.0020. Therefore, a factor of 0.9375 should be multiplied by the strength of the grout core in the equation. By observing Table 6 and Table 7, it can be noticed that the shell peak stress was developed at strain 0.0018 and 0.002 for prisms of *h/t* of 2 and 5, respectively. In addition, the peak stress in the grout cores was developed at higher strain values than the strains for the shell. Therefore, in the current study a lower grout contribution to the prism strength is expected than that of Priestley and Chai Yuk Hon (1984).

4.3.4 Sarhat (2016)

Sarhat (2016) performed a regression analysis based on 171 average masonry compressive strength data points (624 individual prisms). The data points were collected from experimental studies conducted since 1977. Conversion factors were used to account for the different *h/t* values, mortar testing techniques and grout testing techniques. The compressive strength of the prisms ranged from 10 MPa to 50 MPa. The model of Sarhat (2016) is presented in Eq. 4.8. The model is valid for grouted prisms of range of: (a) block strength (based on net area) of 10 to 50 MPa, (b) cylinder grout strength of 10 to 50 MPa, (c) Area net ratio of 0.4 to 0.75, (d) mortar cube strength of less than 30 MPa. Moreover, this equation is limited to a maximum ratio of grout strength to block strength of 1.5 as recommended by Fortes et al. (2014). The loads equation was deduced from the stresses equation and is shown in Eq. 4.9.

$$f_m = 0.29 f_b + 0.1 f_{mr} + 0.21 f_g + 1.51 \quad \text{(MPa, Grout cylinder)} \tag{4.8}$$

$$P_{u_m} = (0.635 f_b + 0.22 f_{mr} + 3.3) A_n + 0.387 f_g A_c \tag{4.9}$$

The equation predicts that the grout contributes by nearly 40% of its strength. Figure 4.15 shows that the equation overestimates the peak stresses for the grouted C-MSBEPs. However, the predicted values are the closest to the experimental results compared to the other models. It is worth noting that the calculation of the point where grout strength equals zero (un-grouted shell) in Figure 4.15 for Sarhat (2016) was done by using the equation introduced by Sarhat and Sherwood (2014).

4.4 Grout cylinders versus grout core prisms stress-strain responses

The stress-strain response of the grout core prisms tested in this experimental work is compared to those of the grout cylinders (see Figure 4.16) for the normal and high strength grout. It is worth noting that the grout core prisms used in this comparison are the wet treated grout core prisms.

For normal strength grout, the cylinder stress-strain curve has a lower peak stress, peak strain and initial stiffness compared to the grout prism. The peak stress resulting from the grout cylinder is 0.76 and 0.7 of the peak stresses of the grout core prisms of *h/t* equal 2 and 5, respectively. This finding agrees with the finding of Drysdale and Hamid (2005) that the strength of molded grout prism is higher than that of the grout cylinder and contradicts the finding of Sturgeon et al. (1980) that the grout core prism strength is 0.74 that of the tested CSA grout cylinder. The peak strain resulting from the cylinder is 0.002 while the peak strains of the grout core prisms are 0.003 for *h/t* = 2 and 0.0028 for *h/t* = 5. This means that the peak strain of the grout core is about 1.5 times the peak strain of the cylinder. Also, the grout cylinder tends to be less stiff than the grout cores.

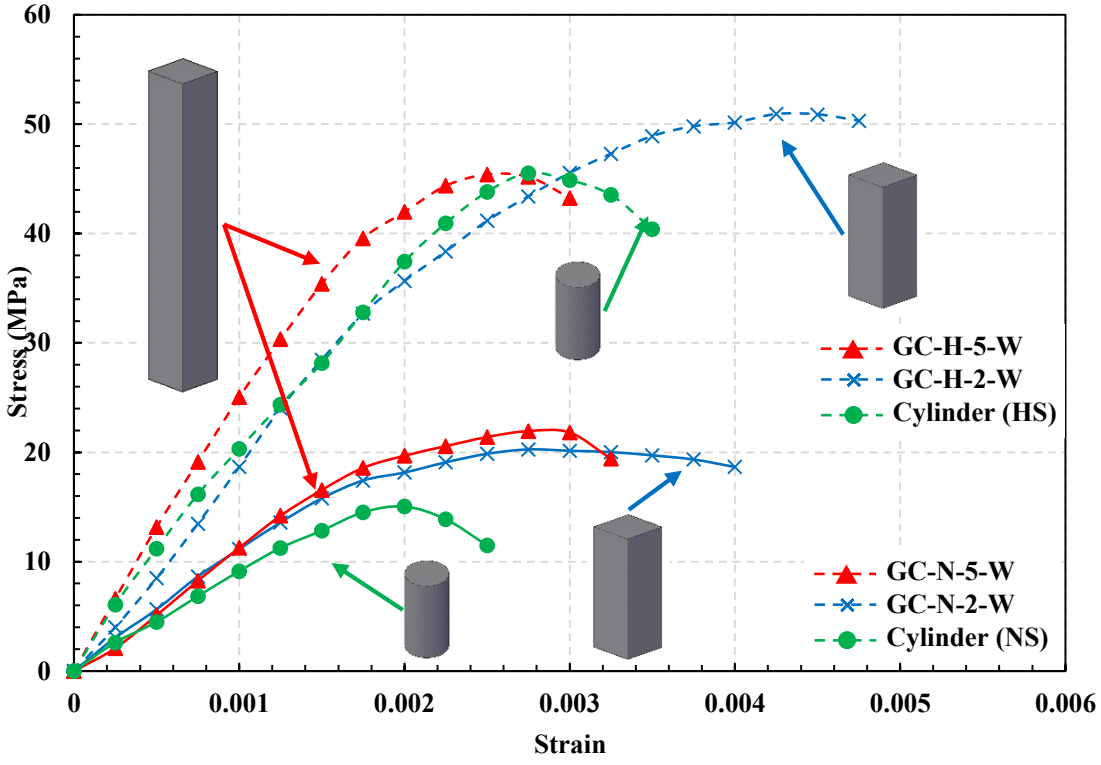

Figure 4-16 Comparison of average stress-strain curves of grout core prisms and grout cylinders

For high strength grout, the cylinder stress-strain curve is generally closer to that of the grout core prism of high aspect ratio. Although it tends to underestimate the initial stiffness, it has similar peak stress and strain. However, when compared to the grout core prism of $h/t = 2$, the cylinder tends to underestimate the peak stress and strain but agrees with the initial stiffness.

Grout core prisms simulate the shape and size of the actual grout core and the water absorption by the shell better than the grout cylinders. Nonetheless, it is believed that neither the grout core prisms nor the grout cylinders accurately replicate the actual grout core of the prism as both specimens neglect the initial lateral tension on the core generated by the shrinkage. This is mainly because the oiled mold walls in the case of the grout cylinders and the paper towels in the case of the grout core prisms hinder the simulation of the bond between the grout core and the shell.

4.5 Superposition of masonry shell and grout core load-displacement curves versus that of the tested boundary elements

The full load-displacement relationships of the BE prisms is compared against the load-displacement relationships of the corresponding shells and air treated grout cores in Figure 4.17. As shown in the figure, for various displacement levels the load resisted by the C-MBE shell is added to the corresponding grout core load to result in the superposition curve, which is compared to the C-MSBEP observed experimental load-displacement curve. The first clear observation is that for samples having $h/t = 5$, the load resisted by the grout core only is higher than that resisted by the corresponding prism. This can be observed by comparing the grout core ultimate load in Table 7 to the C-MSBEP ultimate load in Table 5 even without adding any contribution from the masonry shell. This observation is even clearer in high strength samples where GC-H-5-A and GC-H-5-W resisted almost 400 kN more load than BE-H-5, i.e. 70% more than the prism capacity. It can also be observed from Figure 4.17 that the prism peak strength is achieved at strain comparable to the masonry shell peak strain similar to what was observed by Priestley and Chai Yuk Hon (1984).

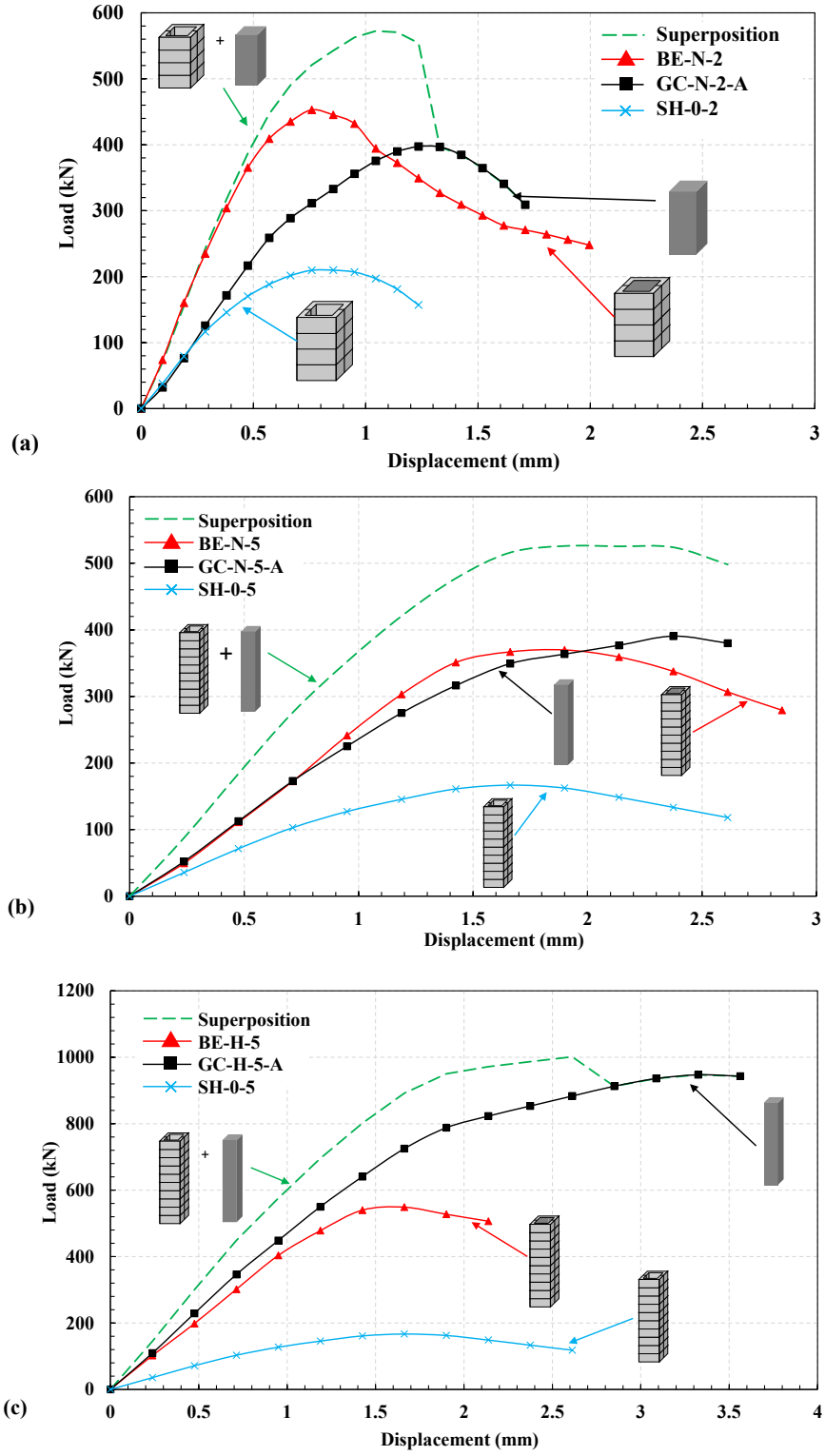

Figure 4-17 Comparison of the load-displacement relationships of BE shells, grouted BE prisms, grout cores, and the superposition: (a) C-MSBEPs having h/t = 2.0 and grouted by normal strength grout, (b) C-MSBEPs having h/t = 5.0 and grouted by normal strength grout, (c) C-MSBEPs having h/t = 5.0 and grouted by high strength grout.

For the BE prisms of normal strength grout and $h/t = 2$, there is a good agreement between the superposition relationship and the tested prism relationship nearly until the cracking of the shell. After that, the superposition overestimates the resistance of the prism with the increase in axial displacement. In other words, the superposition fails to detect the post-peak phase of the prism load-displacement relationship. For the BE prisms of normal strength grout and $h/t = 5$, the superposition tends to overestimate the load capacity of the prism at any displacement. The overestimated load value (superposition load – tested load) tends to increase with the increase of the displacement. Also, the superposition fails in capturing the post-peak response of the prism. For the BE prisms of high strength grout and $h/t = 5$, the superposition tends as well to overestimate the load capacity at any displacement. This overestimation load value again increases with the increase of the displacement. The superposition failure in capturing the post-peak response of the prism is still visible.

4.6 Factors influencing the reduction of the grout stress-strain response in the grouted prism

This study was designed to assess the effect of the above discussed factors on the superposition of strength of the grout core and the shell. The experimental results discussed showed that the treatment (i.e. air versus wet) had negligible effect on the response of the grout core while the increase in the aspect ratio was found to decrease its strength. The CSA A179 (2014) grout cylinders results vary from the grout core prisms stress-strain response. In addition, the size and shape of the grout core were shown to affect the peak stress. However, as shown in the Figure 4.17 all these factors do not fully explain the failure of the grout core and masonry shell superposition in predicting the C-MSBEP load-displacement relationship.

The factor that is believed to have the most effect on the superposition is the bond failure at the interface between the grout and the masonry shell due to grout shrinkage. As shown in Figure 4.18, grout shrinkage causes cracks at the grout-masonry interface. The initial lateral strains acting on the grout perimeter result in decreasing the grout compressive resistance. This leads to less contribution from the grout core to the prism total strength.

This hypothesis would explain why the equation by Priestley and Chai Yuk Hon (1984) is adopted by the New Zealand standard (NZS 2004), even though this equation neglects any

reduction in the grout strength except for the lateral strain compatibility with the masonry shell as it is a common practice in New Zealand to add additives that reduce the grout shrinkage (Voon and Ingham 2006). Therefore, it could be said that Priestley and Chai Yuk Hon (1984) equation may be valid only if non-shrink grout is used.

This conclusion does not contradict with Hedstrom and Hogan (1990) observation that the ASTM molded grout strength matches the grout core strength with only 10% overestimation, because the core samples cut by Hedstrom and Hogan (1990) were from the center of the grout core with area about 33% of the total grout core. Therefore, this sample was away from the cracked area as shown in Figure 4.18. For the masonry prisms tested by Sturgeon et al. (1980), paper towels were used to prevent the bond between the core and the shell. Thus, the stripped core specimens tested showed higher axial compressive strength than the grout in the prisms. Finally, this hypothesis implies an important indication that both the CSA A179 (2014) grout cylinders and the ASTM C1019 (2014) grout prisms are not representative of the actual grout within the C-MSBEP. In addition, to enhance the C-MSBEP stress-strain response, and thus the $f_m^{'}$, the effect of shrinkage should be eliminated.

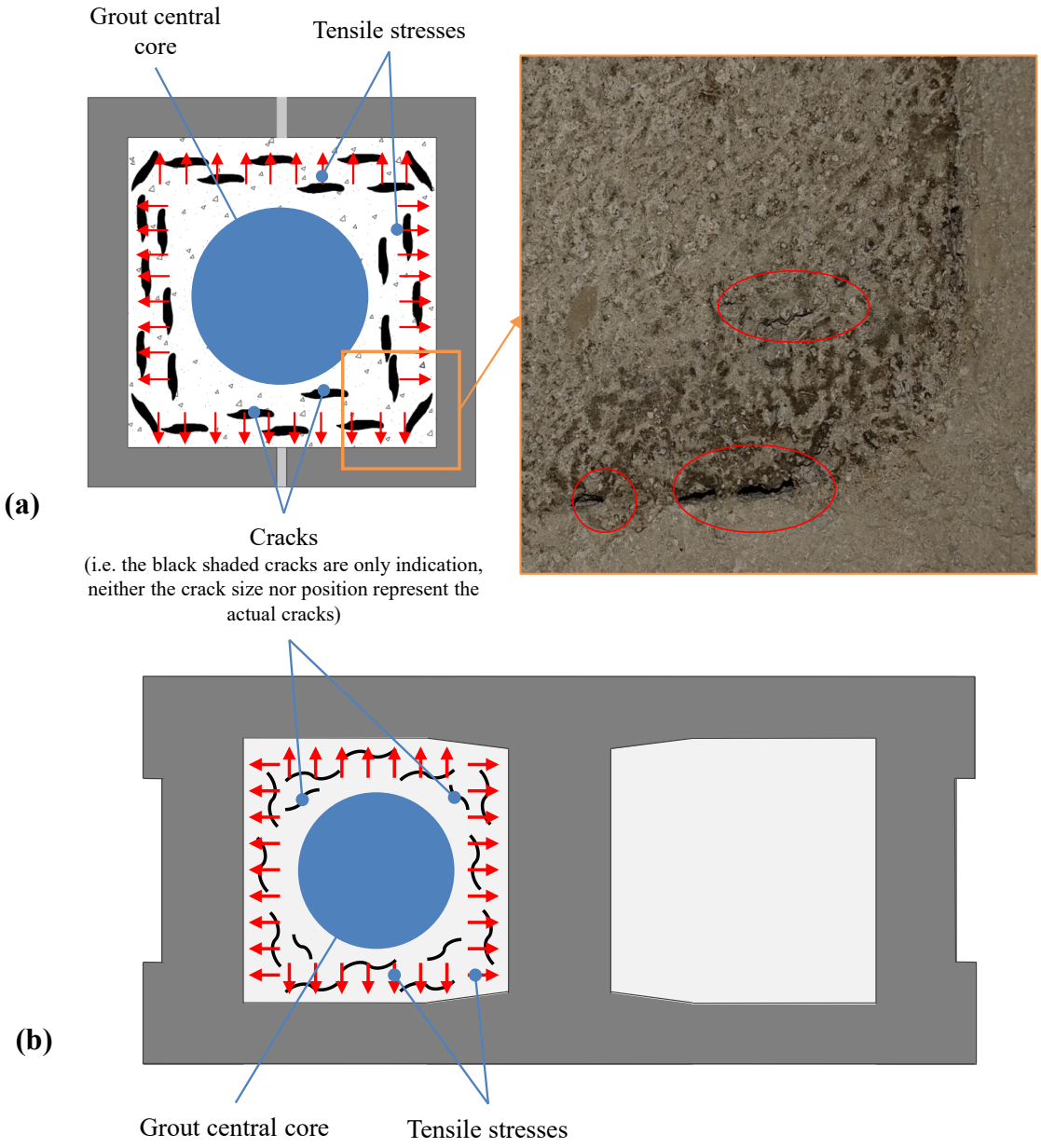

Figure 4-18 Cracked region in the grout cores of (a) Half-scale C-MSBEPs and (b) Full-scale stretcher block prisms

Based on the literature and the experimental work done in this study, a reduction factor α is introduced to the grout strength in Eq. 4.10. This factor α is the multiplication of six reduction factors to account for: shrinkage effect on the grout strength (α_{shr}), shape effect (α_{shp}), size

effect (α_{sz}), aspect ratio (*h/t*) (α_{ar}), water absorption (α_w), and the incompatibility of grout core and masonry shell ultimate strengths (α_{in}).

$$f_m A_g = \alpha f_g A_c + f_{sh} A_n \tag{4.10}$$

$$\alpha = \alpha_{ar}.\alpha_{in}.\alpha_{shp}.\alpha_{shr}.\alpha_{sz}.\alpha_w \tag{4.11}$$

Table 4.8 lists the preliminary value for each reduction factor (α_{ar} , α_{in} , α_{shp} , α_{shr} , α_{sz} and α_w) based on the literature and the experimental work done in this study. An illustration for these reduction factors is presented in Figure 4.19. The proposed equation is compared to the predictive equations discussed before and to the experimental results as shown in Figure 4.15.

The factor α_{shp} which accounts for the difference in shape between the actual grout core (prismatic) and the tested specimen according to CSA (cylinder) is proposed to be 1.5 as suggested by Drysdale and Hamid (2005). The factor α_{sz} which accounts for the difference in size between the tested specimens and the actual grout core is proposed to be 0.88. This value was deduced by comparing the experimental results in this study of the grout cylinders to these of the grout cores specimens of *h/t* = 2.0 and using the value 1.5 to eliminate the shape effect. The factor α_w which accounts for the fact that the actual grout core, unlike the cylinder, is treated inside the shell of the prism and not wet treated is proposed to be 0.98. This value is suggested by the average difference in resulting strength between tested grout core specimens treated between the blocks and these treated in water in this experimental work. The factor α_{ar} which accounts for the difference in aspect ratio between the tested specimen for strength evaluation (cylinder according to CSA or prism according to ASTM) and the actual grout core is proposed to be 0.83. The correction factor used by CSA to eliminate the platen effect between specimens of *h/t* = 5.0 and *h/t* = 2.0 is 0.85 while the correction factor used by ASTM for the same two aspect ratios is 0.82. Therefore, the value used here is chosen to be something in between. The factor α_{in} which accounts for the incompatibility between the stress-strain behaviours of the grout core and the shell is proposed to be 0.94 as suggested by Priestly and Hon (1984). The peak of the grout core occurs at larger strain than that of the shell's peak. At the onset of

reaching the shell's peak stress, the grout core specimens were found to reach percentages of their peak stresses that are close to the precentage suggested by Preistly and Hon (1984). Therefore, the value suggested by Preistly and Hon (1984) was adopted. Finally, the shrinkage is believed to be responsible for the remaining reduction of grout core strength. Therefore, the value for the factor α_{shr} was deduced accordingly and was found to be 0.56.

It should be noted that all the proposed values are preliminary values that need more experimental work in order to be adjusted and to study how these reduction factors can affect one another and how they change with the change in grout strength.

Table 4.8 Proposed values for grout strength reduction factors

Reduction factor	α_{ar}	α_{in}	α_{shp}	α_{shr}	α_{sz}	α_{w}
Proposed Values	0.83	0.94	1.5	0.56	0.88	0.98

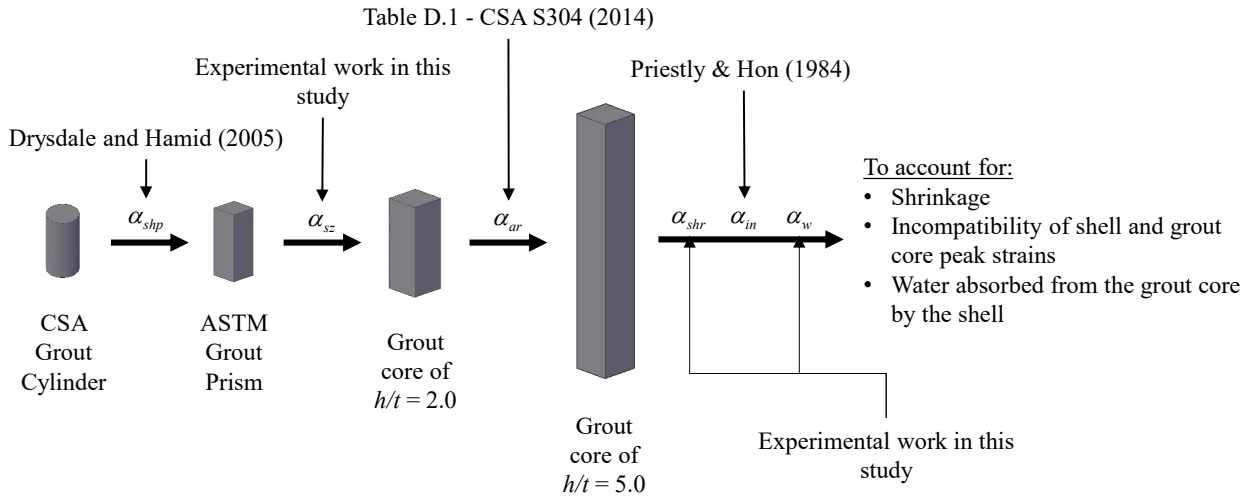

Figure 4-19 Illustration for the factors used in Equation 4.11

Chapter 5

SUMMARY, CONCLUSIONS AND FUTURE WORK

5.1 Summary

In this study, the compressive stress-strain response of half-scale fully-grouted C-MSBEPs and its constituents (i.e. masonry shells and grout cores) are studied and compared to that of half-scale fully-grouted stretcher block prisms. The study investigated the requirements for sampling and testing of prism components as well as the requirements for construction techniques and testing of the prisms in Canadian and US standards. The unit strength method values in these two standards were also considered in the study. In total, 8 fully-grouted masonry prisms, 6 un-grouted masonry shells, 18 grout cores, 9 running-bonded fully-grouted stretcher block prisms, and 9 stack-bonded fully-grouted stretcher block prisms were tested under concentric compression loading up to failure. The matrix includes two prisms' aspect ratios, namely two and five, and two grout strengths, normal (15 MPa) and high (45 MPa) strength. The requirements of the Canadian and US standards for prism construction and testing were summarized and compared and any similarities and discrepancies between the two masonry design standards were highlighted. The effect of these requirements on the masonry compressive strength, f_m, were investigated. Moreover, the unit strength method values in these two standards were evaluated against the experimental results. The effect of prism height to thickness ratio and the block geometry (stretcher versus C-shaped) on the stress-strain relationship of masonry prisms were examined. The experimental results were used to evaluate the predictive ability of four prism compressive strength predictive equations from the literature. The effect of grout height to thickness ratio, grout sample shape and size (cylinder and prism) and grout treatment, air and wet, on the stress-strain relationship was examined on the grout samples. The study provides a simple equation for predicting the peak stress of C-MSBEPs and analytical models for predicting the stress-strain response of CSA and ASTM standard stretcher block prisms and C-MSBEPs.

5.2 Conclusions

The ASTM C1314 (2014) requirements for prism construction affect the resulting f_m. Considering a standard prism *h/t* = 5.0 instead of 2.0 will lead to a failure mode that resembles the mode observed in actual construction. Increasing the prism *h/t* to 5.0 ensures that the prisms are not confined by the loading machine platens during testing. In addition, allowing the prism construction to simulate the actual wall construction in terms of bond pattern used (i.e. stack or running), averts overestimating f'_m when the running bond is used for the actual construction.

Based on the results of the experimental work done, the masonry prisms of *h/t* = 2.0 showed significant increase in peak stress compared to these of *h/t* = 5.0 for the three types of fully-grouted masonry prisms. The effect was least significant on the C-MSBEP peak stress (20% increase compared to 32% in the case of running-bonded stretcher block prisms and 41% in the case of stack-bonded stretcher block prisms). This is attributed to the C-MSBEPs having *l/t* = 1.0 while the stretcher block prisms having *l/t* = 2.0 as shown by Hassanli et al. (2015).

Stretcher block prisms of the same aspect ratio, mortar bedding and block pattern as C-MSBEPs exhibit dissimilar stress-strain responses. C-shaped blocks creates a vertical continuous side-joints and grout core which alter the stress-strain response of the masonry prism resulting in lower peak stress and initial stiffness but higher peak strain.

The standard stretcher block prism and standard C-MSBEP constructed by following the requirements of ASTM C1314 (2014) were found to have significantly different stress-strain responses. The stretcher block prism showed peak stress and peak strain that are 38% and 50% more than these of the C-MSBEP, respectively. This suggests that both stretcher block prism and C-MSBEP shall be tested for a total evaluation of the masonry compressive strength for RMSW with C-MBEs following ASTM requirements. On the other hand, the similarity between the stress-strain responses of the standard stretcher block prism and standard C-MSBEP constructed by following the requirements of CSA S304 (2014), suggests that testing only one type of these prisms would be acceptable for determining the masonry compressive strength for the whole RMSW with C-MBEs following the CSA requirements.

CSA S304 (2014) tabulated masonry compressive strength values were found to underestimate the compressive strength of masonry prisms constructed with stretcher block while overestimate that of C-MSBEPs. On the other hand, MSJC (2013) tabulated values were

found to also underestimate the compressive strength of stretcher block prisms but are approximately equal to the C-MSBEP experimental results.

Two unreinforced masonry stress-strain model were proposed. The first model was developed by modifying the f_m, ε_{mu}, and E_m in Mander's model for unreinforced and unconfined concrete. The second model was developed by modifying the f_m, ε_{mu} in the model of Kent and Park for unreinforced and unconfined concrete. The two models present simple calculations for predicting the full stress-strain curves of C-MSBEPs (h/t = 2.0 or 5.0), the standard CSA S304 (2014) stretcher block prism (running-bonded and face-shell mortar bedded prism of h/t = 5.0), and the standard ASTM C1314 (2014) stretcher block prism (stack-bonded and full mortar bedded prism of h/t = 2.0). The models also allow the transformation between one prism type (i.e. stretcher or C-shaped) and another.

Based on the results of the grout cores tested, it can be concluded that the grout treatment has a negligible effect on the stress-strain response. The average difference in the peak stress between the air and water treated grout cores was 5% for the normal strength grout. The difference was even lower in high strength grout specimens.

The effect of the aspect ratio on the grout strength was lower than the 15% expected from the correction factors suggested by CSA S304 (2014). High strength grout cores of h/t = 2 showed only about 7% increase in strength from the cores of h/t = 5. This percentage is even lower for normal strength grout cores. On the other hand, shells of h/t = 2 showed 25% increase in strength from the cores of h/t = 5.

The size and shape of the grout specimen was found to affect the grout response considerably. Normal strength grout prisms of h/t = 2 when compared to normal strength grout cylinders showed an increase of 32% in strength, 50% in peak strain, and 23% in initial stiffness. In the case of high strength grout, these percentages are 10%, 52% and 13% increase, respectively.

The available strength prediction equations for masonry prisms were found to underestimate or overestimate the strength of C-MSBEPs. The equation provided by Hamid et al. (1978) estimated prims strength that is 40% and 33% lower than the experimental results for normal and high strength grouted prisms respectively. In contrast, the equation provided by Priestley and Chai Yuk Hon (1984) overestimated the strength of the prisms by 29% and 94% for normal and high strength grouted prisms respectively. Hamid et al. (1978) suggested that the excessive bilateral strains exerted by the grout core at high stresses caused a premature splitting failure in

the shell. However, the factors provided in the equation presented in the same study suggest that the grout core, not the shell, is the component that prematurely failed contributing by about 25% of its capacity. On the other hand, Priestley and Chai Yuk Hon (1984) suggested that the grout core contributes by more than 90% of its capacity. According to the study, the core is prevented from developing its full capacity by the fact that the shell's peak stress, which marks the prism failure, occurs at lower strain than that of the grout core. In conclusion, the interaction between the masonry shell and the grout core is not fully investigated in literature which is supported by the gap between the factors used to represent the contribution of each of the masonry prism constituents in the equations discussed.

Superposition of strengths of the masonry shell and the grout core based on area overestimates the strength of the C-MSBEPs. It overestimates the load capacity at any displacement value along the load-displacement curve of the prisms grouted with normal or high strength grouts. It is believed that the main reason for this drawback is the misrepresentation of the strength of the grout in the core. Grout cylinders, grout prisms, and grout core samples cut from grouted prism cells neglect the effect of the restained shrinkage on the grout core. Grout cores bonded to the inner face of the masonry shell is restrained from shrinking which leads to initial bilateral tension on the grout core decreasing its load carrying capacity for axial compression. This leads to considering using non-shrink grout to facilitate higher contribution from the grout core to the prism allowing the core to contribute with its full compressive strength that is developed when tested separately being unbonded from the shell.

A reduction factor α is introduced that is calculated based on six reduction factors to account for different aspect ratios, incompatibility of grout core and masonry shell peak stresses, shape effect, shrinkage effect on the grout strength, size effect, and water absorption from grout core by the shell.

5.3 Recommendations for Future Research

This study opens the door for more future work in this field aiming at enhancing the compressive strength of masonry assemblage and walls. The future work may investigate the effect of each of the reduction factors discussed on one another and their dependency on the grout strength. As the conclusions in this study might have been affected by the limited considered specimens, it is recommended that more BE prisms of different C-shaped block

strengths, different grouts, and mortar strength to be tested and compared to stretcher block prisms. Studying these factors will enhance the understanding of their effect on the stress-strain response of C-MSBEPs. This will also validate the values used in the proposed models and assess the way each of them is affected by each of these factors. The effect of using non-shrink grout on the C-MSBEPs strength and on the validity of the superposition principle is also recommended to be investigated. Along this line, the effect of wetting the masonry prisms before grouting could be investigated aiming that this would reduce the plastic shrinkage of grouted core. It is also recommended that RMSWs with C-MSBEs to be constructed and tested to verify that the local prism response discussed in this study is valid for whole columns and structures. This will also add some valuable data to be used to verify the suitability of using CSA S304 (2014) and MSJC (2013) tabulated values for the prediction of C-MSBEs' and RMSW with BEs capacities.

REFERENCES

Abo El Ezz, A., Seif Eldin, H. M., and Galal, K. (2015). "Influence of confinement reinforcement on the compression stress-strain of grouted reinforced concrete block masonry boundary elements." *Structures*, Elsevier B.V., 2, 32–43.

Albutainy, M., Ashour, A., and Galal, K. (2017). "Effect of Boundary Elements Confinement Level on The Behavriour of Reinforced Masonry Structural Walls with Boundary Elements." *13th Canadian Masonry Symposium*, Halifax, Canada.

ASTM C1019. (2014). "Standard Test Method for Sampling and Testing Grout." ASTM International, West Conshohochken, PA.

ASTM C109. (2013). "Standard Test Method for Compressive Strength of Hydraulic Cement Mortars (Using 2-in. or [50-mm] Cube Specimens)." ASTM International, West Conshohochken, PA.

ASTM C1314. (2014). "Standard Test Method for Compressive Strength of Masonry Prisms." ASTM International, West Conshohocken, PA.

ASTM C140. (2015). "Standard Test Methods for Sampling and Testing Concrete Masonry Units and Related Units." ASTM International, West Conshohocken, PA.

ASTM C469. (2014). "Standard Test Method for Static Modulus of Elasticity and Poisson's Ratio of Concrete in Compression." ASTM International, West Conshohocken, PA.

ASTM C617. (2014). "Standard Practice for Capping Cylindrical Concrete Specimens." ASTM International, West Conshohochken, PA.

Banting, B. R., and El-Dakhakhni, W. W. (2012). "Force- and displacement-based seismic performance parameters for reinforced masonry structural walls with boundary elements." *Journal of Structural Engineering (United States)*, 138(12), 1477–1491.

Boult, B. F. (1979). "Concrete Masonry Prism Testing." *ACI Journal Proceedings*, 76(24), 513–536.

Chahine, G. N., and Drysdale, R. G. (1989). "Influence of Test Conditions on the Compressive Strength and Behaviour of Faceshell Mortar Bedded Concrete Block Prisms." *5th Canadian Masonry Symposium*, University of British Columbia, Vancouver, B.C., Canada, 651–660.

CSA A165. (2014). "CSA Standards on concrete masonry units." Canadian Standards Association, Mississauga, ON, Canada.

CSA A179. (2014). "Mortar and grout for unit masonry." Canadian Standards Association, Toronto, ON, Canada.

CSA S304. (2014). "Design of masonry structures." Canadian Standards Association, Mississauga, ON, Canada.

Drysdale, R. G., and Hamid, A. A. (1979). "Behavior of Concrete Block Masonry Under Axial Compression." *ACI Journal*, 76(6), 707–721.

Drysdale, R. G., and Hamid, A. A. (1982). "Influence of the Characteristcs of the Units on the

Strength of Block Masonry." *Proceedings of the second North American Masonry Conference*, University of Maryland, College Park, MD, USA.

Drysdale, R. G., and Hamid, A. A. (2005). *Masonry Structures Behaviour and Design*. Canada Masonry Design Centre, Mississauga, ON, Canada.

El-Dakhakhni, W., and Ashour, A. (2017). "Seismic Response of Reinforced-Concrete Masonry Shear-Wall Components and Systems: State of the Art." *Journal of Structural Engineering*, 143(9), 03117001.

Ezzeldin, M., El-Dakhakhni, W., and Wiebe, L. (2017). "Experimental Assessment of the System-Level Seismic Performance of an Asymmetrical Reinforced Concrete Block–Wall Building with Boundary Elements." *Journal of Structural Engineering*, 143(8), 04017063.

Fahmy, E. H., and Ghoneim, T. G. M. (1995). "Behaviour of Concrete Block Masonry Prisms under Axial Compression." *Canadian Journal of Civil Engineering*, 22, 898–915.

Fortes, E. S., Parsekian, G. A., and Fonseca, F. S. (2014). "Relationship between the Compressive Strength of Concrete Masonry and the Compressive Strength of Concrete Masonry Units." *Journal of Materials in Civil Engineering*, 27(9), 04014238.

Ganesan, T. P., and Ramamurthy, K. (1992). "Behavior of Concrete Hollow-Block Masonry Prisms under Axial Compression." *Journal of Structural Engineering*, 118(7), 1751–1769.

Hamid, A. A., and Chukwunenye, A. (1986). "Compression Behavior of Concrete Masonry Prisms." *Journal of Structural Engineering*, 112(3), 605–613.

Hamid, A. A., and Drysdale, R. G. (1979). "Suggested Failure Criteria for Grouted Concrete Masonry Under Axial Compression." *ACI Journal*, 76(43), 1047–1061.

Hamid, A. A., Drysdale, R. G., and Heidebrecht, A. C. (1978). "Effect of Grouting on the Strength Characteristics of Concrete Block Masonry." *Proceedings of the North American Masonry Conference*, Boulder, CO.

Hassanli, R., ElGawady, M. A., and Mills, J. E. (2015). "Effect of dimensions on the compressive strength of concrete masonry prisms." *Advances in Civil Engineering Materials*, 4(1).

Hedstrom, E. G., and Hogan, M. B. (1990). "The Properties of Masonry Cgrout in Concrete Masonry." *Masonry: Components to Assemblages, ASTM STP 1063*, ASTM International, 47–62.

Khalaf, F. M. (1996). "Factors Influencing Compressive Strength of Concrete Masonry Prisms." *Magazine of Concrete Research*, 48(175), 95–101.

Khalaf, F. M., Hendry, A. W., and Fairbairn, D. R. (1994). "Study of the compressive strength of blockwork masonry." *ACI Structural Journal*, 91(4), 367–375.

Klinger, T. S. C. and R. E. (1986). "Compressive Strength of Concrete Masonry Prisms." *ACI Journal Proceedings*, 83(1), 88–97.

Korany, Y., and Glanville, J. (2005). "Comparing Masonry Compressive Strength in Various Codes." *Concrete International*, 27(07), 35–40.

Malhotra, V. M. (1976). “Are 4 x 8 Inch Concrete Cylinders as Good as 6 x 12 Inch Cylinders for Quality Control of Concrete?” *ACI Journal Proceedings*, 73(1), 33–36.

Mander, J. B., Priestley, M. J. N., and Park, R. (1988a). “Theoretical Stress-Strain Model for Confined Concrete.” *Journal of Structural Engineering*, 114(8), 1804–1826.

Mander, J. B., Priestley, M. J. N., and Park, R. (1988b). “Observed Stress-Strain Behavior of Confined Concrete.” *Journal of Structural Engineering*, 114(8), 1827–1849.

Martins, R. O. G., Nalon, G. H., Alvarenga, R. de C. S. S. A., Pedroti, L. G., and Ribeiro, J. C. L. (2018). “Influence of blocks and grout on compressive strength and stiffness of concrete masonry prisms.” *Construction and Building Materials*, Elsevier Ltd, 182, 233–241.

Maurenbrecher, A. H. P. (1980a). “Effect of the test procedures on compressive strength of masonry prisms.” *2nd Canadian Masonry Symposium*, Carleton University, Ottawa, ON ,Canada, 119–132.

Maurenbrecher, A. H. P. (1980b). “Effect of the test procedures on compressive strength of masonry prisms.” *2nd Canadian Masonry Symposium*, (922), 119–132.

MSJC. (2013). “Building Code Requirements for Masonry Structures.” *TMS 602-13/ACI 530.1-13/ASCE 6-13*, Masonry Society Joint Committee, Longmont, CO.

NCMA. (2014). “Evaluating The Compressive Strength of Concrete Masonry.” National Concrete Masonry Association, Herndon, Virginia.

Neville, A. M. (1956). “The influence of size of concrete test cubes on me all strength and standard deviation.” *Magazine of Concrete Research*, 8(23), 101–110.

NZS. (2004). “Design of Reinforced Concrete Masonry Structures.” *4230:2004*, New Zealand Standards, Wellington, New Zealand.

Obaidat, A. T., Abo El Ezz, A., and Galal, K. (2017). “Compression behavior of confined concrete masonry boundary elements.” *Engineering Structures*, Elsevier Ltd, 132, 562–575.

Obaidat, A. T., Ashour, A., and Galal, K. (2018). “Stress-strain behavior of C-shaped confined concrete masonry boundary elements of reinforced masonry shear walls.” *Journal of Structural Engineering*, 144(8).

Priestley, M. J. N., and Chai Yuk Hon. (1984). “Prediction of Masonry Compression Strength Part:1.” *New Zealand Concrete Construction*, 28, 11–14.

Rizaee, S., Hagel, M. D., Kaheh, P., and Shrive, N. (2016). “Comparison of compressive strength of concrete block masonry prisms and solid concrete prisms.” *16th International Brick and Block Masonry Conference: IBMAC*, London, UK, 1839–1846.

Romagna, R. H., and Roman, H. R. (2002). “Compressive Strength of Grouted and Un-grouted Concrete Block Masonry.” *Proceedings of the British Masonry Society*, 399–404.

Sarhat, S. R. (2016). “The Size Effect and Strain Effect in Reinforced Masonry.” Carleton University.

Sarhat, S. R., and Sherwood, E. G. (2014). “The prediction of compressive strength of ungrouted

hollow concrete block masonry." *Construction and Building Materials*, Elsevier Ltd, 58, 111–121.

Scrivener, J. C., and Baker, L. R. (1988). "Factors Influencing Grouted Masonry Prism Compressive Strength." *Proceedings of 8th International Brick/Block Masonry Conference*, Ireland, 874–883.

Shedid, M. T., El-Dakhakhni, W. W., and Drysdale, R. G. (2010). "Alternative Strategies to Enhance the Seismic Performance of Reinforced Concrete-Block Shear Wall Systems." *Journal of Structural Engineering*, 136(6), 676–689.

Sturgeon, G. R., Longworth, J., and Warwaruk, J. (1980). *An Investigation of Reinforced Concrete Block Masonry Columns*. *University of Alberta Structural Engineering Report No. 91*, Edmenton, AB, Canada.

Voon, K. C., and Ingham, J. M. (2006). "Experimental in-plane shear strength investigation of reinforced concrete masonry walls." *Journal of Structural Engineering*, 132(3), 400–408.

Appendix A

EXPERIMENTAL WORK

Appendix A.1 **Material Characterization**

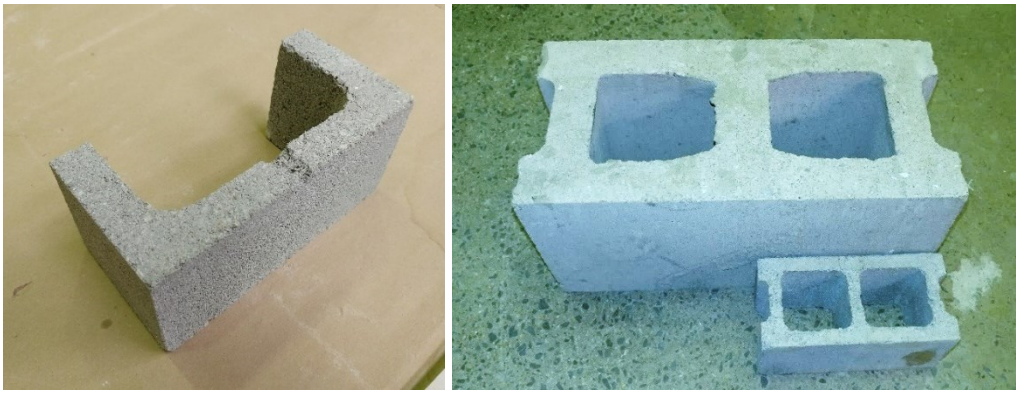

Figure A-1 Half-scale C-shaped block and Half-scale stretcher block compared to full-scale stretcher block

Figure A-2 Capping of stretcher blocks

Figure A-3 Failure of Stretcher blocks

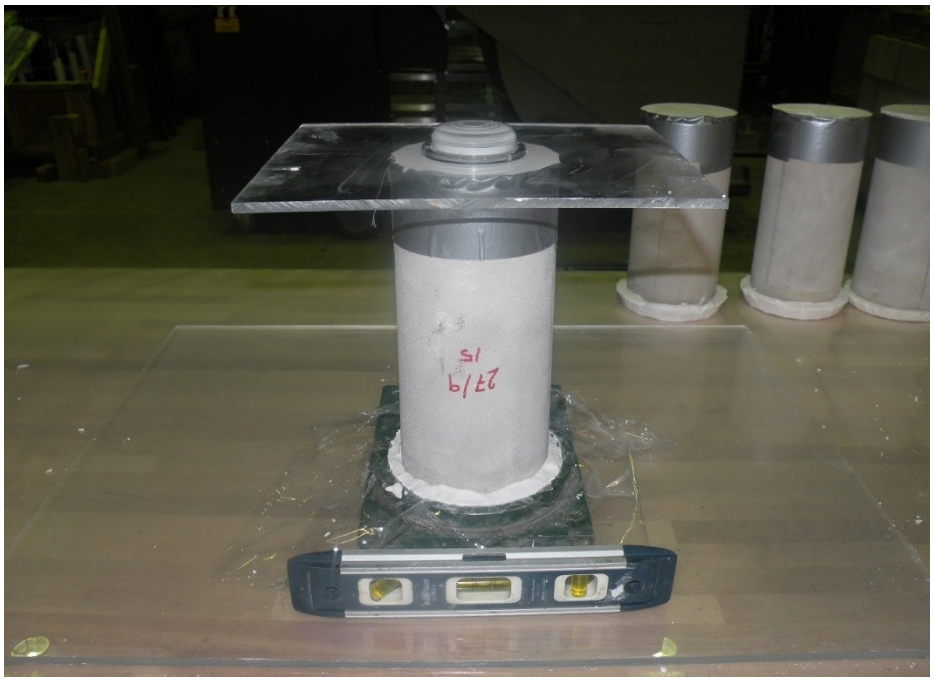

Figure A-4 Capping of grout cylinders

Figure A-5 Failure of grout cylinders

Figure A-6 Failure of ASTM grout prisms

Figure A-7 Sampling and tamping of mortar cubes

Appendix A.2 **Construction of Specimens**

Figure A-8 Building the specimens by the certified mason

Figure A-9 Stretcher block prisms and C-MSBEPs during construction

Figure A-10 Grouting the masonry prisms

Figure A-11 Keeping the prisms in sealed water tight bags

Figure A-12 Wet treatment of the grout cores

Figure A-13 Stretcher prisms of h/t = 2.0 before testing

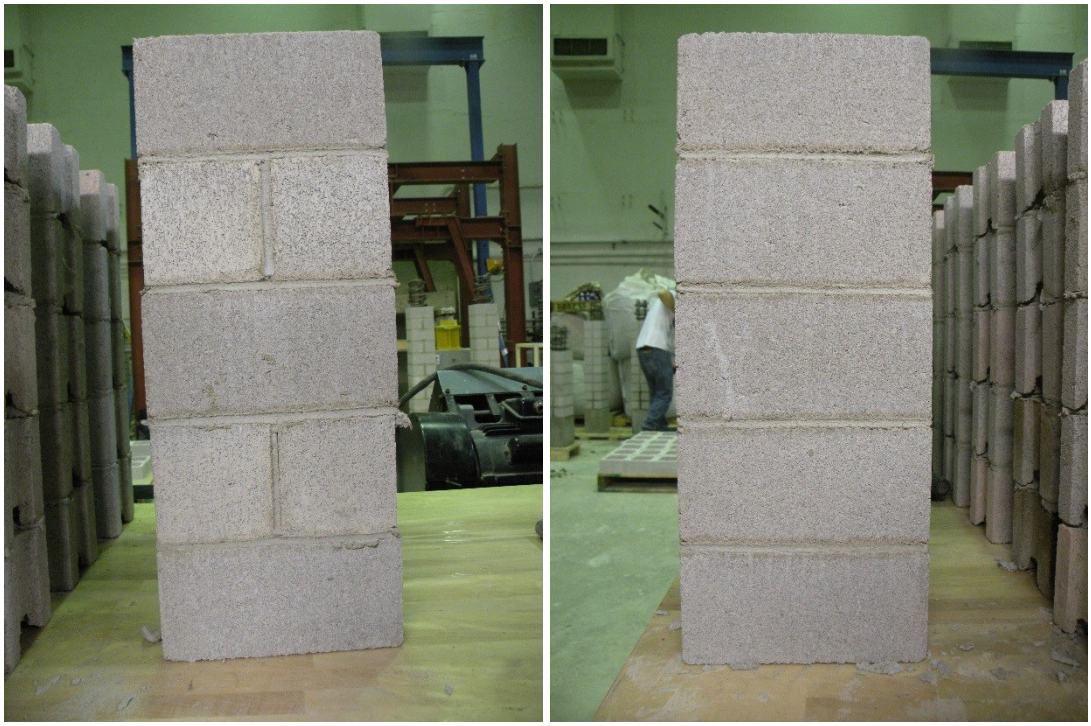

Figure A-14 Stretcher prisms of h/t = 5.0 before testing

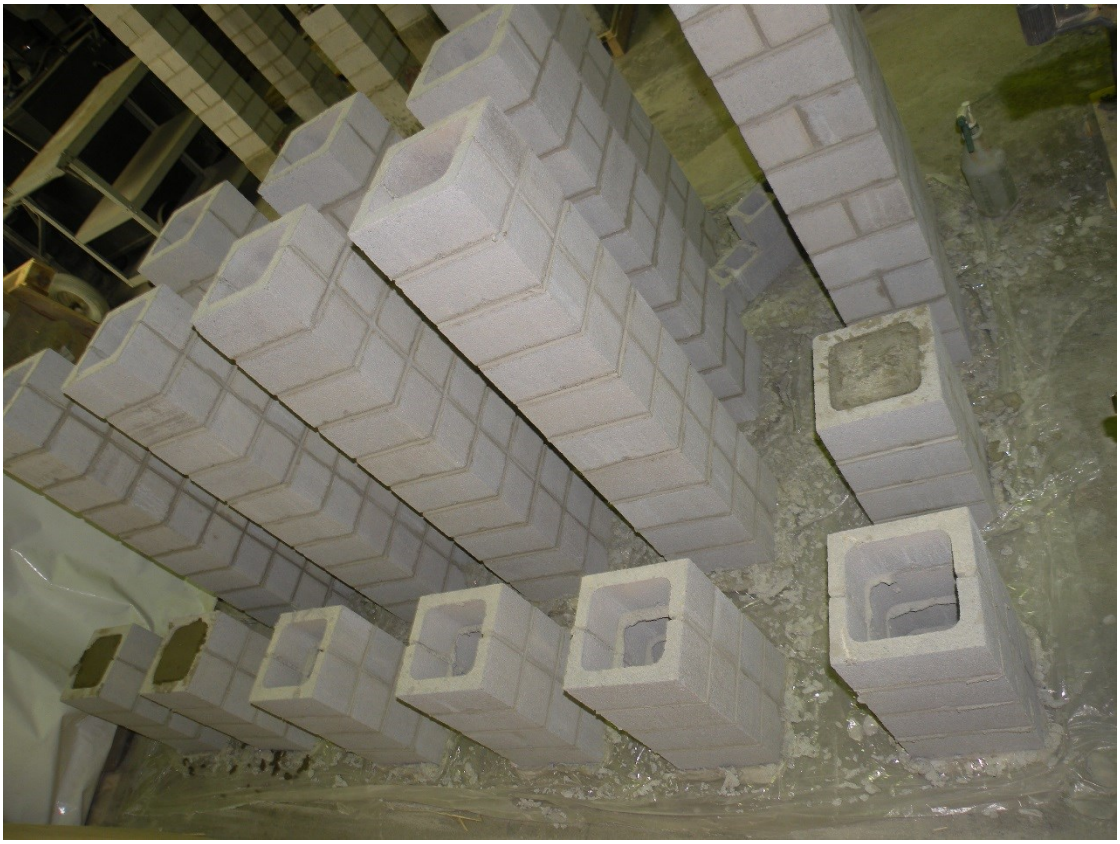

Figure A-15 C-MSBEPs before testing

Appendix A.3 **Specimens after Testing**

Figure A-16 Stretcher block prisms after testing

Figure A-17 C-MSBEPs after testing